



Norwegian University of
Science and Technology

Numerical Study on Wave Drift Loading on Slender Marine Structures

Julie Vadholm

Marine Technology

Submission date: July 2017

Supervisor: Marilena Greco, IMT

Co-supervisor: Finn-Christian W. Hanssen, Moss Maritime
Babak Ommani, IMT

Norwegian University of Science and Technology
Department of Marine Technology



MASTER THESIS IN MARINE TECHNOLOGY

Spring 2017

FOR

Julie Vadholm

Numerical study on wave drift loading on slender marine structures

(Numerisk studie av bølgedriftlaster på slanke marine konstruksjoner)

During the 1990s, some research showed that viscous effects contributed to a substantial increase in wave drift loads in high sea states for slender structures. Recently, the viscous contribution has been suggested as a possible explanation for some accidents with mooring line failures. In those cases, the sea states were within the operational limits for the mooring systems. This suggests that there exists a knowledge gap in connection with the wave loading. To account for viscous drift contributions, the state-of-the-art approach in the industry is to apply Morison equation to model drag loads on slender members. In the wave-drift problem, the most important contributions (both viscous and non-viscous) originate from the part of the structure in the free-surface zone. Here the uncertainties related to choice of drag coefficient is large, both due to nonlinear wave kinematics, local wave-body interactions leading to non-uniform water rise-up along the structure, and possibly due to variations in relevant flow parameters. Recently an empirical formula for the wave drift loads has been proposed within the "EXWAVE JIP" project for semis and other column-based floating platforms.

Objective

The present master thesis aims to contribute in enhancing the knowledge on the relevant effects for wave drift loading on slender marine structures. This will be done numerically, performing 2D and 3D simulations of the problem. As preliminary study, a project-thesis work examined relevant literature and identified an open-source CFD solver to carry out numerical investigations of the problem. The solver was verified for wave propagation and wave interaction against a fixed structure, assuming 2D flow conditions. Accuracy and numerical convergence were studied.

The master-thesis work should be carried out in steps as follows:

1. Summarize major findings/outcomes from the project thesis.
2. Complement the literature study initiated in the project thesis.
3. Apply the selected CFD solver to study a 2D problem with incident (regular and bi-chromatic) waves interacting with a fixed body mimicking a platform column. Examine the loads on the structure and discuss contributions from linear and nonlinear effects as a function of the incident-wave parameters and the body slenderness.
4. Compare results from selected cases of step 3 against a potential-flow fully nonlinear solution to assess importance of viscous effects.
5. Select relevant incident-wave parameters from the investigations in step 3 and 4 and apply the CFD solver to study a 3D problem with incident waves interacting with a fixed body mimicking a platform column. The body beam-to-draft ratio should be selected from the 2D body geometries used in step 3 and 4. Examine the loads on the structure and discuss importance of 3D effects.
6. Compare the drift-load results from the 3D simulations against the predictions from the available empirical formula recently proposed within the "EXWAVE JIP" project.
7. Summarize the results and provide suggestions for future research investigations.

The work may show to be more extensive than anticipated. Some topics may therefore be left out after discussion with the supervisor without any negative influence on the grading.

The candidate should in his report give a personal contribution to the solution of the problem formulated in this text. All assumptions and conclusions must be supported by mathematical models and/or references to physical effects in a logical manner.

The candidate should apply all available sources to find relevant literature and information on the actual problem.

The thesis should be organised in a rational manner to give a clear presentation of the work in terms of exposition of results, assessments, and conclusions. It is important that the text is well written and that tables and figures are used to support the verbal presentation. The thesis should be complete, but still as short as possible. In particular, the text should be brief and to the point, with a clear language. Telegraphic language should be avoided.

The thesis must contain the following elements: the text defining the scope (i.e. this text), preface (outlining project-work steps and acknowledgements), abstract (providing the summary), table of contents, main body of thesis, conclusions with recommendations for further work, list of symbols and acronyms, references and (optional) appendices. All figures, tables and equations shall be numerated.

The supervisor may require that the candidate, in an early stage of the work, present a written plan for the completion of the work. The plan should include budget for the use of computer and laboratory resources that will be charged to the department. Overruns shall be reported to the supervisor.

From the thesis, it should be possible to identify the work carried out by the candidate and what has been found in the available literature. It is important to give references to the original source for theories and experimental results.

Supervisor : Marilena Greco
Co-supervisor : Finn-Christian W. Hanssen
Co-supervisor : Babak Ommani
Deadline : 28 August 2017

Marilena Greco
Supervisor

Preface

This is a master thesis within marine hydrodynamics concerning a numerical study on the wave drift loading on slender marine structures as a part of the study program Marine Technology at the Norwegian University of Science and Technology in Trondheim. The work has mainly been carried out from April to August 2017. The work is a continuation of the preliminary project study carried out from January to March 2017. The work has been performed in cooperation with Moss Maritime who initially suggested the topic and emphasized the importance of research within this particular area. Moss Maritime has provided a co-supervisor who has supported me throughout the work with this master thesis.

The master thesis covers a brief introduction to the relevant theory related to the problem, a description of the current methods used to calculate and predict the wave drift forces, the methodology behind the numerical study by use of openFOAM, a summary of the results, discussion of the main findings and recommendations for further work. A considerable amount of time has been used to modify the numerical wave tank in OpenFOAM developed during the project phase to include a damping area, by coupling the existing cases to the toolbox waves2foam. In addition, performing computational analyses with openFOAM is of course time consuming.

Trondheim, 2017-07-30

Julie Vadholm

Acknowledgement

I would like to thank my supervisor, Marilena Greco, for the support while working with the master thesis and for discussing and answering all my questions during our weekly meetings. I would also like to thank my co-supervisors Babak Ommani from SINTEF Ocean and NTNU and Finn-Christian W. Hanssen from Moss Maritime. I would like to thank Babak for all the hours he has used to help me moving forward with OpenFOAM, guide me when I have had trouble with the simulations and answered all my questions. I would like to thank Finn-Christian for always being available and answering my questions regarding the relevant theory behind the thesis, providing me with relevant literature and post processing methods and valuable discussions concerning the results. I would also like to thank Moss Maritime for being positive and helpful and proposing a master topic of importance for the maritime industry. I would also like to thank Carl Trygve Stansberg for answering my questions regarding the new empirical formula proposed by MARINTEK and helping me find additional literature. At last I would like to thank Kjell Larsen and Statoil for providing me with some up-to-date model test results.

J.V.

Summary

This master thesis presents the first step in the investigation of wave drift forces acting on slender structures through numerical simulations. Basic theory is presented along with an overview of how the problem is treated in the industry and a description of the most commonly used methods. The numerical study of how the wave drift forces act on a 2D geometry is performed using the computational fluid dynamics (CFD) program OpenFOAM. The effect of viscosity is also investigated. This is an in-depth study focusing on the methodology behind the problem and presents the initial part of the comprehensive study of wave drift forces on semi-submersible platforms. The study is a continuation of the preliminary project performed from January to March 2017.

Recent mooring line failures in the North Sea occurring at lower sea states than the design sea states indicate the need for an investigation of the existing load prediction methods. A full understanding of the problem is not yet obtained, even though many studies have been carried out during the recent years. Several studies suggest that the wave drift forces are higher than initially anticipated, especially the viscous contribution. Wave drift forces are of higher order and can be difficult to calculate accurately. Potential flow theory is often applied together with simplified viscous theory. However, these methods have shown to under-predict the drift forces. The viscous model is often based on the drag term of Morison's equation. The drag coefficient is case dependent and difficult to predict accurately without the use of model tests. Predictions of wave drift forces using model tests, CFD analysis and development of simplified empirical formulas are still an active research field with the purpose of understanding the underlying physics properly.

The analysis using OpenFOAM is performed for a 2D column of quadratic cross section mimicking one of the columns of a semi-submersible platform. The column is fixed in space, meaning that

the diffraction problem is investigated. The column is subjected to both regular and bi-chromatic waves with wave height 4.5, 6 and 7 m. The wave conditions have been chosen based on parameters presented in relevant literature. The ratio between wave length to body size is always such that the wave classifies as a long wave. The waves are generated in two ways; by a numerical wavemaker and by using the built-in feature of the toolbox waves2Foam, both based on first-order wave theory. An initial convergence study is performed in order to investigate the correct time step to be used. The choices made during the modelling and simulations are discussed along with the presented results. Selected inviscid cases have also been simulated in order to investigate the effect of viscosity.

The presented results show that the expected dominating frequencies are present in the spectra of the forces and wave elevation. For the bi-chromatic wave cases, the mean drift force in surge is proportional to more than the wave amplitude squared. The slow drift forces are also clearly increasing for higher wave amplitudes. Furthermore, the results show that the viscous contribution to the wave drift loads is small and that non-viscous flow separation is present at the sharp corners at the bottom of the column. The grid resolution might have been too low in order to fully capture some details of the viscous effects, and a finer mesh could have been applied in order to investigate this further. Future investigation of this problem would benefit from building up a 3D case to study the importance of three-dimensional effects with an enhanced grid refinement.

Sammendrag

Denne masteroppgaven studerer bølgedriftskreftene på en slank konstruksjon gjennom numeriske simuleringer. Grunnleggende teori og en oversikt over hvordan problemet er behandlet i industrien og hvilke metoder som er mest brukt blir presentert. Det numeriske studiet av bølgedriftskrefter på en 2D geometri er gjennomført ved bruk av CFD-programmet OpenFOAM. Effekten av viskositet har også blitt undersøkt. Studiet har fokusert på metodikken bak problemet og presenterer det første steget i det omfattende studiet av bølgedriftskrefter på halvt nedsenkbare plattformer. Studiet bygger på resultatene fra det innledende prosjektet som ble gjennomført fra januar til mars 2017.

De siste årene har det oppstått flere brudd på ankerliner i Nordsjøen, selv ved lavere laster enn det de er designet for. Dette indikerer at det er et behov for å undersøke de gjeldende lastberegningemetodene. En fullstendig forståelse av problemet er ennå ikke oppnådd, på tross av at det har blitt gjennomført mange studier på dette området de siste årene. De fleste studiene bemerker at bølgedriftskreftene er større enn tidligere antatt, særlig det viskøse bidraget. Bølgedriftskrefter er høyere ordens krefter og kan være vanskelig å beregne nøyaktig. Ofte er forenklet potensialteori brukt sammen med enkle viskøse metoder som er basert på Morisons likning. Drag-koeffisienten varierer ut fra tilfelle og er vanskelig å predikere uten sammenlikning opp mot modelltester. Prediksjon av bølgedriftskrefter ved hjelp av modelltester, CFD analyser og utvikling av empiriske formler er fortsatt interessante forskingsfelt i arbeidet mot å forstå den bakenforliggende fysikken korrekt.

Den numeriske analysen ved hjelp av OpenFOAM er utført for en 2D cylinder med kvadratisk tverrsnitt, som skal etterlikne en av søylene i en halvt nedsenkbar plattform. Søylene er fastholdt og diffraksjonsproblemet er studert. Søylene har blitt utsatt for både regulære og bikromatiske bølger med høyde 4.5, 6 og 7.5 m. Bølgeparametrene er valgt på grunnlag av det som er presentert i

relevant faglitteratur. Forholdet bølgelengde over søylebredde er valgt slik at bølgene er klassifisert som lange. Bølgene er generert på to forskjellige måter; med en numerisk bølgegenerator og ved å bruke den innebygde metoden i verktøyskassen waves2Foam. Begge er basert på førsteordens bølge teori. En enkel konvergensstudie er gjennomført for å bestemme hvilket tidssteg som skal brukes i simuleringen. Noen simuleringer har også blitt gjennomført uten viskositet.

De presenterte resultatene viser at de forventede dominante frekvensene er synlige i kraft- og bølgehevingsspekteret. Koeffisientene til den gjennomsnittlige driftskraften i jag øker med mer enn kvadratet av bølgeamplituden, det samme gjelder for den saktevarierende kraften. Resultatene viser videre at det viskøse bidraget er lite og at ikke-viskøs separasjon oppstår ved søylens hjørner. Elementstørrelsen kan ha vært for stor til å kunne kartlegge de viskøse effektene korrekt og elementstørrelsen bør minkes for å studere dette videre. Videre arbeid med dette problemet vil dra nytte av å gå videre til 3D for å undersøke kreftene og effekten av viskositet nøyere, og å minke elementstørrelsen i et større område under søylen.

Nomenclature

Acronyms

- 2D** Two-dimensional
- 3D** Three-dimensional
- CFD** Computational Fluid Dynamics
- QTF** Quadratic Transfer Function
- KC** Keulegan-Carpenter number
- BC** Boundary Condition
- FFT** Fast Fourier Transform
- DOF** Degree Of Freedom
- TLP** Tension Leg Platform
- JIP** Joint Industry Project
- VOF** Volume Of Fluid

Symbols

B	Bredth [m]
L	Length [m]
ω	Rotational frequency [rad/s]
f	Frequency [1/s]
T	Wave period [s]
λ	Wave length [m]
C_D	Drag coefficient [-]
p	Pressure [Pa]
ϕ	Velocity potential [m^2/s]
ρ	Density [kg/m^3]
A_j	Wave amplitude of wave component j [m]
A_R	Reflected wave amplitude [m]
A_T	Transmitted wave amplitude [m]
ζ_a	Incident wave amplitude [m]
g_i	Gravitational acceleration [m/s^2]
ϵ	Phase angle [rad]
T_{ij}^{is}	Second order transfer functions connected to sine term
T_{ij}^{ic}	Second order transfer functions connected to cosine term
F_i	Force component i [N]
F_D	Drift force [N]
F_V	Viscous force [N]
M_y	Moment about y-axis [Nm]
U	Velocity [m/s]
u_i	Velocity vector [m/s]
U_M	Velocity amplitude of oscillatory flow [m/s]
D	Diameter [m]
A	Area [m^2]
Cu	Current [m/s]
H	Wave height [m]

η	Wave elevation [m]
H_s	Significant wave height [m]
T_p	Peak period [s]
k	Wave number [rad/m]
μ	Dynamic viscosity [$kg/(m \cdot s)$]
δ_{ij}	Kronecker delta [-]
x	Displacement in x [m]
z	Displacement in z [m]
$S(z)$	Wave maker stroke [m]
$S(\omega_j)$	Wave spectrum [$m^2 s$]
Co	Courant number [-]
e_{ij}	Strain rate tensor [1/s]
h	Water depth [m]
T_{oc}	Oscillation period [s]
w	Relaxation weight [-]
α	Volume fraction [-]
m	exponent [-]
a_n	Coefficients in Fourier transformation [-]
b_n	Coefficients in Fourier transformation [-]

Contents

Preface	III
Acknowledgement	IV
Summary	VI
Sammendrag	IX
Nomenclature	XI
Acronyms	XI
Symbols	XII
1 Introduction	1
1.1 Background and Motivation	1
1.2 Objective and Scope	2
1.3 Challenges With the Numerical Study	3
1.4 Outline of Project Thesis	3
2 Introduction to wave drift forces	5
2.1 The Theory of Wave Drift Forces	5
2.1.1 Potential-Flow Theory Approach	6
2.1.2 Viscous Effects	9
2.2 Results and Methods Covered in Literature	10
2.3 Result from Preliminary Numerical Study	13
3 Description of Method	15

3.1	Introduction to OpenFOAM	15
3.2	Solver	16
3.3	Computational Power	17
3.4	Domain and Mesh Generation	17
3.5	Wave Making	18
3.6	Damping	20
3.7	Time Variables	22
3.8	Post-Processing	22
4	Modelling and Simulation	25
4.1	Domain Geometry	25
4.2	Body Geometry	27
4.3	Wave Parameters	28
4.3.1	Regular Waves	28
4.3.2	Bi-chromatic Waves	29
4.4	Damping Parameters	32
4.5	Adjusting Time Variables	33
4.6	Post Processing	35
5	Results	37
5.1	Regular Waves	37
5.1.1	Wave Elevation Results	37
5.1.2	Force Results	38
5.2	Bi-Chromatic Waves	42
5.2.1	Results from paraView	42
5.2.2	Wave Elevation Results	44
5.2.3	Force Results	46
5.3	Inviscid Flow Case	56
5.3.1	Wave Elevation Results	56
5.3.2	Force Results	57
6	Discussion	61

6.1	Regular Waves	61
6.2	Bi-Chromatic Waves	62
6.3	Inviscid Flow Case	65
6.4	General Remarks	65
7	Conclusions and Recommendations for Further Work	67
7.1	Conclusion	67
7.2	Recommendations for Further Work	67
A	OpenFOAM Details	73
A.1	Overview of OpenFOAM Case Set-Up	73
A.2	Boundary Conditions and Explanation	75
B	Additional Simulation Results	77
B.1	Regular Waves	77
B.1.1	Wave Elevation Results	77
B.1.2	Force Results	78
B.2	Bi-Chromatic Waves	81
B.2.1	Wave Elevation Results	81
B.2.2	Force Results	82
B.3	Inviscid Flow Case	84
B.3.1	Wave Elevation Results	84
B.3.2	Force Results	85
C	MATLAB Scripts	87
C.1	Case Generation Script	87
C.2	Post-Processing Scripts	95
C.2.1	FFT of Wave Elevation	95
C.2.2	FFT of Force Data	98
C.2.3	Fourier Analysis of Force Data	103
C.2.4	Input Function in fourier_analysist001.m	107
C.2.5	Input Function in fourier_comp.m	107

C.2.6 Script Used to Plot Mean Drift Force Coefficients 107

List of Figures

3.1	Flap-type wavemaker	19
3.2	Wave particle orbits (Pettersen; 2007)	19
3.3	User interface of paraView	23
4.1	Domain geometry	26
4.2	Domain with mesh	26
4.3	Close-up of domain with mesh	27
4.4	Location of probes	27
4.5	Domain with mesh and volume fraction	27
4.6	Body geometry	28
4.7	Force time series for simulation using a wavemaker	30
4.8	Force time series for simulation using waves2Foam	31
4.9	Overview of waves in the domain with mesh	32
4.10	Waves at the inlet of the domain with mesh	32
4.11	Waves around the body	32
4.12	Comparison of time step and simulated and theoretical wave elevation for $H=4.5$ m	33
4.13	Comparison of time step and simulated and theoretical wave elevation for $H=6$ m	33
4.14	Comparison of time step and simulated and theoretical wave elevation for $H=7$ m	34
5.1	Regular waves: wave elevation analysis for $H = 6m$ and $T = 12s$	37
5.2	Regular waves: force time series for $H = 6m$ and $T = 12s$	38
5.3	Regular waves: force spectrum for $H = 6m$ and $T = 12s$	39
5.4	Regular waves: coefficients of mean drift force	39
5.5	Regular waves: coefficients of force in x direction	40

5.6 Regular waves: coefficients of force in z direction 40

5.7 Regular waves: coefficients of moment about y axis 40

5.8 Plot of the dynamic pressure distribution during wave propagation 42

5.9 Plot of fluid velocity during wave propagation 42

5.10 Plot of fluid velocity vectors around the body 42

5.11 Plot of fluid velocity vectors at the inlet 43

5.12 Plot of velocity vectors around the body for $H=4.5$ m and $d\omega = 0.05$ at $t=700$ s . . 43

5.13 Plot of velocity vectors around the body for $H=6$ m and $d\omega = 0.05$ at $t=700$ s . . . 43

5.14 Plot of velocity vectors around the body for $H=7.5$ m and $d\omega = 0.05$ at $t=700$ s . . 43

5.15 Plot of velocity around body for $H=4.5$ m and $d\omega = 0.05$ at two different time instants 44

5.16 Bi-chromatic waves with $d\omega = 0.05$: wave elevation time series for $H = 4.5m$. . . 44

5.17 Bi-chromatic waves with $d\omega = 0.05$: wave elevation time series and spectrum for
 $H = 6m$ 45

5.18 Bi-chromatic waves with $d\omega = 0.07$: wave elevation time series and spectrum for
 $H = 6m$ 45

5.19 Bi-chromatic waves with $d\omega = 0.05$: wave elevation time series for $H = 7.5m$. . . 46

5.20 Bi-chromatic waves with $d\omega = 0.05$: force time series for $H = 4.5m$ 47

5.21 Bi-chromatic waves with $d\omega = 0.05$: force spectrum for $H = 4.5m$ 47

5.22 Bi-chromatic waves with $d\omega = 0.05$: force time series for $H = 6m$ 48

5.23 Bi-chromatic waves with $d\omega = 0.05$: force spectrum for $H = 6m$ 48

5.24 Bi-chromatic waves with $d\omega = 0.07$: force time series for $H = 6m$ 49

5.25 Bi-chromatic waves with $d\omega = 0.07$: force spectrum for $H = 6m$ 49

5.26 Bi-chromatic waves with $d\omega = 0.05$: force time series for $H = 7.5m$ 50

5.27 Bi-chromatic waves with $d\omega = 0.05$: force spectrum for $H = 7.5m$ 50

5.28 Bi-chromatic waves: coefficients of mean drift force in x direction 51

5.29 Bi-chromatic waves: coefficients of mean drift force in z direction 51

5.30 Bi-chromatic waves: coefficients of mean drift moment in y direction 52

5.31 Bi-chromatic waves: slow drift force coefficient in x direction 52

5.32 Bi-chromatic waves: slow drift force coefficient in z direction 52

5.33 Bi-chromatic waves: slow drift moment coefficient about y 53

5.34	Bi-chromatic waves: first-order force coefficients for $d\omega = 0.05$	53
5.35	Bi-chromatic waves: first-order force coefficients for $d\omega = 0.07$	53
5.36	Bi-chromatic waves: third order force coefficients for $d\omega = 0.05$	54
5.37	Inviscid flow case with $d\omega = 0.05$: wave elevation time series and spectrum for $H = 6m$	56
5.38	Inviscid flow case with $d\omega = 0.05$: plot of velocity vectors around the column . . .	57
5.39	Inviscid flow case with $d\omega = 0.05$: force time series for $H = 6m$	57
5.40	Inviscid flow case with $d\omega = 0.05$: force spectrum for $H = 6m$	58
5.41	Inviscid and viscous flow results for $d\omega = 0.05$: mean drift force coefficients	58
5.42	Inviscid and viscous flow results for $d\omega = 0.05$: first-order force coefficients	59
5.43	Inviscid and viscous flow results for $d\omega = 0.05$: slow drift force coefficients	59
A.1	Overview of initial programming set-up	73
A.2	Overview of programming set-up with result folders	74
B.1	Regular waves: wave elevation analysis for $H = 4.5m$	77
B.2	Regular waves: wave elevation analysis for $H = 7.5m$	78
B.3	Regular waves: force time series for $H = 4.5m$	78
B.4	Regular waves: force spectrum for $H = 4.5m$	79
B.5	Regular waves: force time series for $H = 7.5m$	79
B.6	Regular waves: force spectrum for $H = 7.5m$	80
B.7	Bi-chromatic waves with $d\omega = 0.07$: wave elevation time series for $H = 4.5m$. . .	81
B.8	Bi-chromatic waves with $d\omega = 0.07$: wave elevation time series for $H = 7.5m$. . .	81
B.9	Bi-chromatic waves with $d\omega = 0.07$: force time series for $H = 4.5m$	82
B.10	Bi-chromatic waves with $d\omega = 0.07$: force spectrum for $H = 4.5m$	82
B.11	Bi-chromatic waves with $d\omega = 0.07$: force time series for $H = 7.5m$	83
B.12	Bi-chromatic waves with $d\omega = 0.07$: force spectrum for $H = 7.5m$	83
B.13	Inviscid flow case with $d\omega = 0.05$: wave elevation time series and spectrum for $H = 4.5m$	84
B.14	Inviscid flow case with $d\omega = 0.05$: wave elevation time series and spectrum for $H = 7.5m$	84

LIST OF FIGURES

B.15 Inviscid flow case with $d\omega = 0.05$: force time serie for $H = 4.5m$ 85

B.16 Inviscid flow case with $d\omega = 0.05$: force spectrum for $H = 4.5m$ 85

B.17 Inviscid flow case with $d\omega = 0.05$: force time series for $H = 7.5m$ 86

B.18 Inviscid flow case with $d\omega = 0.05$: force spectrum for $H = 7.5m$ 86

List of Tables

4.1	Wave parameters for regular wave runs with $T = 12$ s	29
4.2	Result from wave maker generated waves of $T=12$ s	29
4.3	Result from waves2Foam generated waves of $T=12$ s	29
4.4	Wave parameters for bi-chromatic wave runs with $H = 4.5$ m	30
4.5	Wave parameters for bi-chromatic wave runs with $H = 6$ m	31
4.6	Wave parameters for bi-chromatic wave runs with $H = 7.5$ m	31
5.1	Regular waves: percentage change of force coefficient from lowest to highest amplitude	41
5.2	Percentage change of mean drift force coefficient from lowest to highest amplitude	54
5.3	Percentage change of slow drift force coefficient from lowest to highest amplitude	54
5.4	Percentage change of first-order force coefficient from lowest to highest amplitude for $d\omega = 0.05$	54
5.5	Percentage change of first-order force coefficient from lowest to highest amplitude for $d\omega = 0.07$	55
A.1	Boundary Conditions	75
A.2	Boundary Condition Description (CFD Direct; 2016)	76

Chapter 1

Introduction

1.1 Background and Motivation

Recent mooring line failures of semi-submersibles in the North Sea occurring at sea states lower than the design sea states, indicate that the predicted loads on these structures used in the design phase are too low in some wave conditions. This has emphasized a need for further investigation and improvement of the design predictions. Several studies have been carried out over the past years, but a full understanding of the problem is not yet obtained. However, several studies suggest that the wave forces, and especially the slow drift forces, are higher than anticipated. Wave drift forces are of higher order, which can be difficult to calculate accurately. Usually, potential flow theory is assumed to be applicable, which is further simplified by Newman's approximation using the first-order linear potential solutions. Comparison of model test results and results from potential-flow codes show that potential codes generally under-predict the loads for slender structures, particularly when the wave height increases. New empirical formulas are also developed in order to prevent underestimation of the mooring line loads, but the accuracy and validity of these formulas are not yet fully understood.

It has been shown that the viscous contribution to wave drift loading increases considerably with increased wave steepness, and is of particular interest in long waves where the viscous forces are dominating. Several studies have suggested that the viscous contribution to the wave drift loads is larger than previously anticipated. In the industry, the drag term of Morison's equation is used to

account for viscous effects in potential theory. Drag coefficients are found empirically by tuning against model tests. As stated by many studies, the most important contributions to the wave drift loads, both potential and viscous, originate in the free-surface zone. The free surface zone is the part of the structure which is in and out of water and there exist some uncertainties regarding the correct choice of drag coefficient in this region in particular. The free surface zone is associated with non-linearities both in the incoming and diffracted wave field, which make it difficult to obtain accurate results with a simplified drag formulation.

Ideally, wave loads should be calculated using the Navier Stokes equations as the governing equation when viscous effects are of importance. Due to the large processor capacity needed to perform these calculations, it can be very time consuming and expensive. However, due to the technological development within the area of computer performance, it becomes increasingly important to test and verify the Navier Stokes solvers for such problems.

1.2 Objective and Scope

This master thesis is exploring the Navier Stokes solver OpenFOAM for calculation of the wave drift forces on a slender cylinder of quadratic cross section in 2D, fixed in space. The cylinder is subjected to selected wave conditions including regular and bi-chromatic waves. The work is a continuation of a preliminary study performed from January to March 2017.

The main objectives of this project have been to

- Apply the Navier Stokes solver OpenFOAM on a two-dimensional problem for a fixed cylinder in monochromatic and bi-chromatic waves
- Analyse the results in order to identify and discuss the wave drift forces
- Investigate the viscous contribution to the wave drift forces

1.3 Challenges With the Numerical Study

The simulations with OpenFOAM are partly done on a regular MacBook Pro computer and partly on the supercomputer Vilje, which is owned by both NTNU and the Norwegian Meteorological Institute. The processing capacity and storage possibilities of the personal computer are limited, and the number of elements and simulation time have therefore been kept low. In addition, OpenFOAM is Linux based, and has therefore been run using the program VirtualBox. VirtualBox makes it possible to run a different guest operative system than the existing operative system, but the program is only allowed to use a limited part of the computer's processing capacity. This may have increased the time needed to perform the analyses. In addition, VirtualBox makes the data handling challenging, as the only way of connecting the guest with the host operative system is via a shared folder. This often requires several loops of copying and transferring data back and forth, which is time consuming. Time limitations is always an issue when performing CFD analyses, however, having access to Vilje has made it possible to run several cases at the same time and decrease the time step.

A new toolbox for openFOAM called waves2Foam has been applied. This includes built-in methods to create wave damping areas and a new wave generation method, different from the wave maker used in the preliminary project. A considerable amount of time has been spent on getting familiar with these methods. Therefore, the thesis work has been limited to deal with the 2D problem. The project has been restricted to the diffraction problem, and the thesis represents the first step in the systematic approach in order to numerically study the wave drift forces. The focus has been on the methodology behind the study, and the simulated cases represent a small part of the real and more complex problem, where also 3D effects and wave radiation effects are anticipated to be important.

1.4 Outline of Project Thesis

Chapter 2 gives a brief introduction to the basic theory regarding wave drift forces, covers findings in available and relevant literature and summarises major findings from the initial project work.

Chapter 3 covers the general method used in the numerical study and the analysis of the results.

Chapter 4 contains explanations and discussion of the choices made during the modelling of the domain and waves and throughout the simulations.

Chapter 5 includes force and wave elevation results from the simulations and visual illustrations from selected time instants of the runs.

Chapter 6 discusses the results presented in *Chapter 5*.

Chapter 7 includes conclusions from the performed work and the obtained results, and provides suggestions for further investigation and research of the problem.

Chapter 2

Introduction to wave drift forces

This chapter will cover the theory of wave drift forces, a brief summary of selected literature and results obtained during the preliminary study of this problem performed from January to March 2017.

2.1 The Theory of Wave Drift Forces

Unlike linear wave forces with a zero mean value, wave drift forces are, in the framework of potential flow perturbation theory, second-order forces which generally have non-zero mean values. Wave drift forces can be divided into mean drift forces and difference-wave frequency forces, which are slowly varying loads. The slowly varying loads oscillate with low frequencies caused by sea states with more than one wave frequency component present (Greco; 2012). With two wave frequencies, ω_j and ω_i , the difference frequency is $\Delta\omega = \omega_i - \omega_j$. The second-order forces are often neglected because they might be small compared to the first-order force, but they are important for structures with low natural frequencies. Because the wave drift forces are of higher order and proportional to the wave amplitude squared, A^2 , the importance of these forces typically increase with increasing wave height (Greco; 2012).

2.1.1 Potential-Flow Theory Approach

Methods based on potential flow theory are widely used to calculate the wave drift forces because of their simplicity and due to the viscous contribution often being small enough to be neglected (Berthelsen et al. (2009) and Stansberg et al. (1998)). The higher order forces can be calculated by performing a perturbation analysis while keeping the terms up to the order of interest. For instance, starting from Bernoulli's equation and performing a perturbation analysis keeping the second-order terms, the pressure accurate to the second-order can be expressed as (Greco; 2012)

$$p = -\rho g z - \rho \frac{\partial \phi_1}{\partial t} - \rho \frac{\partial \phi_2}{\partial t} - \rho \frac{1}{2} \nabla \phi_1 \nabla \phi_1 \quad (2.1)$$

where p is pressure, ρ is the density of water, ϕ_1 and ϕ_2 are the first and second-order velocity potentials, g is the gravitational acceleration and z is the vertical position. Bernoulli's equation, Equation 2.1, includes both first and second-order potentials and products between the gradient of the first-order potentials. As an example, the result of squaring the x-derivative of the first-order potential, $\phi_{01} = A \cos(\omega t + \epsilon)$, is

$$\left(\frac{\partial \phi}{\partial x}\right)^2 = \frac{A^2}{2} + \frac{A^2 \cos[2(\omega t + \epsilon)]}{2} \quad (2.2)$$

where A is the wave amplitude of the wave component and ϵ is the phase angle. As shown in Equation 2.2 this second-order term contributes to a non-zero mean load (Greco; 2012).

Mean Wave Drift Load

In potential-flow theory, the mean wave drift forces originate from the diffraction and radiation of waves from the body. This implies that these loads are greater for large structures compared to the wave length, because of their capability of wave making. The mean wave drift forces can be estimated through either direct pressure integration or conservation of fluid momentum. Unlike for the slowly-varying loads, it can be shown that it is only the first-order velocity potential that contributes to the mean drift force. Hence, the mean drift force can be obtained from a linear potential-flow analysis.

For a body in first-order incident waves, diffraction occurs because of the presence of the body and radiation because of the body motions. A simple way of calculating the mean wave drift of a 2D body is described by Maruo's formula, Equation 2.3, where the incident waves can split into the sum of transmitted and reflected waves with amplitudes A_T and A_R , respectively. The transmitted waves are the sum of incident waves, radiated waves and diffracted waves on the downstream side while the reflected waves include the radiated and diffracted waves on the upstream side. The largest mean wave drift forces using the formula occur when there are no transmitted waves or when A_R is very large. This can occur when waves are propagating towards a vertical fixed wall, if the waves are short compared to the encountering structure or if the body motions are large as a consequence of heave resonance (Faltinsen; 1990).

$$\bar{F} = \frac{\rho g}{2} A_R^2 \quad (2.3)$$

The mean wave drift force is proportional to the wave amplitude squared (Faltinsen; 1990), which means that the transfer function can be written as $\overline{F_i(\omega)}/\zeta_a^2$. The transfer functions are of importance, because they can be used to estimate the mean drift loads in irregular waves from the results in regular waves by dividing the irregular waves into N regular wave components and summing over all the components as given below (Faltinsen; 1990).

$$\bar{F}_i = \sum_{j=1}^N \frac{\overline{F_i(\omega_j)}}{\zeta_a^2} A_j^2 \quad (2.4)$$

F_i is the force in the i-th direction, ζ_a is the incident wave amplitude and A_j is the amplitude of the j-th wave component.

Difference-Wave-Frequency Oscillations: Slow Drift Loads

According to Faltinsen (1990), slow drift motions are resonance oscillations at low frequencies compared to the incoming wave frequency. The slow drift motions are caused by loads connected to second-order difference frequency effects. These non-linear loads can be critical for moored structures with large natural periods if resonance occurs. The long period and small frequency

imply that the linear wave radiation damping is small and that viscous contribution to damping may be important. This means that slow drift motions can be larger than linear motion in certain conditions.

Slow drift forces are caused by a sea state consisting of waves with at least two different frequencies, ω_i and ω_j . Both first and second-order velocity potentials contribute to slowly varying loads. An expression for the slow drift forces up to the second-order is given below (Faltinsen; 1990).

$$F_i^{SV} = \zeta_{a1}\zeta_{a2}T_{12}^{ic} \cos[(\omega_2 - \omega_1)t + (\epsilon_2 - \epsilon_1)] + \zeta_{a1}\zeta_{a2}T_{12}^{is} \sin[(\omega_2 - \omega_1)t + (\epsilon_2 - \epsilon_1)] \quad (2.5)$$

Where T_{12}^{is} and T_{12}^{ic} are the second-order quadratic transfer functions (QTF) for the slow drift loads which are independent of sea state, but functions of the frequencies ω_i and ω_j (Faltinsen; 1990). ϵ is the phase angle and ζ is the wave amplitude. This formula can be modified to be used for a wave spectrum $S(\omega)$, by splitting the spectrum into regular wave components with amplitudes $A_j = \sqrt{2S(\omega_j)\Delta\omega}$ and performing a double summation over all the wave components. By using this method, both the mean and slowly varying forces are found. The diagonal of the QTF matrix constitutes the mean drift load and the off-diagonal values are related to the slow drift loads.

Generally, the second-order potential must be included in order to calculate the slow drift forces. However, through Newman approximation, given below, the calculations are simplified considerably, because the slowly varying loads then can be predicted based on the results from a linear analysis (Faltinsen; 1990).

$$T_{jk}^{ic} = T_{kj}^{ic} = \frac{1}{2}(T_{jj}^{ic} + T_{kk}^{ic}) \quad (2.6)$$

$$T_{jk}^{is} = -T_{kj}^{is} = 0 \quad (2.7)$$

The formulas above indicate the same as taking the values of the transfer functions along the line $\omega_k \approx \omega_j$, i.e. the mean drift force, given that the difference $\omega_k - \omega_j$ is small. According to Faltinsen (1990), Newman approximation can be used when 1) the small difference frequencies and large oscillation periods are of interest and 2) when the transfer functions, T_{jk}^{ic} and T_{jk}^{is} does not change much with frequency around the main diagonal. Newman approximation should not be used when T_{jk}^{ic} has a pronounced maxima or minima close to the line $\omega_j = \omega_k$. If both the conditions are

satisfied, then

$$T_{jj}^{ic} \cong T_{kk}^{ic} \quad (2.8)$$

and

$$0.5(T_{jj}^{ic} + T_{kk}^{ic}) \cong \sqrt{T_{jj}^{ic} T_{kk}^{ic}} \quad (2.9)$$

Introducing the mentioned simplifications, the resulting force expression for the slowly varying force becomes (Faltinsen; 1990)

$$F_i^{SV} \cong \sum_{j=1}^N \sum_{k=1}^N A_j A_k \sqrt{T_{jj}^{ic} T_{kk}^{ic}} \cos[(\omega_k - \omega_j)t + (\epsilon_k - \epsilon_j)] \quad (2.10)$$

This expression depends on the transfer functions of the mean drift loads and the first-order solution in regular waves, and ϕ_2 does not need to be calculated. Potential-flow theory with Newman's approximation is widely used in industry (Berthelsen et al.; 2009).

2.1.2 Viscous Effects

When the waves are long compared to the structure and the wave height increases, viscous effects become increasingly important relative to the potential-flow loads, because the viscous contribution is of higher order than second. Long waves are related to small wave generation causing less drift loads due to potential drift. In order to add the viscous effects to the potential-flow theory methods, the drag term of Morison's equation, Equation 2.11, based on strip theory is widely used in the industry (Berthelsen et al.; 2009). Morison's equation is a long wave approximation, valid when $\lambda/D \gtrsim 5$ for calculation of wave loads on cylindrical structures (Faltinsen; 1990). The drag term of Morison's equation is given below.

$$F_V = - \int_L \frac{\rho}{2} C_D U |U| dl \quad (2.11)$$

C_D is the drag coefficient, L is the length of the structure and U is the velocity perpendicular to the cylinder axis. The resulting force when the expression is integrated up to the instantaneous free surface is proportional to the wave amplitude cubed (Dev and Pinkster; 1995). This means that viscous load in the wave zone becomes very important for high waves that are long compared to

the structure. The drag coefficient must be empirically determined and is dependent on several flow variables (Faltinsen; 1990).

The choice of drag coefficient is not straightforward. The most accurate way of estimating C_D is by using results from model tests. However, the drag coefficient can also be estimated using the Keulegan-Carpenter number, KC-number, which is defined as (Faltinsen; 1990)

$$KC = \frac{U_M T}{D} \quad (2.12)$$

where U_M is the velocity of an oscillatory planar flow, T is the oscillation period and D is the characteristic cross-section dimension of the structure. From a defined KC-number, C_D can be found from relations and graphs based on previous experiments (Faltinsen; 1990).

2.2 Results and Methods Covered in Literature

A brief literature study has been performed, which covers some of the methods and results emphasized in existing studies of drift forces in cases where both potential and viscous loads matter. From the literature study, different methods used to calculate wave drift forces have been investigated. Research within this field are based on numerical, empirical and experimental methods in order to as accurately as possible analyse the wave drift forces and response. Model tests are often used to validate the results obtained using empirical formulas or numerical methods.

Most of the literature investigated agree that results from methods based on potential-flow theory show discrepancies when compared to experimental results regarding the wave drift forces on semi-submersibles (Berthelsen et al. (2009), Stansberg et al. (1998), Hu and Zhou (2015), Stansberg et al. (2016)). The potential-flow theory methods are most commonly based on Newman's approximation. Large deviations are observed in cases where the waves are long and for high sea states. When the viscous effects are added to the potential-flow theory solutions, the results show better agreement. Therefore, viscous effects are expected to be the main reason for the discrepancies towards results based on potential-flow theory. The studies also show that the relative

importance of the viscous contribution increases with increasing wave height and wave length. In order to calculate the viscous contribution, the most common approach is through Morison's equation. The results are most accurate if the drag term, C_D , is tuned against model tests and separate drag coefficients are introduced for the free surface zone (Berthelsen et al.; 2009). C_D is case dependent and choosing a large value may result in too large damping (Berthelsen et al. (2009), Stansberg et al. (1998)).

An empirical formula for calculation of the wave drift forces on slender structures has been proposed by a joint industry project (JIP) called EXWAVE (Stansberg and Nestegård; 2014). The formula includes the effect of current, and has been tested for different kinds of semi-submersible platforms and compared to experimental and numerical results. It shows good agreement in some cases and discrepancy in other (Stansberg et al.; 2016) without indicating a clear trend or pattern. The formula is given below.

$$F = \frac{F_D(\omega, U, H_s)}{A^2} = f_{d,pot}(1 + C_p U) + b(GU + H_s) \quad (2.13)$$

$$b = b' D_{sum}$$

$$D_{sum} = \Sigma D_i$$

$$b' = k \cdot P$$

$$P = \exp(-1.25(kD_0)^2)$$

The formula consists of two terms, the first one is related to the potential flow and the second accounts for the viscous effects. $f_{d,pot}$ is the second-order mean wave drift coefficient calculated from first-order potential-flow theory. It can be found from potential-flow codes like WAMIT. WAMIT is a linear and second-order potential-flow program based on the panel method, where the output is in the frequency domain (WAMIT; 2017). C_p is the wave-current interaction coefficient from potential-flow theory and is set to be 0.25 in the EXWAVE study. b is the viscous drift, D_{sum} is the sum of the column diameters, b' accounts for the upper limit of frequency where the viscous effects are important, k is the wave number, D_0 is the diameter of the main columns, U is the current velocity parallel to the waves, A is the wave amplitude and H_s is the significant wave height.

G, the viscous wave-current interaction term, is empirically determined and is equal to 10 in the EXWAVE study.

Model tests of semi-submersibles with the purpose of investigating the wave drift forces have recently been performed, and the results have been compared to the empirical formula (Fonseca (2016), Thys and Ambrahamsen (2016), Braaten (2016)). One of the semi-submersibles consists of columns with squared cross section with rounded corners (Fonseca; 2016), whereas the other two consist of circular columns (Thys and Ambrahamsen (2016), Braaten (2016)). The two semi-submersibles with circular columns differ by the size and number of columns. One of them consists of several small interconnecting cylinders in addition to the larger main columns. The reports show that there is a difference in the results for the three semi-submersibles. The large quadratic columns cause a considerable amount of wave radiation, which is visible from additional peaks in the force coefficient plots. Another finding is that the force in the low frequency region is largest for the semi-submersible with the largest amount of columns. This is most likely due to the viscous effects as a consequence of large periods and small cylinder diameters of the interconnecting cylinders. For the two semi-submersibles with circular cross section, the interaction of the cylinders is visible in the results through less smooth force coefficient plots.

As for the geometry of the semi-submersibles investigated and covered in the literature, most are of squared section with rounded corners (Berthelsen et al. (2009), Stansberg et al. (1998), Hu and Zhou (2015), Fonseca (2016)). The draught is about 20 meters and the diameter of the columns are about 15 meters.

A 3D numerical study on the wave run-up and forces on a vertical fixed squared cylinder in regular waves has recently been published (Ali et al.; 2017). The main goal with the study was to validate and verify the computational fluid dynamics software OpenFOAM in prediction of wave run-up. The waves were validated against analytical and experimental results, and it was concluded that openFOAM can produce results in good agreement with experimental data and that the accuracy is satisfactory. The method used in this study is quite similar to the one used in this master thesis, although the parameters differ. The experimental results used for verification have been taken from Stansberg et al. (2005). This study also include an introductory CFD study on a circular vertical column in which significant non-linear contributions are observed in the free surface area.

2.3 Result from Preliminary Numerical Study

The project thesis, performed from January to March 2017, covered a preliminary analysis of the forces acting on a simple 2D geometry by use of the Navier Stokes solver OpenFOAM. For a simple 2D geometry, useful observations and experiences were made. The results from this CFD study were compared to model test results for the same body and wave parameters presented in the paper by [Tanizawa et al. \(1999\)](#).

The most important experience from the initial numerical study has been that the numerical wave tank needs to be made such that the resulting force time series is sufficiently long and not affected by reflected waves. Because the desired waves to be investigated are long compared to the structure, there will be a considerable amount of transmitted waves, which eventually will reflect back from the downstream boundary wall. Results show that the wave drift force for the particular case investigated is higher when the body is exposed to the reflected waves from the wall. In order to avoid this effect, the wave tank can be made very long ([Stansberg et al.; 2005](#)), as done in the preliminary project, or by introducing a damping zone in the downstream end of the wave tank. The last alternative is desirable because it involves a smaller domain, less elements and thus a shorter simulation time. The results from the analysis also show that that the wave drift force is sensitive with regards to the wetted surface, which means that the elements in the free surface zone need to be small enough to get accurate results. Another valuable experience is the quick increase in computational time associated with decreasing the element size and time step. However, the over-all numerical results match the experimental reference results quite well, which validates the use of the numerical method and the simulation variables for the particular case tested.

Chapter 3

Description of Method

This chapter covers the general methodology used in the numerical study. It contains descriptions of the CFD software, solver, mesh generation, wave generation, wave damping method, the choice of time variables and post-processing methods.

3.1 Introduction to OpenFOAM

In order to numerically find the wave drift loads on a slender structure, the Navier Stokes solver OpenFOAM (Open Source Field Operation and Manipulation) has been used. OpenFOAM is an open source code to perform Computational Fluid Dynamics (CFD) simulations. The code is based on the programming language C++ and consists of different solvers and utilities designed to solve specific problems and perform tasks with data manipulation (CFD Direct; 2016). OpenFOAM comes with a post-processing utility based on ParaView, which is an open-source visualisation application (CFD Direct; 2016). The structure of the program can be found in Appendix B. In this thesis OpenFOAM is used to create a numerical wave tank in order to simulate wave drift loads on fixed slender surface-piercing structures in a viscous fluid. The Navier Stokes equations, conservation of momentum, and continuity equation, conservation of mass (see Equation 3.1 and 3.2 (Kundu and Cohen; 2007)), are solved for the defined elements in the domain for each time step.

$$\rho \frac{Du_i}{Dt} = -\frac{\partial p}{\partial x_i} + \rho g_i + \frac{\partial}{\partial x_j} \left[2\mu e_{ij} - \frac{2}{3}\mu(\nabla \cdot u_i)\delta_{ij} \right] \quad (3.1)$$

$$\frac{\partial \rho}{\partial t} + \nabla \cdot (\rho u) = 0 \quad (3.2)$$

u_i is the velocity, μ is the dynamic viscosity, e_{ij} is the strain rate tensor and δ_{ij} is the Kronecker delta function.

For an incompressible fluid, like water can be considered as in most cases, the conservation of momentum of the Navier Stokes equations reduces to Equation 3.3 (Kundu and Cohen; 2007).

$$\rho \frac{Du_i}{Dt} = -\frac{\partial p}{\partial x_i} + \rho g_i + \mu \nabla^2 u_i \quad (3.3)$$

A chosen set of cases with zero viscosity have also been run in order to investigate the effect of viscosity on the forces. By defining the viscosity to be zero, $\mu = 0$, the Navier Stokes equations reduces to the Euler equation as given in Equation 3.4 (Kundu and Cohen; 2007).

$$\rho \frac{Du_i}{Dt} = -\nabla p + \rho g_i \quad (3.4)$$

3.2 Solver

OpenFOAM includes different solvers for different applications. In the preliminary project the solver `interFoam` was used, which is valid for two incompressible and isothermal fluids. The solver is based on VOF (Volume Of Fluid) phase-fraction to capture the interface between the fluid. The two fluids are air and water. The solver can be used even though air is not incompressible, because the force from the air is small compared to the force from the water. Using VOF method, fluids are specified by giving the desired elements a defined phase-fraction at the initial time step where 1 corresponds to 100 % water and 0 corresponds to 100 % air. Due to the issue of damping, described

in Chapter 2 Section 2.3, a new solver called waveFoam is used, which is a part of the toolkit waves2Foam. This solver is very similar to interFoam, but together with waves2foam it includes more features as will be covered later. The simulations have been run using a laminar turbulence model, which means that the flow behaviour is assumed to be laminar, and turbulence has not been modelled. The location of the separation points in a general boundary layer depends on the flow being laminar or turbulent, but because the investigated geometry has sharp corners, the separation points are known.

3.3 Computational Power

The simulations are partly run on a personal MacBook Pro computer via Ubuntu Linux on Virtual Box and partly on the super computer, Vilje, owned by both NTNU and the Norwegian Meteorological Institute. Vilje runs the operative system SUSE Linux Enterprise Server 11 and have 1404 nodes with 16 cores per node ([Hpc Group; 2017](#)).

3.4 Domain and Mesh Generation

The domain of the numerical wave tank and the initial mesh generation has been made using blockMesh, a built-in utility of OpenFOAM. The coordinates of the tank boundaries are defined, and origo is placed upstream at the left bottom corner. For the 2D case, the thickness of the wave tank is set to be 0.1 meters. The overall dimensions of the wave tank are based on the wave parameters and will be presented in the next chapter. 70 % of the domain is water, while the rest is air. The utility snappyHexMesh has been used in order to generate a finer mesh around geometries and in the free surface zone, such that the surface elevation is defined as accurately as possible and such that there is no artificial numerical damping. In the free surface zone, the ratio between the wave height and the element size in the vertical direction, $H/\Delta z$, should ideally be larger than 10, and the ratio of wave length to horizontal element size, $\lambda/\Delta x$, should be larger than 20. In addition, the elements should have a shape close to a quadrat. The mesh size increases outside the

free surface region. SnappyHexMesh uses the existing blockMesh domain and refines the mesh according to specified refinement levels in desired regions and around defined geometries described in separate STL-files. The STL-files contains the information about the geometry and describes the surface of an object approximated by triangles (3D Systems; 2017).

In addition, the domain boundaries must be defined, and there exist a variety of possible boundary conditions that need to be chosen based on the problem and relevant theory. The boundaries of relevance in this thesis is the bottom of the wave tank, inlet and outlet wall, the sides of the wave tank, the cylinder boundaries and the boundary defining the vertical end of the wave tank.

3.5 Wave Making

During the first phase of this study the waves were generated in a similar way as in the preliminary project work. Because the results from the project were compared to experimental results, the waves were made using a numerical wavemaker based on first-order wavemaker theory. The wavemaker was made by imposing a special boundary condition at the upstream (left) wall, so that the wall acted as a wavemaker. The wave motion induced by a wavemaker can be determined well from linear wave theory (Dean and Dalrymple; 1991). The waves are generated by forced oscillation of the flap, or the upstream wall boundary. The flap type wavemaker is analogue with a vertical wall being able to rotate about a point. The wavemaker concept is described in figure 3.1. The wavemaker has a horizontal displacement and a surface respectively described by the following equations (Dean and Dalrymple; 1991).

$$x = S(z) \sin \omega t \quad (3.5)$$

$S(z)$ is the wavemaker stroke. The ratio of wave height to stroke, $\frac{H}{S}$, satisfying the Laplace equation and the boundary conditions, is described by the following equation for a flap type wavemaker.

$$\frac{H}{S(0)} = 4 \left(\frac{\sinh kh}{kh} \right) \frac{kh \sinh kh - \cosh kh + 1}{\sinh 2kh + 2kh} \quad (3.6)$$

k is the wave number for the progressive wave, h is the depth and $z = 0$ corresponds to the calm water level. The resulting wave elevation can be described by the following equation.

$$\eta = \frac{H}{S(0)} \cos(kx - \omega t) \quad (3.7)$$

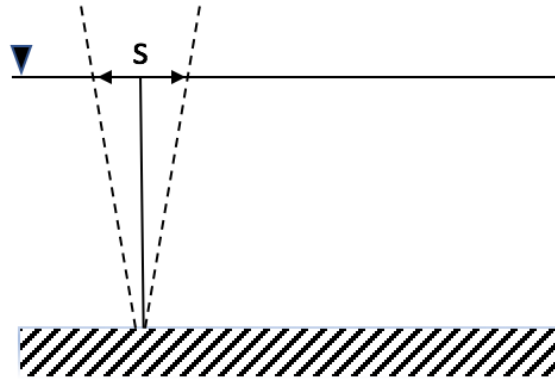


Figure 3.1: *Flap-type wavemaker*

The goal has been to create the numerical wave tank as identical as a real wave tank environment as possible. A flap type wave maker was initially of interest, because deep water is considered and the desired wave particle orbits are circular and not elliptical, as is the case for shallow water. This phenomenon is shown in figure 3.2 taken from [Pettersen \(2007\)](#). The flap type wave maker is more efficient in resembling deep-water wave conditions ([Dean and Dalrymple; 1991](#)).

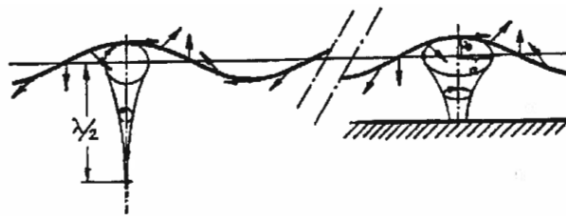


Figure 3.2: *Wave particle orbits* ([Pettersen; 2007](#))

However, a new method of generating the waves has been implemented through the work with this thesis. The method is a part of the toolkit waves2Foam. waves2Foam ([Jacobsen; 2011](#)) is a library made in order to handle the free surface wave generation and damping better than the basic openFOAM library. waves2Foam is built for the exact purpose of surface waves and is based on VOF (Volume of Fluid) method, which is also the base of the interFoam solver used in the project work. The library contains different wave theories, which means that different kinds of waves

easily can be made without having to modify the wave maker. Stokes first-order wave theory has been used, which generates linear waves described by the same equations as for the wavemaker generated waves, Equation 3.7.

The wave length, period and height have been decided upon by looking at the wave conditions used in the literature and former studies regarding wave drift forces on semi-submersibles.

In order to trace the surface elevation and analyse the waves, the actual free surface is measured at different locations in the wave tank during the simulations. This is done by saving the vertical position of the elements that have the volume fraction closest to the value of 0.5, which indicate that the element is in a fluid state between air and water. It is valuable to trace the wave elevation at different locations in the wave tank in order to investigate how the waves are propagating both with time and in space.

3.6 Damping

A very long wave tank was used in the preliminary analysis done during the project work in order to generate a long enough steady state force time series without disturbance from the reflecting waves. The project report emphasizes the need of a damping area for further analysis of the problem in order to limit the number of elements that comes with a large domain. With a damping area present, the domain can be made much smaller while preventing reflection of waves from the boundaries and avoid interference with the force results.

There exist several methods of wave damping, for instance stretching the mesh in the end of the wave tank, create a beach and construct a sponge layer to absorb the energy. The simplest and most straight forward method is stretching the mesh. This has been tested, but because the waves investigated in this project are long, the method of stretching the mesh is not efficient. The method requires a smooth increase of the element size in order to avoid that the elements act as walls and reflect the waves. This requires a very long domain for the waves to be satisfactory damped. Due to the complexity of damping the waves properly, the toolkit `waves2Foam` has been introduced. It is important to note that the goal with this master project is to investigate the wave drift forces on a

slender body and not to make a perfect wave tank. Therefore, more time has been spent on trying to make a simple working wave tank that is good enough, rather than developing and validating different methods to make the perfect wave tank.

waves2Foam defines specific areas for damping and wave generation, called relaxation zones. Different geometries for the damping area are available, which makes it convenient to use for a variety of cases. As a default, damping areas at the inlet and at the outlet must be defined.

The damping zone in the waves2Foam toolkit is based on certain relaxation weights, w , included in the equations for volume fraction and velocity. These equations are updated and solved every time step in the relaxation zones. The equations are given below, Equation 3.8 and 3.9

$$u = (1 - w)u_{target} + wu_{computed} \quad (3.8)$$

$$\alpha = (1 - w)\alpha_{target} + w\alpha_{computed} \quad (3.9)$$

α_{target} and u_{target} are the volume fraction and velocity at the outlet boundary and $\alpha_{computed}$ and $u_{computed}$ are the values calculated from the Navier Stokes Equations. There are different ways of calculating the relaxation weight, w . Anyhow, the weight is defined to be 1 at the start of the outlet damping area and decrease to zero at the end of the outlet damping area or at the outlet wall. For the inlet, the opposite is defined, the weight is 1 at the end of the inlet damping area and zero at the inlet boundary, corresponding to the beginning of the inlet damping area. The default way of defining the weight is exponential with an exponent, m , of 3.5. The equation is given below, Equation 3.10.

$$w = 1 - \frac{\exp(\sigma^m) - 1}{\exp(1) - 1} \quad (3.10)$$

3.7 Time Variables

There are several time variables that need to be defined in order for the simulation to run. An appropriate simulation time must be chosen. The simulation time is dependent on how much time it takes before the simulation reaches steady state, and how long the force time series need to be for the analysis and the Fourier transformation to become accurate enough.

Another variable to be decided upon is the time step. The time step is chosen based on the wave period, the element size and the Courant number. The Courant number is defined as $Co = \frac{\delta t |U|}{\delta x}$, which is the time step multiplied by the velocity through the cell divided by the element size in the direction of the velocity. According to [CFD Direct \(2016\)](#), temporal accuracy and numerical stability is obtained when the Courant number is less than one. Therefore, the final time step is chosen in accordance with the element size in order to assure a Courant number smaller than one.

The last time variable, `writeInterval`, defines how often the results are going to be saved. The force time series and the wave elevation time series are saved at each time step and are independent of the `writeInterval` variable. Therefore, the saved results are only used to visualize and investigate the flow characteristics in `paraView`, and there is no need to save the results too often.

3.8 Post-Processing

`paraView` has been used to get a first impression of the results, visualise the waves on the body and to check the mesh generation. A picture of the user interface of `paraView` is shown in [Figure 3.3](#). Matlab is used for further analysis, because it is faster and more convenient when interpreting the results.

In order to study the wave generation and find the actual wave height and period, the wave elevation time series are transformed into the frequency domain through the FFT (Fast Fourier Transformation) function in Matlab and the wave amplitudes and frequencies are collected. This method is also used for the force time series in order to investigate the frequency of the force peaks.

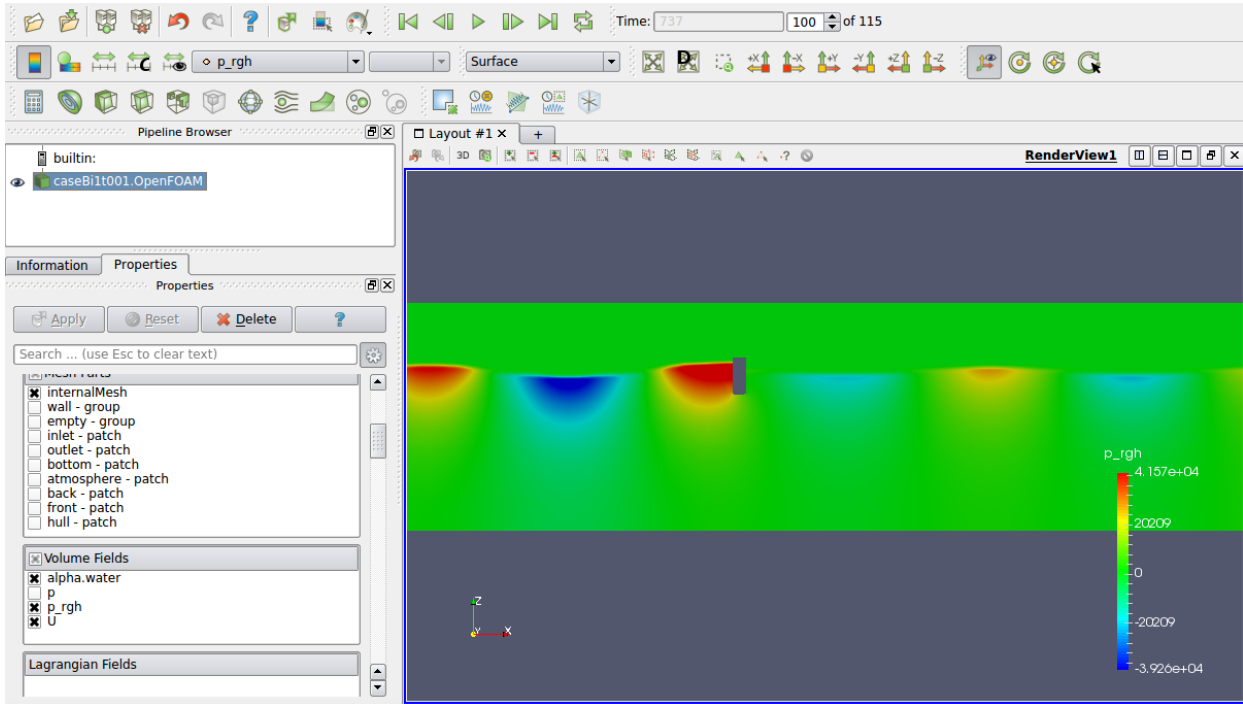


Figure 3.3: User interface of paraView

In order to further evaluate and interpret the force results from the time domain simulations, the time series are transformed into Fourier series. A force time series can be described by a Fourier series as shown below

$$F(t) = \frac{a_0}{2} + \sum_{n=1}^{\infty} (a_n \cos(n\omega t) + b_n \sin(n\omega t)) \quad (3.11)$$

$$a_0 = \frac{1}{N \cdot T} \int_{t_1}^{t_1 + N \cdot T} f(t) dt$$

$$a_n = \frac{1}{N \cdot T} \int_{t_1}^{t_1 + N \cdot T} f(t) \sin(n\omega t) dt$$

$$b_n = \frac{1}{N \cdot T} \int_{t_1}^{t_1 + N \cdot T} f(t) \cos(n\omega t) dt$$

The first coefficient, a_0 , corresponds to the mean force, a_n and b_n are the amplitude of the oscillating, harmonic force, n defines up to which order of harmonics the analysis is to be performed, T is the period, N is the number of periods and decides the size of the time series interval used in the Fourier analysis and t_1 is the start of the interval. In order to perform a good and accurate Fourier Transformation, the interval of the time series used in the analysis has to be where steady-state is obtained. The interval should also be chosen such that it includes a complete number of wave

periods. The Fourier transformations of the force time series in this project have been performed in Matlab by use of a script made by one of the co-supervisors of this project, Finn-Christian W. Hanssen. The script outputs the mean wave drift force in x and z-direction, mean moment about the y-axis, the harmonic forces in x and z-direction up to the chosen order, the moment in y-direction up to the chosen order and the slow drift force in x and z direction and moment about y.

The mean force coefficients in x and z direction are made dimensionless by $\rho g L A^2$ and the moment by $\rho g L B A^2$. The slow drift force in x and z-direction are made dimensionless by $\rho g L A^2$ and the slow drift moment about y by $\rho g B L A^2$. The first to third-order coefficients in x direction are made dimensionless by $\rho g L d A$, in z direction by $\rho g L B A$ and the moment about y by $\rho g L B d A$. L [m] is the length of the column in y-direction and is the same as the thickness of the wave tank in 2D, A [m] is the wave amplitude, B [m] is the breadth of the column in x-direction and d [m] is the draft of the column.

Chapter 4

Modelling and Simulation

This chapter is discussing and summarising the choices made during the pre-processing, simulation and post processing of the cases. All the case files have been generated through a MATLAB script based on a script made by one of the co-supervisors, Babak Ommani. This has made the change of parameters simple and clean. The chosen parameters are defined in or calculated by the script which further generates the OpenFOAM case files in the correct folder and directories. The MATLAB script can be found in Appendix C.

4.1 Domain Geometry

The chosen geometry of the wave tank can be seen in figure 4.1. The wave tank length, L , is made 11 times the incident wave length, λ . To satisfy the deep water condition the depth has been set to 0.5λ . As stated in Chapter 3, the water covers 70 % of the wave tank. The applied boundary conditions are presented and explained in Appendix A.2. As in the preliminary project, a flap-type wavemaker is first placed at the left, upstream boundary to generate waves. The damping area is placed at the downstream, right, end of the wave tank and can be seen in figure 4.1 by the striped region.

In order to trace the free surface as accurately as possible and due to the recommendations presented in the report from the preliminary project, the free surface is further refined. The initial blockMesh

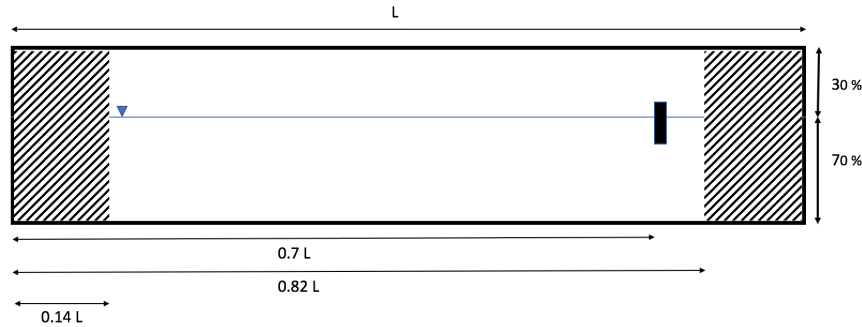


Figure 4.1: *Domain geometry*

grid has 20 elements per wave length and a refinement level of 3 is defined in the free surface zone and close to the body using the snappyHexMesh utility. This causes the smallest element size to be approximately 1.4 m, which means that the ideal ratio of 10 elements per wave height is not fulfilled, as can be seen from the wave parameters presented in Section 4.3. Although it would be desirable to have a smaller element size in the vertical direction, the choice of element size is a matter of available time and necessary accuracy. However, in the horizontal direction, the amount of elements more than fulfil the recommended amount discussed in Chapter 3. Because the simulation variables are connected, a smaller element size requires a smaller time step, which also increase the simulation time considerably. Figure 4.2 and 4.3 show the meshed wave tank domain as presented in paraView.

Due to the simplicity and convenience of the method, another way of generating waves using waves2Foam has been implemented and is used to create all the results to be presented in Chapter 5. The new cases using waves2Foam also contains a damping area at the inlet as shown in figure 4.1. This was not present in the domain for the cases generating waves with the wavemaker.

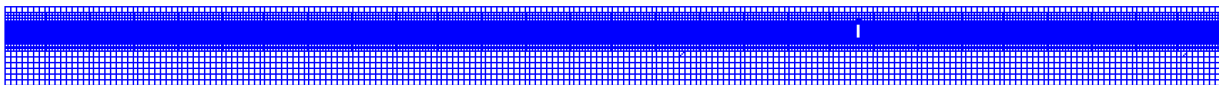


Figure 4.2: *Domain with mesh*

The locations of the probes for measuring the actual wave elevation during the simulations are shown in figure 4.4. Because the probes are placed at different locations along the wave tank, it is possible to trace the wave propagation and validate that the generated waves are as expected. The

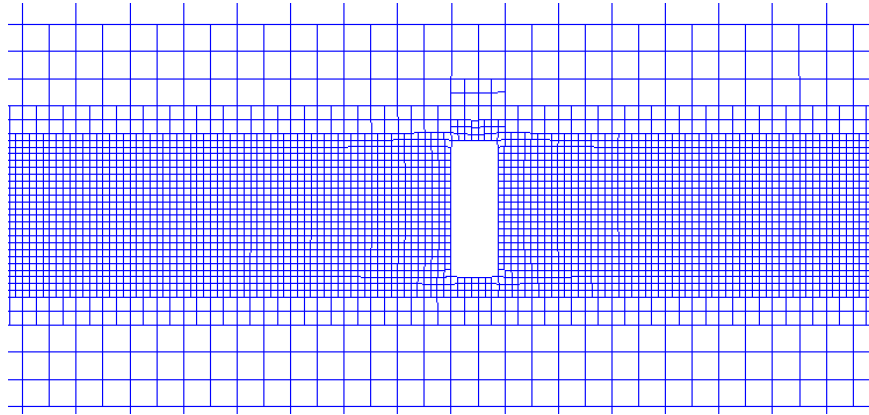


Figure 4.3: Close-up of domain with mesh

wave elevation results presented in Chapter 5 are collected from the probe located one cylinder diameter in front of the cylinder, the rest of the probes are only used for validation.

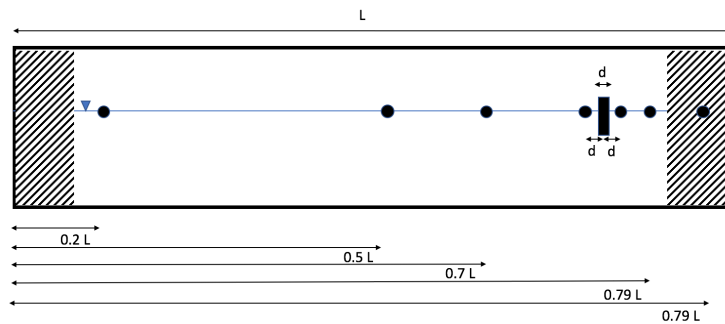


Figure 4.4: Location of probes

The full domain with the mesh and the volume fraction is shown in figure 4.5. Red corresponds to water and blue corresponds to air.

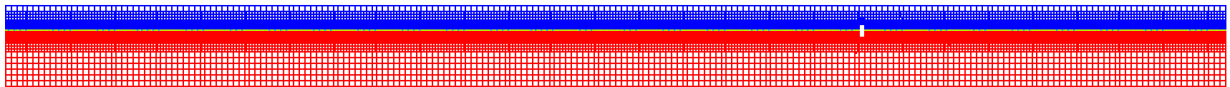


Figure 4.5: Domain with mesh and volume fraction

4.2 Body Geometry

The chosen body geometry is shown in figure 4.6. Due to the waves being long and that slender bodies will be the main focus in this thesis, only one body geometry is studied. It is assumed

that changing the geometry within the slender body condition in 2D will not affect the drift force considerably. In the 2D case, vortex shedding and separation will only occur from the bottom corners of the 2D cylinder. The chosen geometry is inspired by and chosen based on relevant geometry in literature.

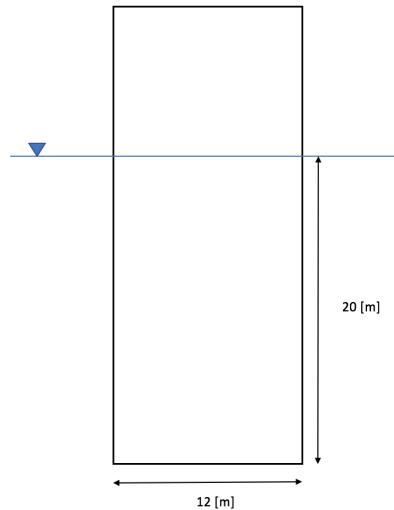


Figure 4.6: *Body geometry*

4.3 Wave Parameters

Both regular and bi-chromatic waves have been simulated. The wave parameters are presented below.

4.3.1 Regular Waves

First a set of regular wave runs with varying wave heights has been performed. The wave parameters of these runs are summarised in table 4.1. The wave period is long and is chosen based on literature and previous studies of the wave drift forces ([Berthelsen et al. \(2009\)](#), [Stansberg et al. \(1998\)](#), [Stansberg and Nestegård \(2014\)](#)). Results from these studies show that the viscous contribution to the wave drift forces increases for longer waves and larger wave heights. Even though it is interesting to investigate and study waves with a high steepness, the chosen cases have smaller

steepness than $1/30$, because it can be difficult to model steeper waves in openFoam. In order to accurately model steep waves, the elements must be even smaller which requires a further reduction of the time step and the computational time will increase quickly.

Table 4.1: Wave parameters for regular wave runs with $T = 12$ s

Run	Wave length [m]	Wave height [m]	Steepness $H/\lambda[-]$	$\lambda/D[m]$
1	224.8	4.5	1/50	18.7
2	224.8	6	1/37	18.7
3	224.8	7.5	1/30	18.7

The regular wave cases listed in Table 4.1 have been run for waves both generated with the wave maker created in the project phase and with the waves2Foam toolkit in order to test if the toolkit could be used for the remaining of the simulations. These simulations were run with a time step of 0.05 s. The resulting wave elevation from these simulations are shown in Table 4.2 and 4.3. The force time series are shown in Figure 4.7 and 4.8.

Table 4.2: Result from wave maker generated waves of $T=12$ s

	Run 1	Run 2	Run 3
Actual wave amplitude [m]	1.899	2.521	3.035

Table 4.3: Result from waves2Foam generated waves of $T=12$ s

	Run 1	Run 2	Run 3
Actual wave amplitude [m]	1.950	2.595	3.067

Looking at the wave elevation results, it is clear that wave generation using waves2Foam creates a wave with an amplitude somewhat closer to the theoretical value. Regarding the force time series, the figures show similar results for the steady state region. Because the plots show quite similar results, waves2foam has been considered valid to use for the remaining of the simulations.

4.3.2 Bi-chromatic Waves

The cases performed for bi-chromatic waves are summarised in the three tables below, Table 4.4, 4.5 and 4.6. The difference frequencies are chosen to be in the range of natural periods of

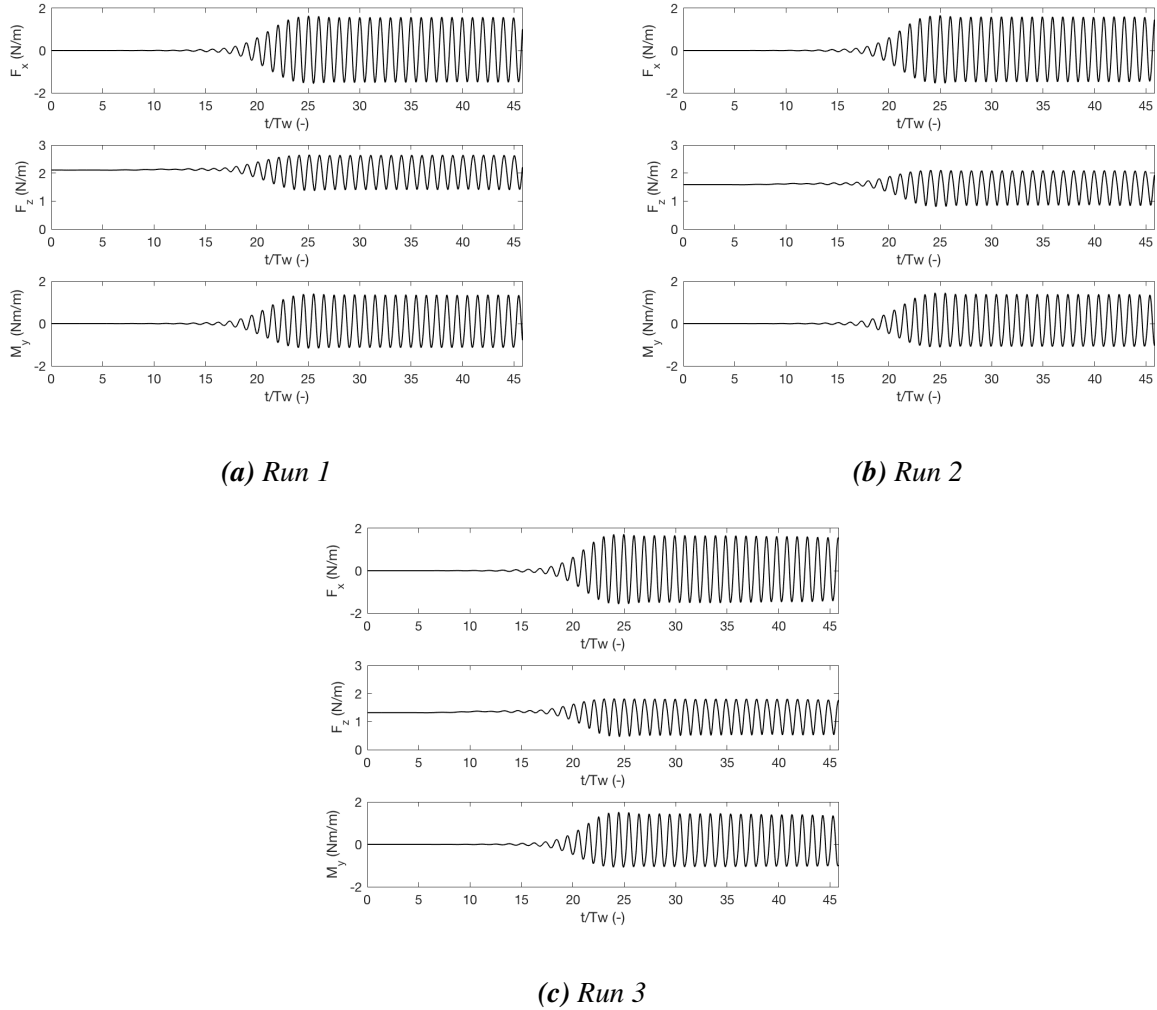


Figure 4.7: Force time series for simulation using a wavemaker

semi-submersibles covered in literature. This is of relevance because sea states containing these frequencies can be the most severe conditions regarding slow drift wave loads and excitation. Moored semi-submersibles generally have a natural period in surge of about 100 s. The two chosen difference frequencies correspond to slowly varying periods of 125.6 s and 89.8 s. Simulations are done for three different wave heights and two different difference frequencies in order to investigate how they are related to the resulting wave loads.

Table 4.4: Wave parameters for bi-chromatic wave runs with $H = 4.5$ m

Run	$\omega_1 - \omega_2$ [rad/s]	T_1 [s]	T_2 [s]	$H/\lambda_1[-]$	$H/\lambda_2[-]$	$\lambda_1/D[-]$	$\lambda_2/D[-]$
1	0.05	12	13.27	1/50	1/65	18.7	22.9
2	0.07	12	13.85	1/50	1/66	18.7	25.0

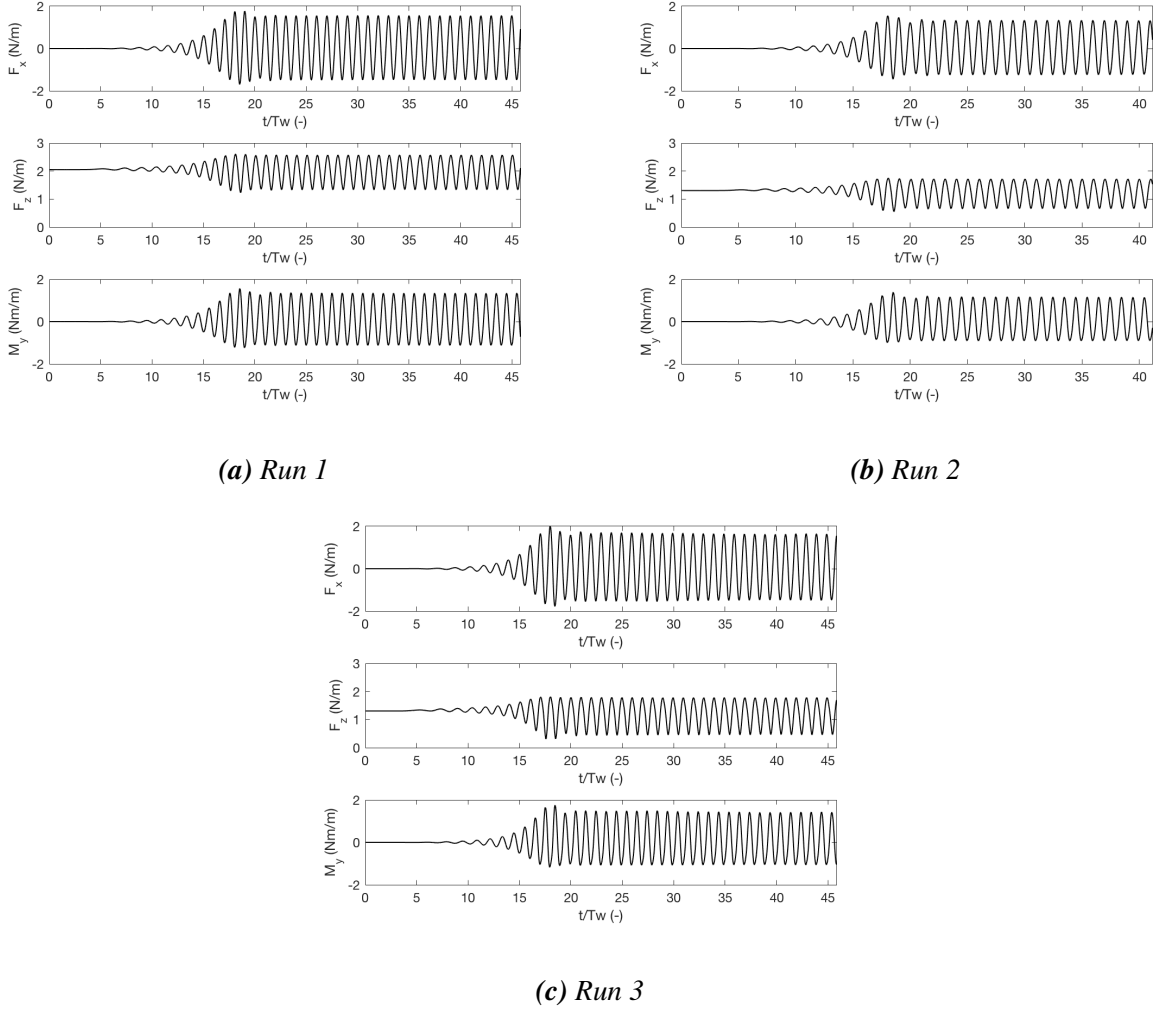


Figure 4.8: Force time series for simulation using waves2Foam

Table 4.5: Wave parameters for bi-chromatic wave runs with $H = 6\text{ m}$

Run	$\omega_1 - \omega_2$ [rad/s]	T_1 [s]	T_2 [s]	H/λ_1 [-]	H/λ_2 [-]	λ_1/D [-]	λ_2/D [-]
1	0.05	12	13.27	1/37	1/46	18.7	22.9
2	0.07	12	13.85	1/37	1/50	18.7	25.0

Table 4.6: Wave parameters for bi-chromatic wave runs with $H = 7.5\text{ m}$

Run	$\omega_1 - \omega_2$ [rad/s]	T_1 [s]	T_2 [s]	H/λ_1 [-]	H/λ_2 [-]	λ_1/D [-]	λ_2/D [-]
1	0.05	12	13.27	1/30	1/37	18.7	22.9
2	0.07	12	13.85	1/30	1/40	18.7	25.0

The cases summarised in Table 4.4 to 4.6 are also simulated without the body present in order to only investigate and analyse the wave propagation. In addition, the cases with a difference

frequency of 0.05 rad/s have been simulated with zero viscosity, $\mu = 0 \text{ kg/(m}\cdot\text{s)}$, in order to investigate the viscous contribution to the forces. The results from these simulations are solutions of the Euler equation.

Figure 4.9, 4.10 and 4.11 show details of the wave propagation for a wave height of 6 m and difference frequency of 0.05 rad/s.

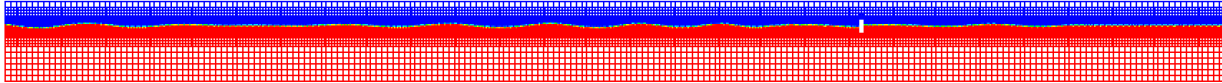


Figure 4.9: *Overview of waves in the domain with mesh*

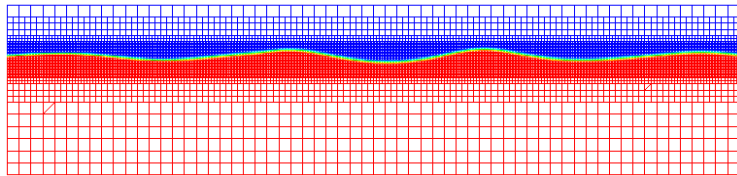


Figure 4.10: *Waves at the inlet of the domain with mesh*

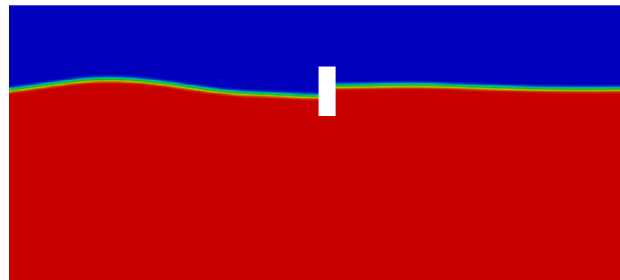


Figure 4.11: *Waves around the body*

4.4 Damping Parameters

The relaxation weight has been defined through an exponential function, as explained in Chapter 3, where the exponent, m , in Equation 3.10 has been set to 3.5. The relaxation area is rectangular and is defined at the inlet and at the outlet of the domain.

4.5 Adjusting Time Variables

The initial time step used in the simulations was 0.05 s, and was chosen based on the smallest element size, which is found in the free surface area and is approximately 1.4 m, together with the Courant Number. With a time step of 0.05 s, element size of 1.4 m and a phase velocity of approximately 18 m/s, the resulting Courant number is $Co = 0.64$ which is below 1. After studying the wave elevation results and getting access to Vilje, the time step has been reduced to 0.01 s. Comparison of the simulated and theoretical wave elevation, according to linear wave theory, for the time steps 0.05 s and 0.01 s can be seen in figure 4.12, 4.13 and 4.14, corresponding to the regular waves presented in Table 4.1 with wave height 4.5, 6 and 7.5 m.

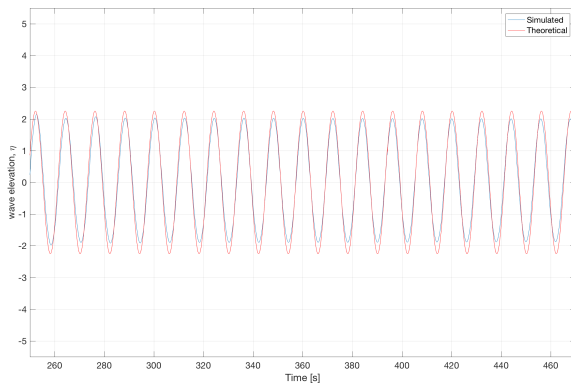
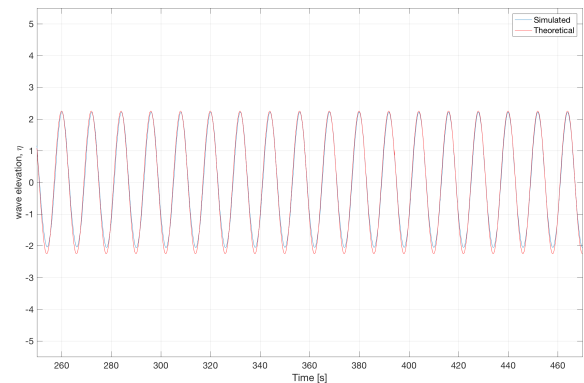
(a) $\Delta t = 0.05$ (b) $\Delta t = 0.01$

Figure 4.12: Comparison of time step and simulated and theoretical wave elevation for $H=4.5$ m

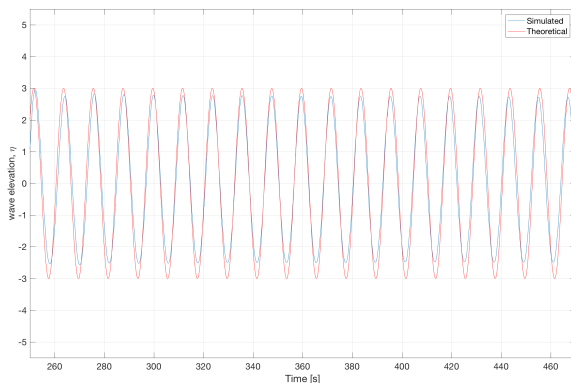
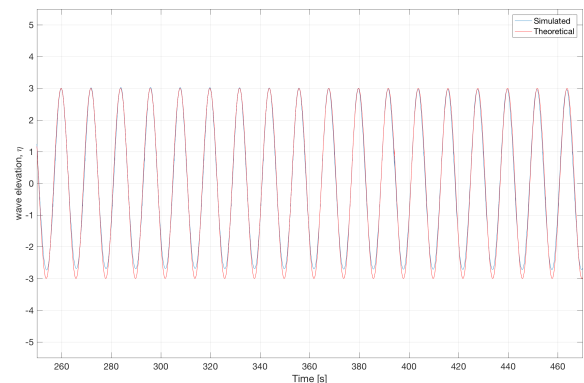
(a) $\Delta t = 0.05$ (b) $\Delta t = 0.01$

Figure 4.13: Comparison of time step and simulated and theoretical wave elevation for $H=6$ m

4.6 Post Processing

Fonseca et al. (2011) is used as an inspiration for the post-processing methods and appearance of the results presented in Chapter 5. The post processing of the results from the simulations consist of mostly Fourier analyses of the force and wave elevation time series. For the analysis to be accurate enough, the data interval used must be taken from where steady state has been reached, as discussed in Chapter 3. For the regular waves, the analysed interval from the time series consists of 10 wave periods, $10 \cdot T$ [s], and the interval starts at the time equal to 30 wave periods, $30 \cdot T$ s. For the irregular waves, 4 periods of the envelope of the waves are used in the analysis and the start of the interval depends on the difference frequency of the bi-chromatic wave. With a difference frequency of 0.05 [rad/s] the interval starts at $2.22 \cdot T$ s and for a difference frequency of 0.07 [rad/s] the interval starts at $4.05 \cdot T$ s. This is decided upon through close investigation of the time series. The nominal amplitude has been used to non-dimensionalize the forces, because it is difficult to measure the exact actual wave amplitude of the wave components at the location of the body in case of bi-chromatic waves from the simulations.

A selection of the MATLAB scripts used for post processing of the results are included in Appendix C.

The main interest throughout this thesis has been towards the mean wave drift and slow drift forces, and the presented results are reflecting this.

Chapter 5

Results from the Numerical Study

5.1 Regular Waves

This section includes a selection of both the wave elevation results and the force results from the regular wave simulations. The results will be discussed in Chapter 6.

5.1.1 Wave Elevation Results

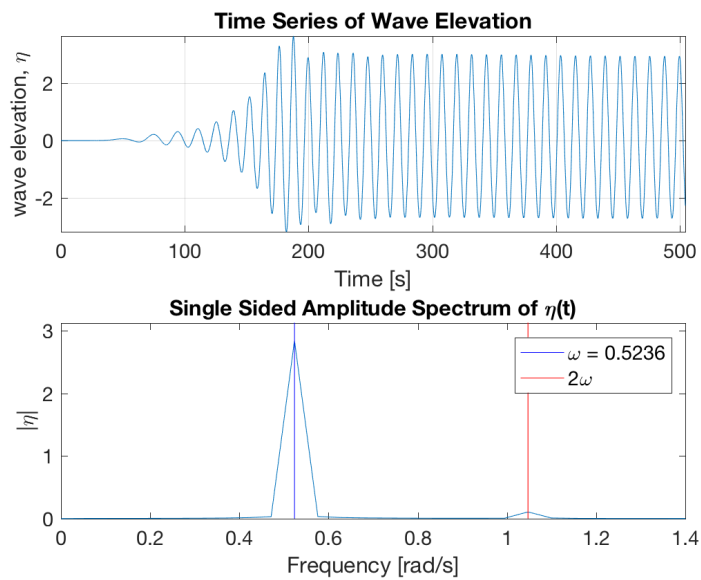


Figure 5.1: Regular waves: wave elevation analysis for $H = 6m$ and $T = 12s$

The time series of the wave elevation and the wave elevation spectrum from the regular wave simulations with wave amplitude 6 m and period 12 s are shown in figure 5.1. The vertical lines in the spectra show the most important existing frequencies in the wave condition. ω has the unit [rad/s]. The wave elevation data is measured at the probe located one cylinder diameter upstream of the body. The results from the remaining simulations can be found in Appendix B.

5.1.2 Force Results

Figure 5.2 show the force time series and Figure 5.3 show the force spectrum from the Fourier analysis of the force time series for wave height 6 m and period 12 s. The colored lines show the frequencies of the force peaks and the y-axis marks the peaks of the mean force. The results for the remaining simulations can be found in Appendix B.

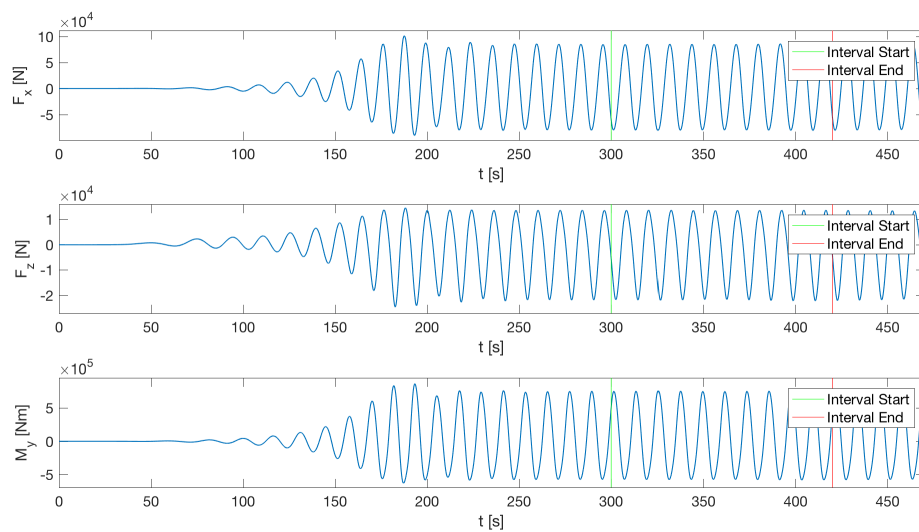


Figure 5.2: Regular waves: force time series for $H = 6m$ and $T = 12s$

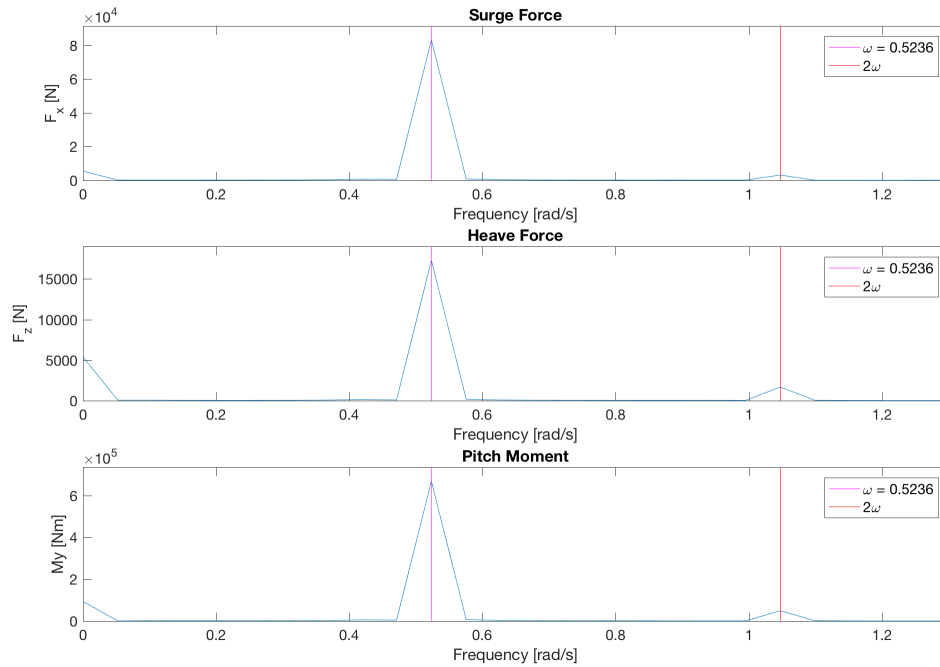


Figure 5.3: Regular waves: force spectrum for $H = 6m$ and $T = 12s$

The force coefficients from the regular wave simulations with wave period 12 s are shown in figure 5.4 to 5.7.

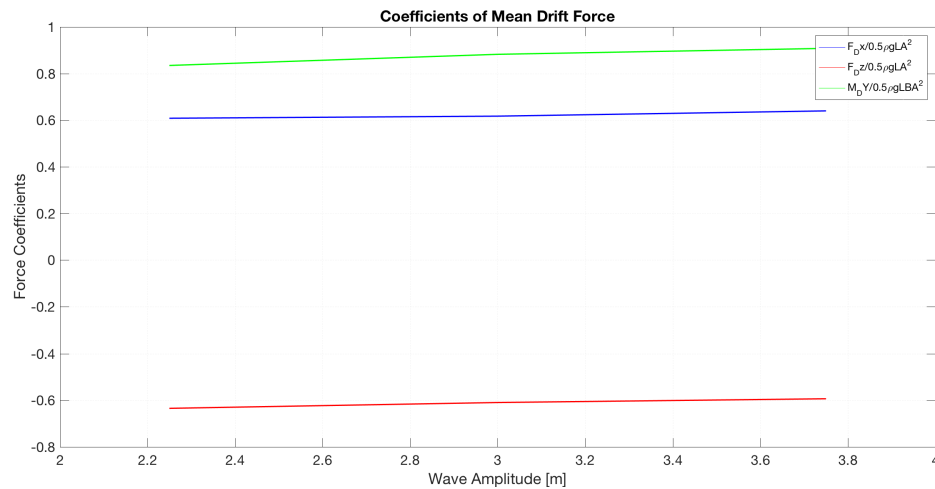


Figure 5.4: Regular waves: coefficients of mean drift force

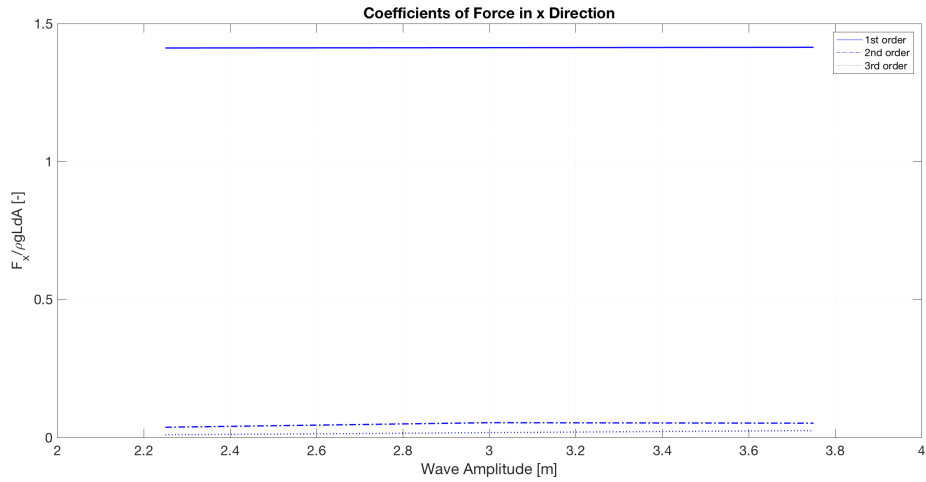


Figure 5.5: Regular waves: coefficients of force in x direction

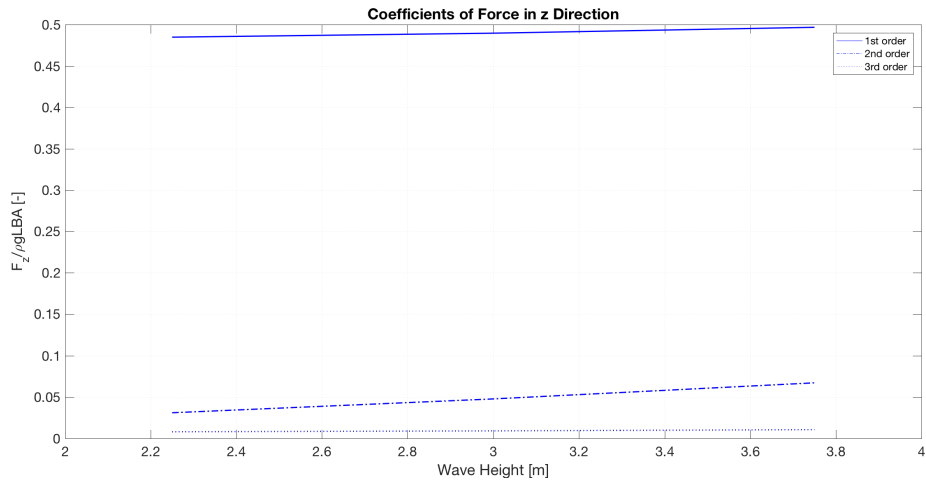


Figure 5.6: Regular waves: coefficients of force in z direction

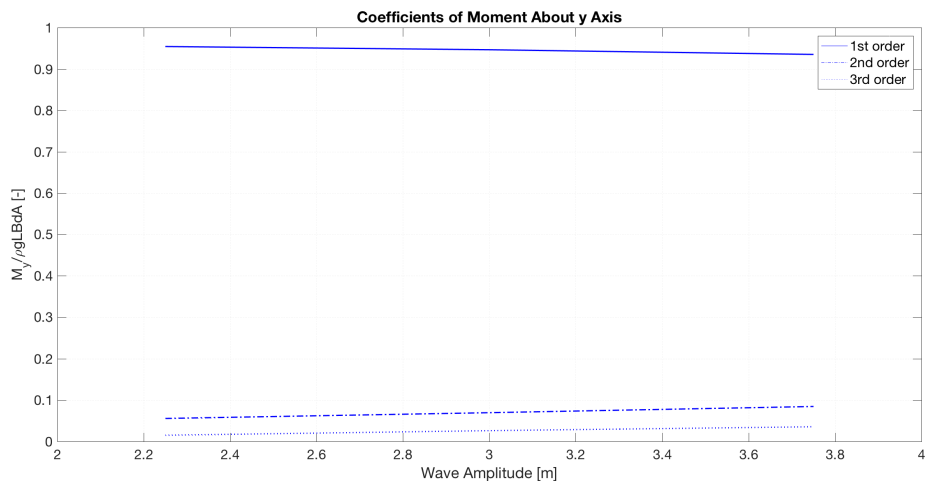


Figure 5.7: Regular waves: coefficients of moment about y axis

Table 5.2 summarises the percentage of change of the force coefficients presented in Figure 5.4 to 5.7.

Table 5.1: *Regular waves: percentage change of force coefficient from lowest to highest amplitude*

Force Direction	Mean Drift	1. Order
Force in x	5.19 %	0.17 %
Force in z	-6.48 %	2.46 %
Moment about y	8.78 %	-2.00 %

5.2 Bi-Chromatic Waves

This section includes a selection of the wave elevation and force results from the bi-chromatic wave simulations. In addition, it contains pictures and illustrations from the simulations made in paraView.

5.2.1 Results from paraView

The figures below are taken from post processing in paraView of results from the simulations of bi-chromatic waves with a difference frequency of 0.05 rad/s and where the two individual wave components have a wave height of 6 m.

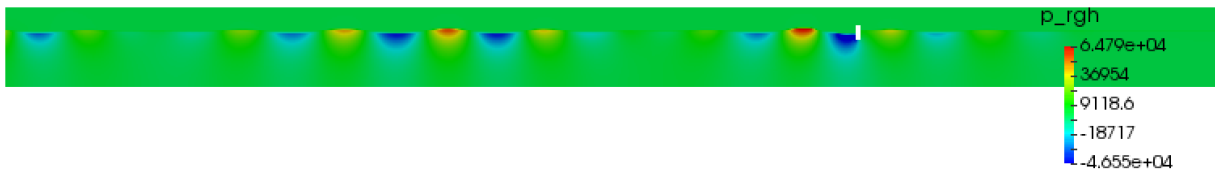


Figure 5.8: *Plot of the dynamic pressure distribution during wave propagation*

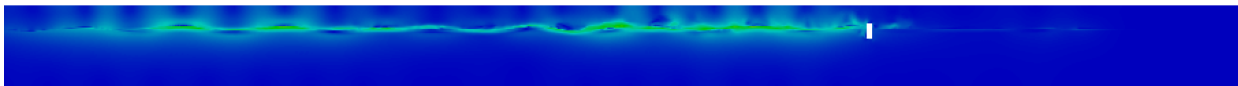


Figure 5.9: *Plot of fluid velocity during wave propagation*

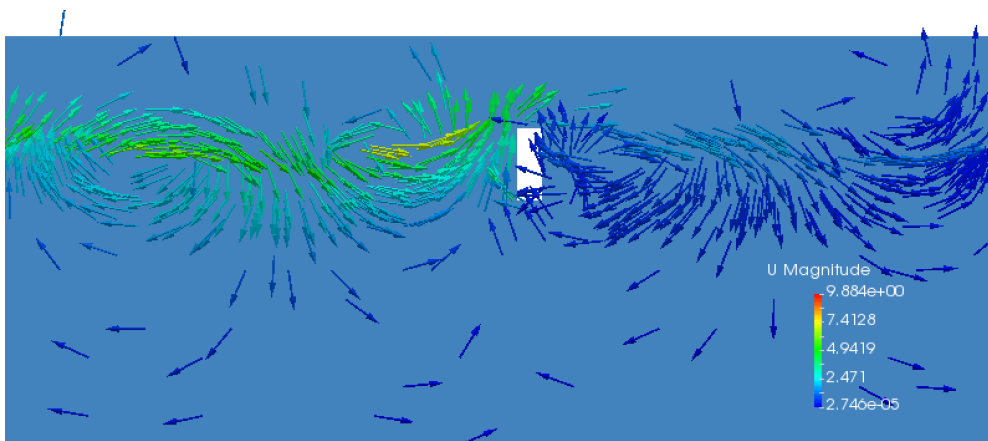


Figure 5.10: *Plot of fluid velocity vectors around the body*

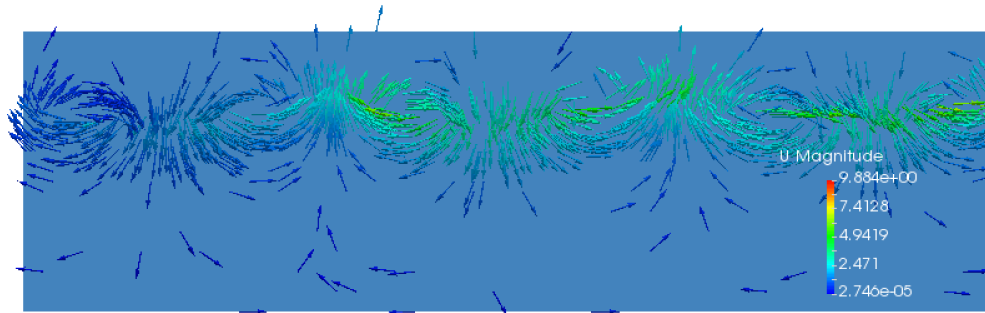


Figure 5.11: *Plot of fluid velocity vectors at the inlet*

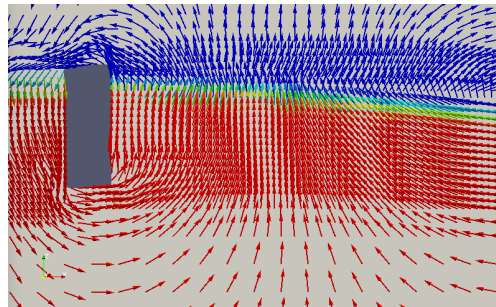


Figure 5.12: *Plot of velocity vectors around the body for $H=4.5$ m and $d\omega = 0.05$ at $t=700$ s*

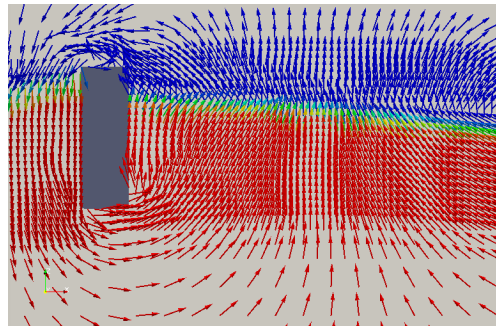


Figure 5.13: *Plot of velocity vectors around the body for $H=6$ m and $d\omega = 0.05$ at $t=700$ s*

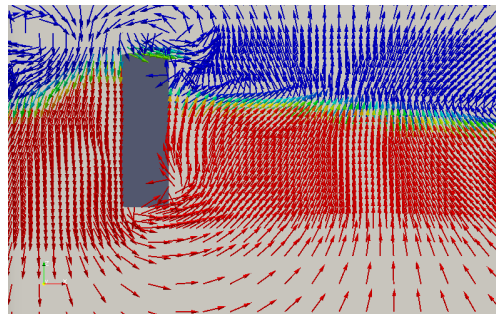


Figure 5.14: *Plot of velocity vectors around the body for $H=7.5$ m and $d\omega = 0.05$ at $t=700$ s*

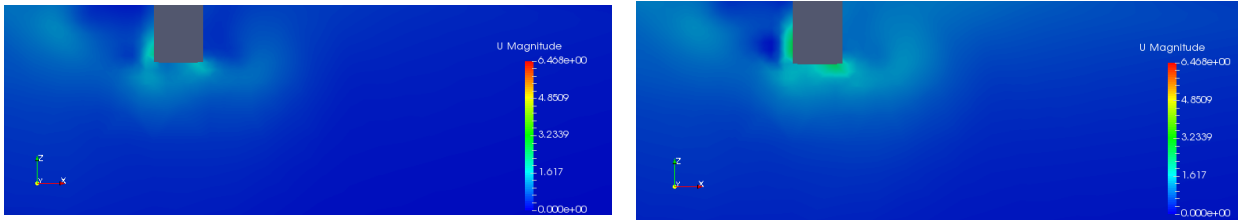


Figure 5.15: Plot of velocity around body for $H=4.5$ m and $d\omega = 0.05$ at two different time instants

5.2.2 Wave Elevation Results

Figures 5.16 to 5.19 show the time series of the wave elevation together with the spectra of the time series made from the interval marked on the plot. The wave elevation data is measured at the probe located one cylinder diameter upstream of the body. Selected results from the runs with bi-chromatic waves with a difference frequency of 0.05 rad/s and wave height 4.5, 6 and 7.5 m and difference frequency of 0.07 rad/s for wave height 6 m are included, the results for the remaining simulations can be found in Appendix B.

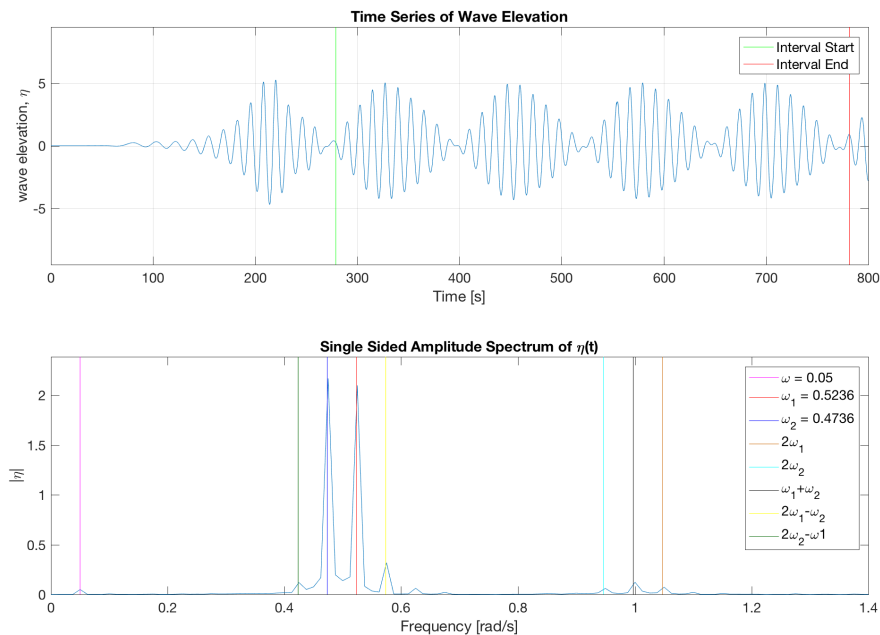


Figure 5.16: Bi-chromatic waves with $d\omega = 0.05$: wave elevation time series for $H = 4.5$ m

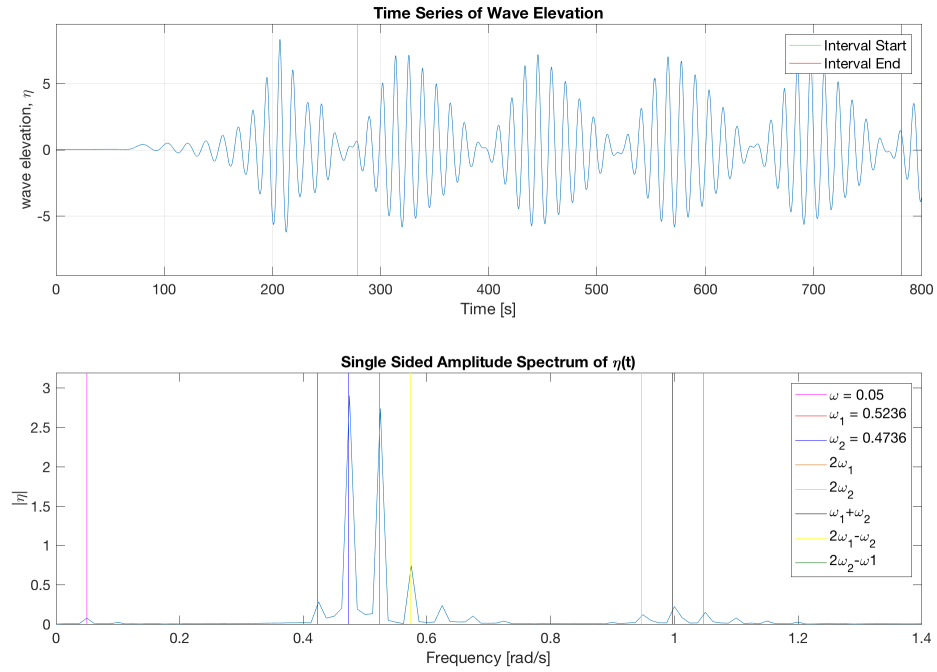


Figure 5.17: Bi-chromatic waves with $d\omega = 0.05$: wave elevation time series and spectrum for $H = 6m$

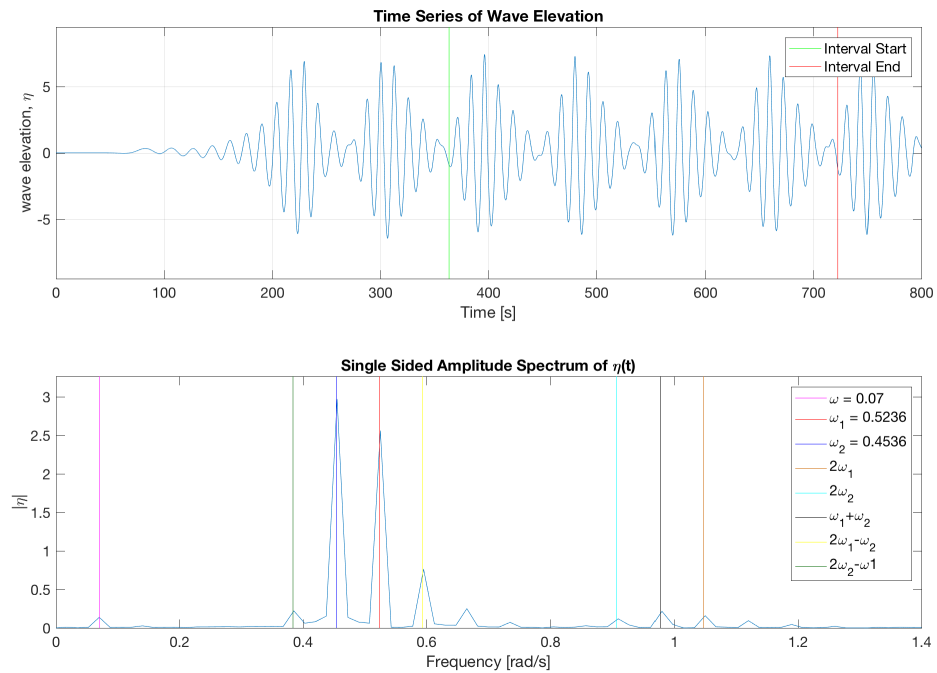


Figure 5.18: Bi-chromatic waves with $d\omega = 0.07$: wave elevation time series and spectrum for $H = 6m$

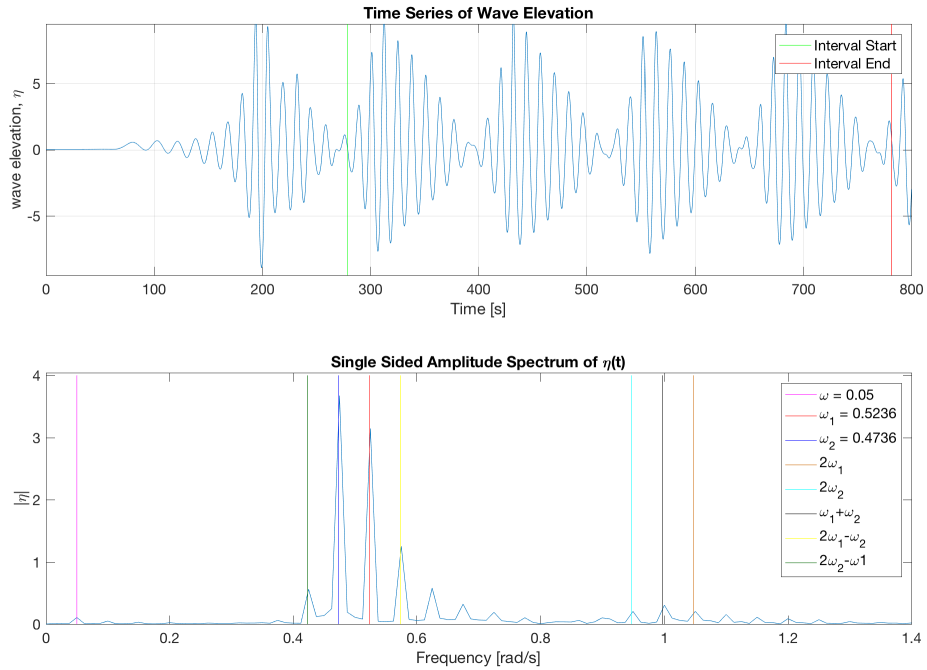


Figure 5.19: Bi-chromatic waves with $d\omega = 0.05$: wave elevation time series for $H = 7.5m$

5.2.3 Force Results

Figure 5.20 to 5.27 show the force time series and the spectra from the Fourier analysis of the force time series. The time series interval used in the Fourier analysis is marked in the plots of the time series. The colored lines in the plots of the spectra show the frequencies of the force peaks. The unit of ω is rad/s.

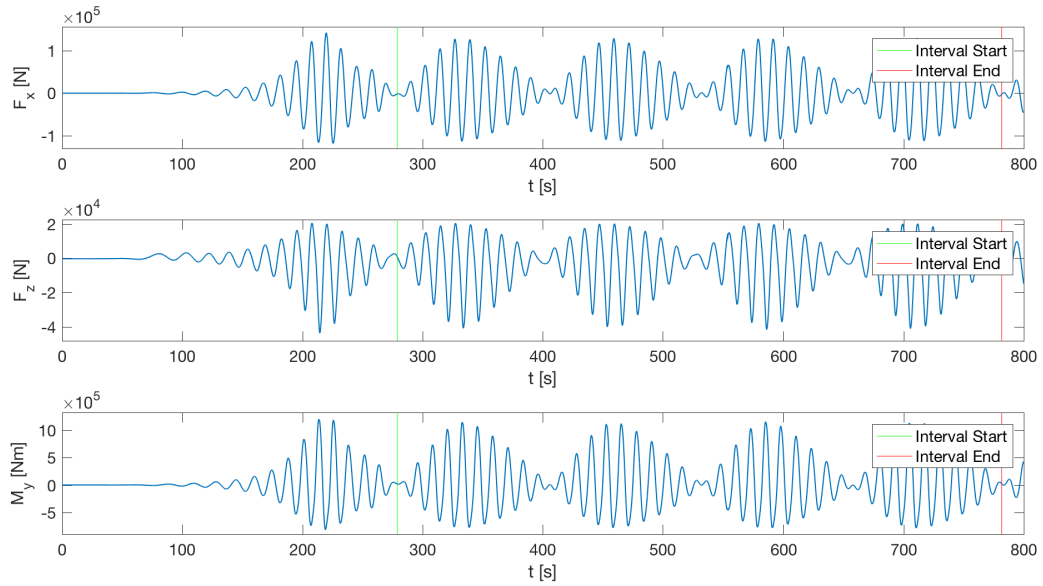


Figure 5.20: Bi-chromatic waves with $d\omega = 0.05$: force time series for $H = 4.5m$

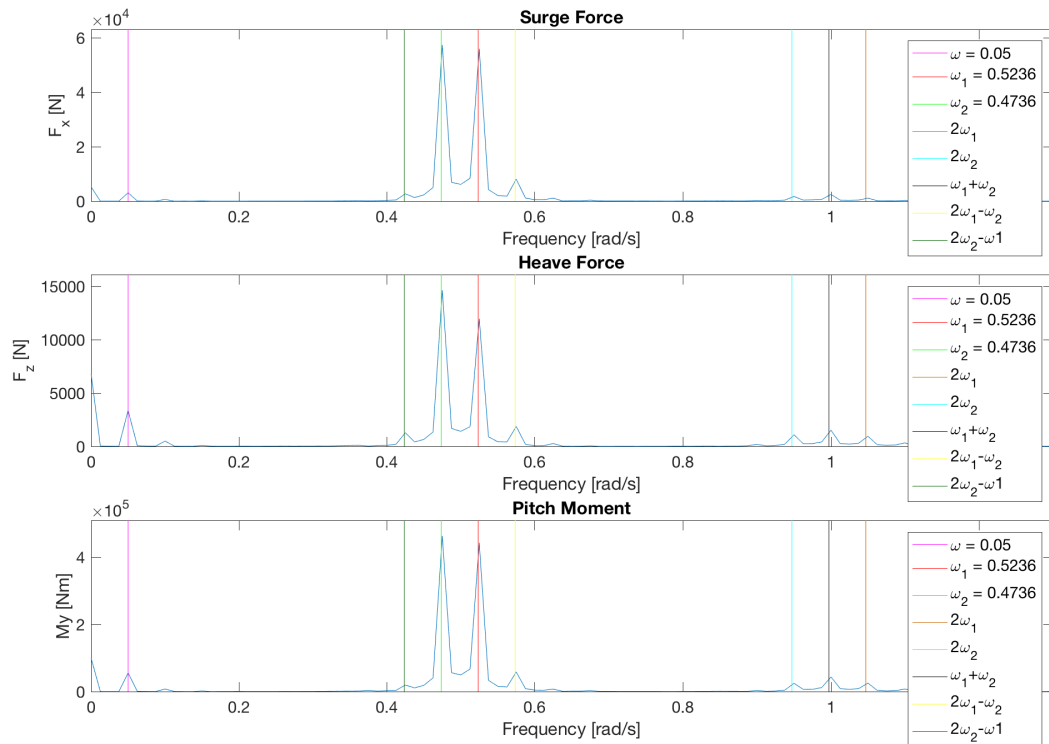


Figure 5.21: Bi-chromatic waves with $d\omega = 0.05$: force spectrum for $H = 4.5m$

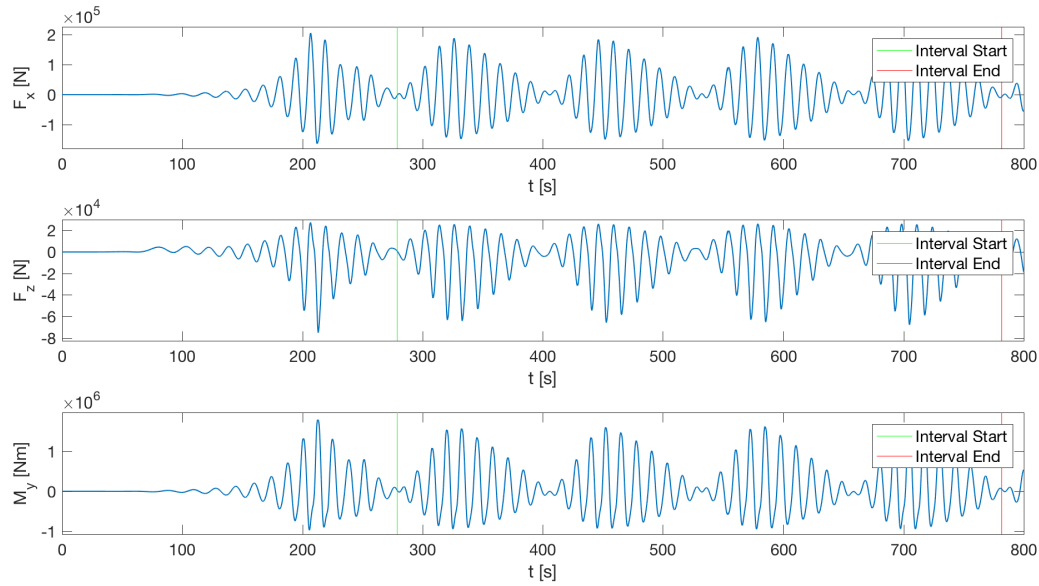


Figure 5.22: Bi-chromatic waves with $d\omega = 0.05$: force time series for $H = 6m$

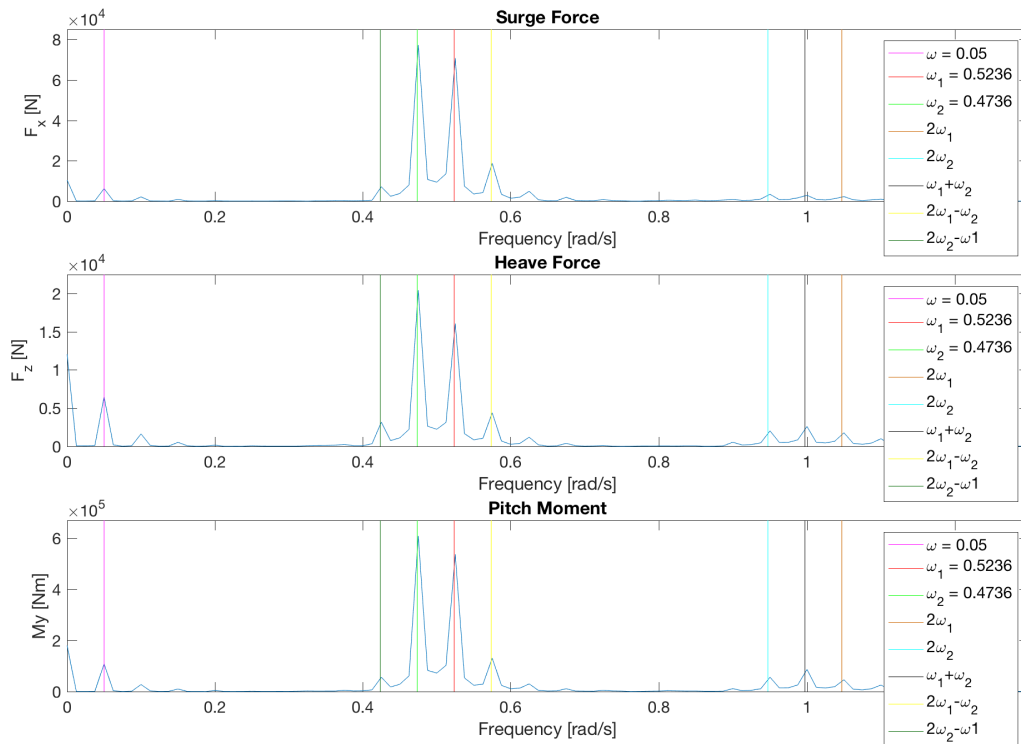


Figure 5.23: Bi-chromatic waves with $d\omega = 0.05$: force spectrum for $H = 6m$

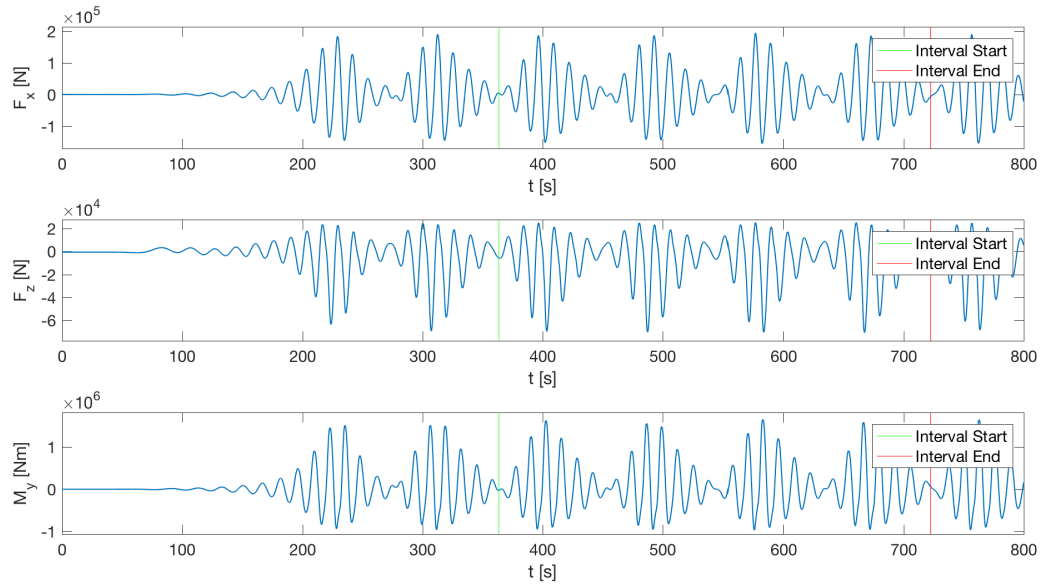


Figure 5.24: Bi-chromatic waves with $d\omega = 0.07$: force time series for $H = 6m$

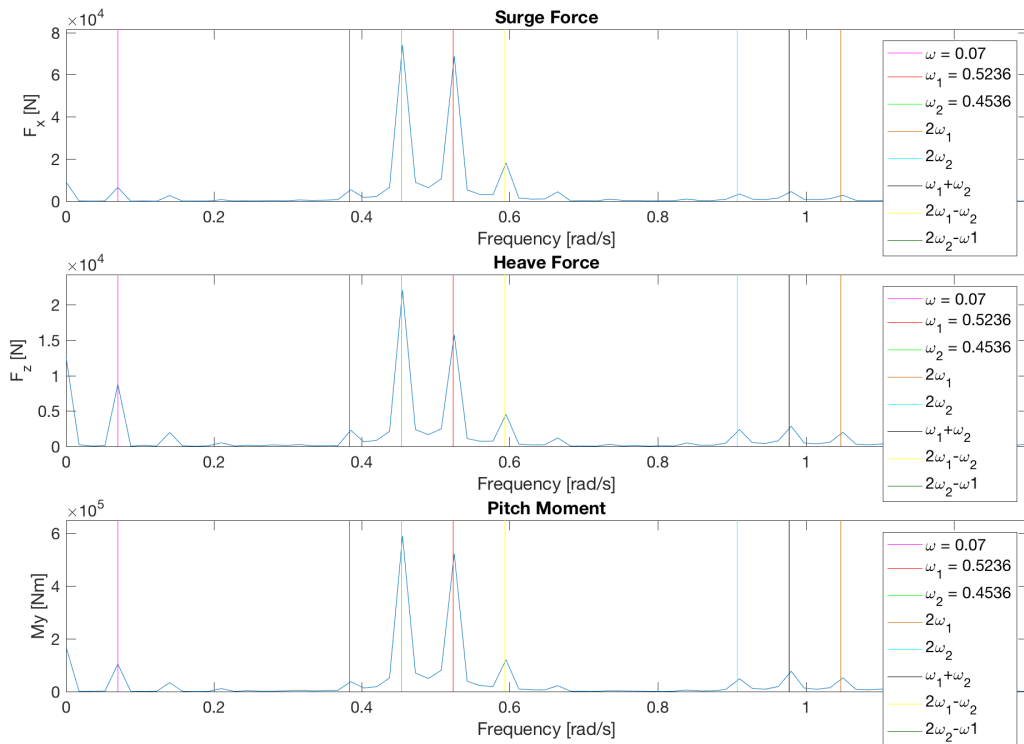


Figure 5.25: Bi-chromatic waves with $d\omega = 0.07$: force spectrum for $H = 6m$

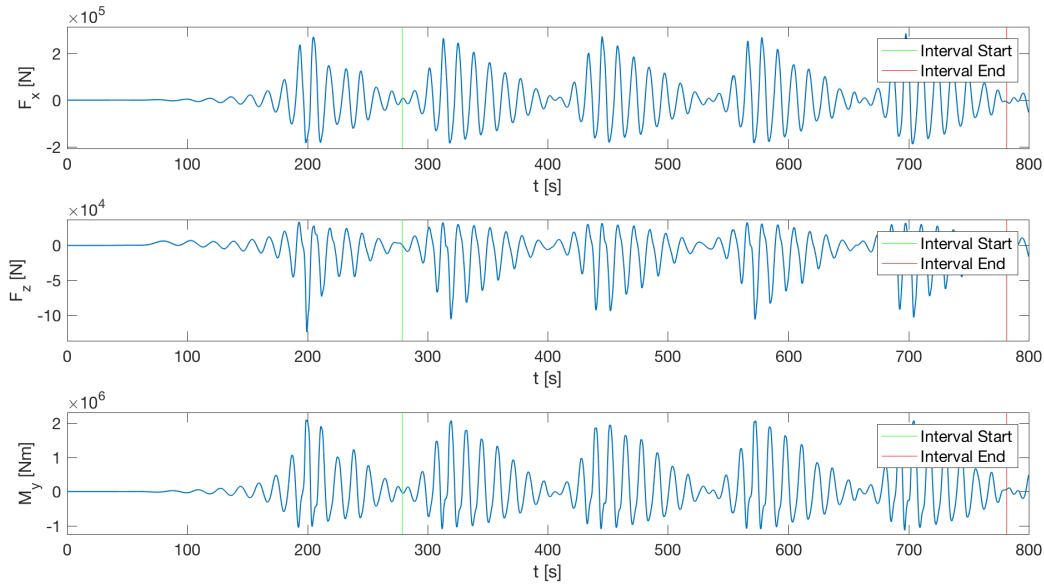


Figure 5.26: Bi-chromatic waves with $d\omega = 0.05$: force time series for $H = 7.5m$

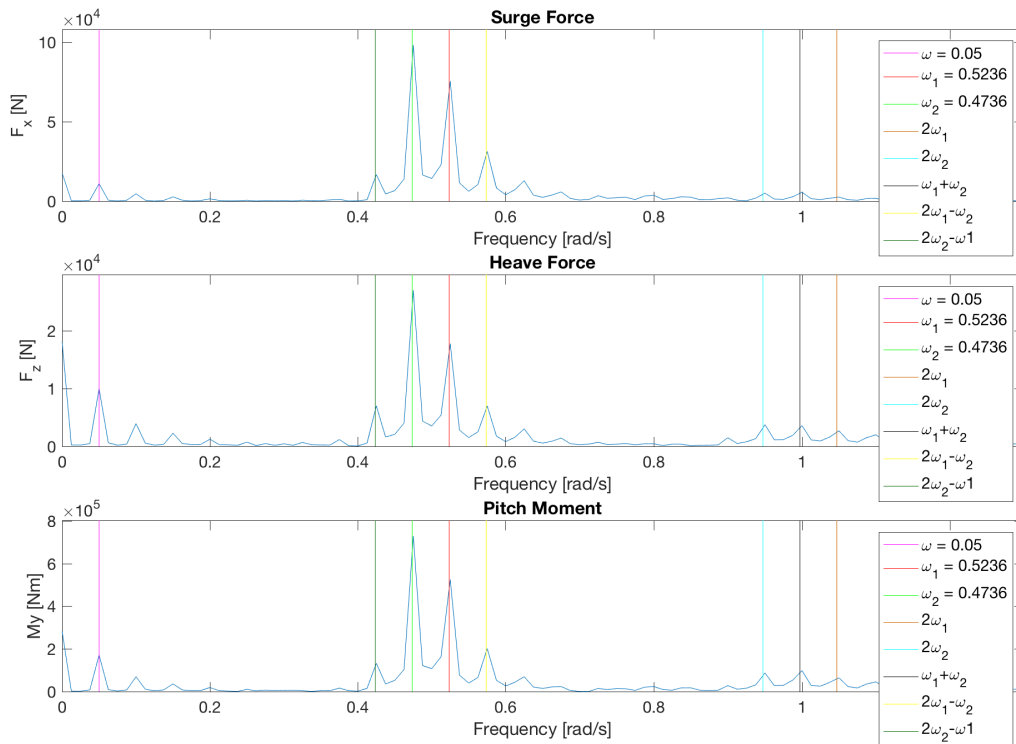


Figure 5.27: Bi-chromatic waves with $d\omega = 0.05$: force spectrum for $H = 7.5m$

The mean drift force coefficients for the runs with bi-chromatic waves are shown in figure 5.28 to 5.30. The slow drift coefficients are presented in figure 5.31 to 5.33. The first-order force coefficients related to the single wave components' frequency for the bi-chromatic runs with a difference frequency of 0.05 rad/s and 0.07 rad/s are presented in figure 5.34 and 5.35, respectively. The third order force coefficients related to the frequencies $2\omega_1 - \omega_2$ and $2\omega_2 - \omega_1$ are plotted in figure 5.36.

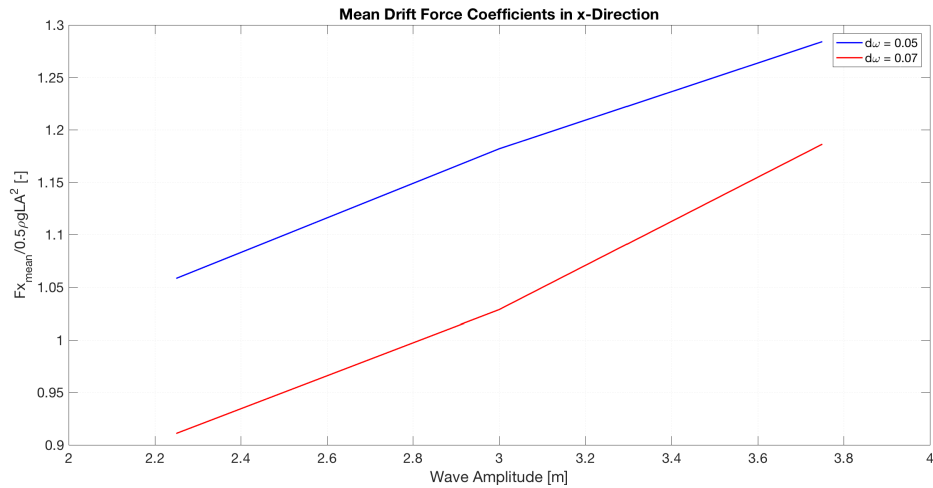


Figure 5.28: Bi-chromatic waves: coefficients of mean drift force in x direction

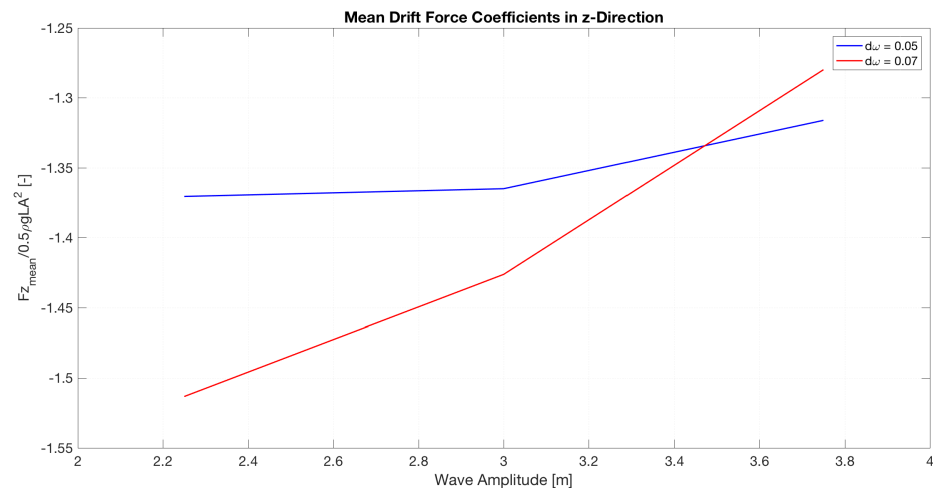


Figure 5.29: Bi-chromatic waves: coefficients of mean drift force in z direction

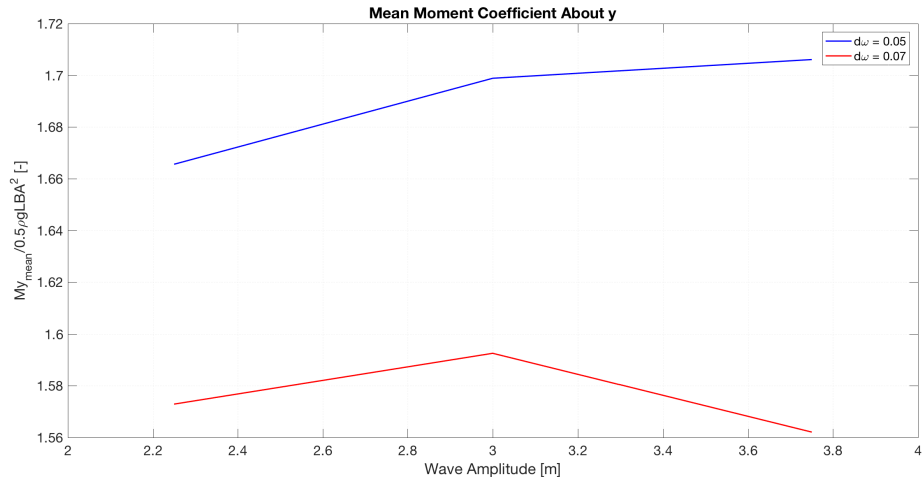


Figure 5.30: Bi-chromatic waves: coefficients of mean drift moment in y direction

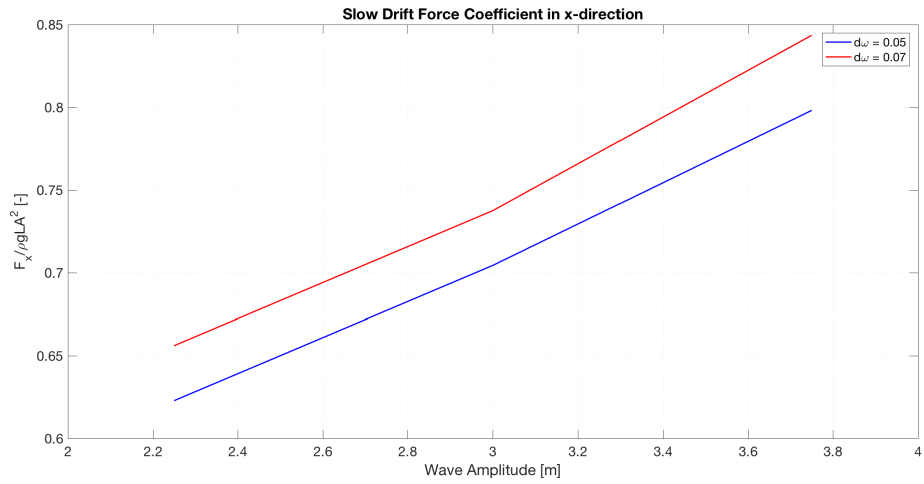


Figure 5.31: Bi-chromatic waves: slow drift force coefficient in x direction

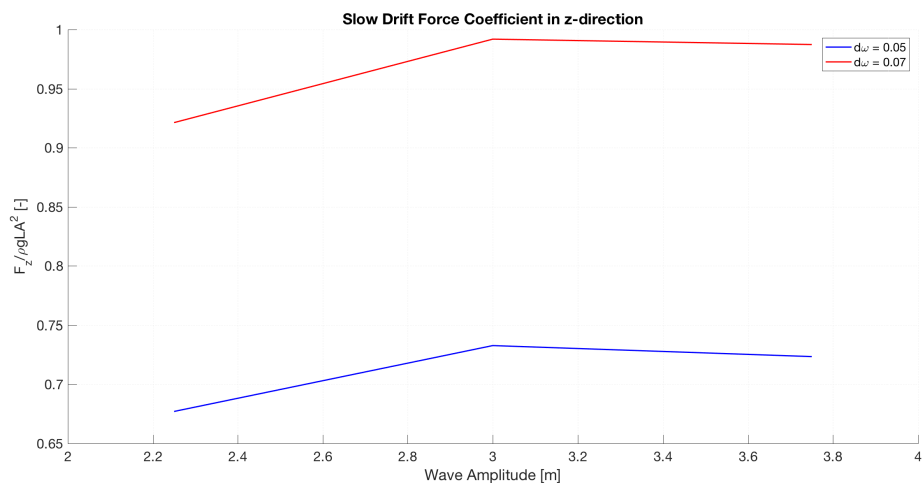


Figure 5.32: Bi-chromatic waves: slow drift force coefficient in z direction

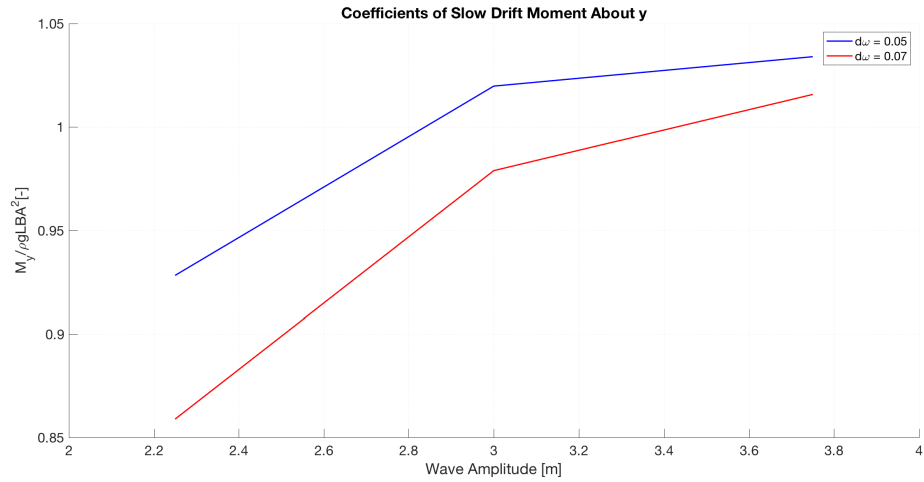


Figure 5.33: Bi-chromatic waves: slow drift moment coefficient about y

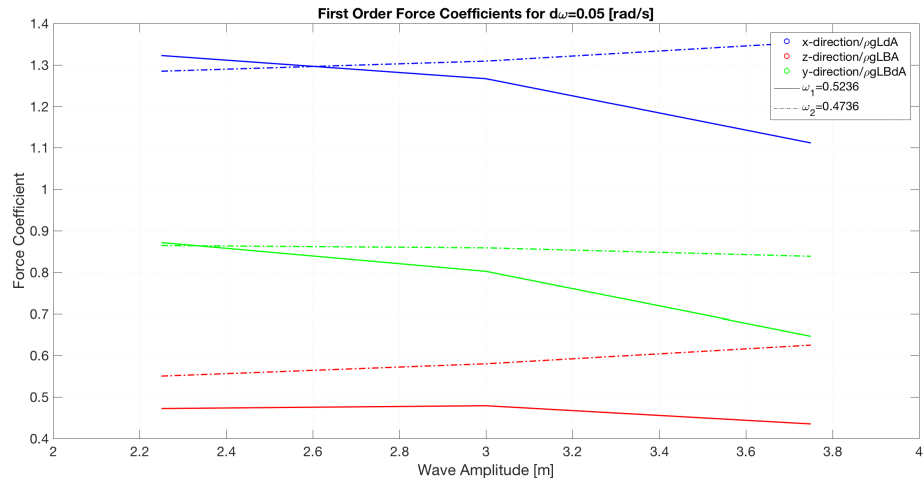


Figure 5.34: Bi-chromatic waves: first-order force coefficients for $d\omega = 0.05$

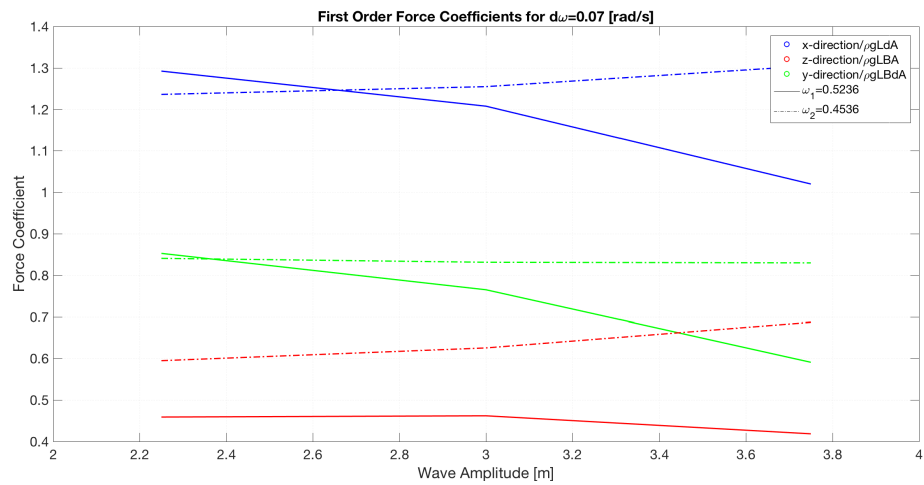


Figure 5.35: Bi-chromatic waves: first-order force coefficients for $d\omega = 0.07$

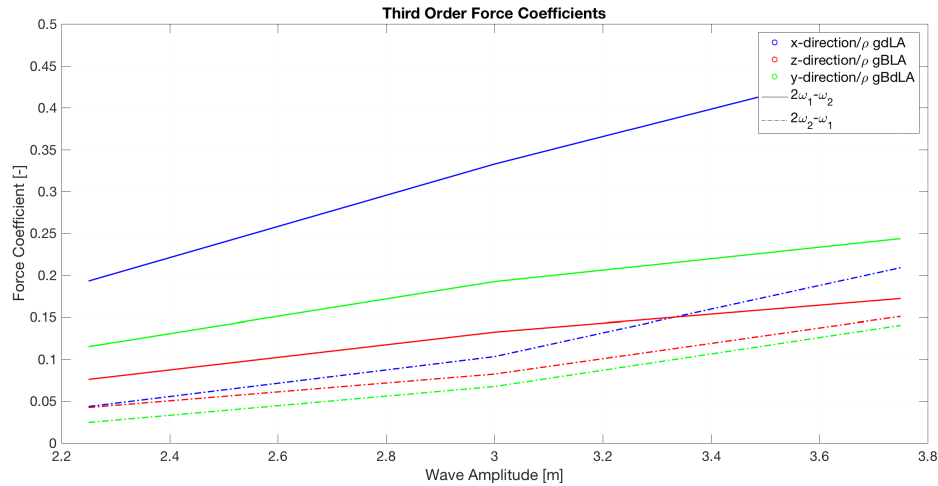


Figure 5.36: Bi-chromatic waves: third order force coefficients for $d\omega = 0.05$

The following tables show the percentage of change of the presented force coefficients from smallest to largest amplitude. Table 5.2 shows the mean drift force, 5.3 shows the slow drift force and 5.4 and 5.5 show the first-order force.

Table 5.2: Percentage change of mean drift force coefficient from lowest to highest amplitude

Force Direction	$d\omega = 0.05$	$d\omega = 0.07$
Force in x	21.32 %	30.23 %
Force in z	-3.97 %	- 15.42 %
Moment about y	2.43 %	- 0.69 %

Table 5.3: Percentage change of slow drift force coefficient from lowest to highest amplitude

Force Direction	$d\omega = 0.05$	$d\omega = 0.07$
Force in x	28.14 %	28.58 %
Force in z	6.86 %	7.17 %
Moment about y	11.40 %	18.26 %

Table 5.4: Percentage change of first-order force coefficient from lowest to highest amplitude for $d\omega = 0.05$

Force Direction	$\omega_1 = 0.5236$	$\omega_2 = 0.4736$
Force in x	-15.94 %	5.46 %
Force in z	-7.86 %	13.56 %
Moment about y	-25.83 %	-3.00 %

Table 5.5: *Percentage change of first-order force coefficient from lowest to highest amplitude for $d\omega = 0.07$*

Force Direction	$\omega_1 = 0.5236$	$\omega_2 = 0.4536$
Force in x	-21.07 %	5.59 %
Force in z	-8.81 %	15.50 %
Moment about y	-30.68 %	-1.29 %

5.3 Inviscid Flow Case

Selected results from the inviscid flow simulations for bi-chromatic waves with a difference frequency of 0.05 rad/s and zero viscosity, $\mu = 0 \text{ kg/(m} \cdot \text{s)}$, are included in this section. The rest of the results and figures are included in Appendix B.

5.3.1 Wave Elevation Results

The wave elevation results from the inviscid simulation with bi-chromatic waves of height $H = 6\text{m}$ are presented in figure 5.37.

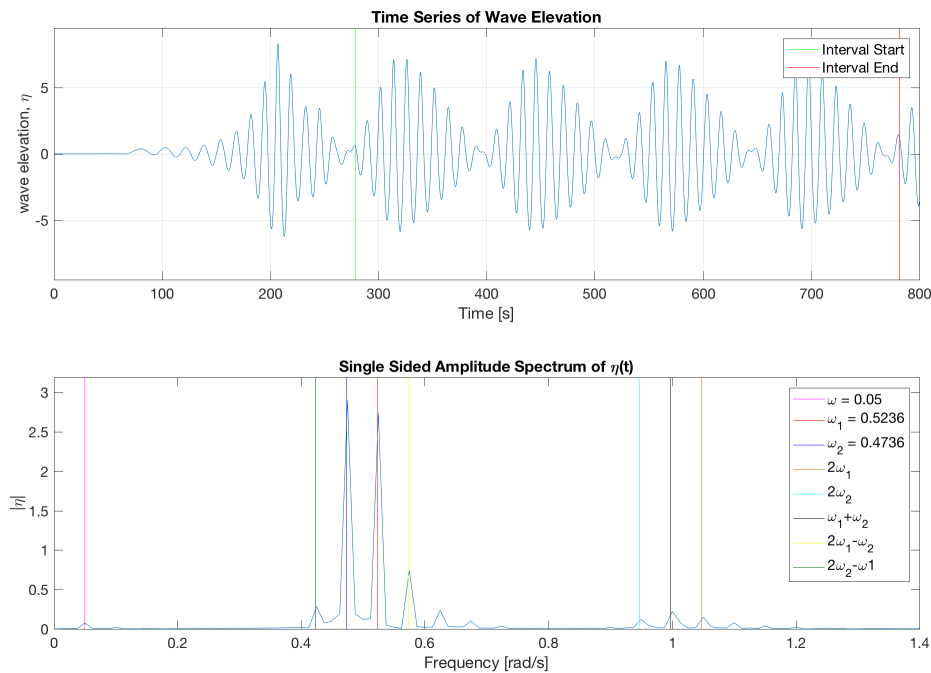


Figure 5.37: Inviscid flow case with $d\omega = 0.05$: wave elevation time series and spectrum for $H = 6\text{m}$

A plot of the velocity vectors around the column is shown in Figure 5.38.

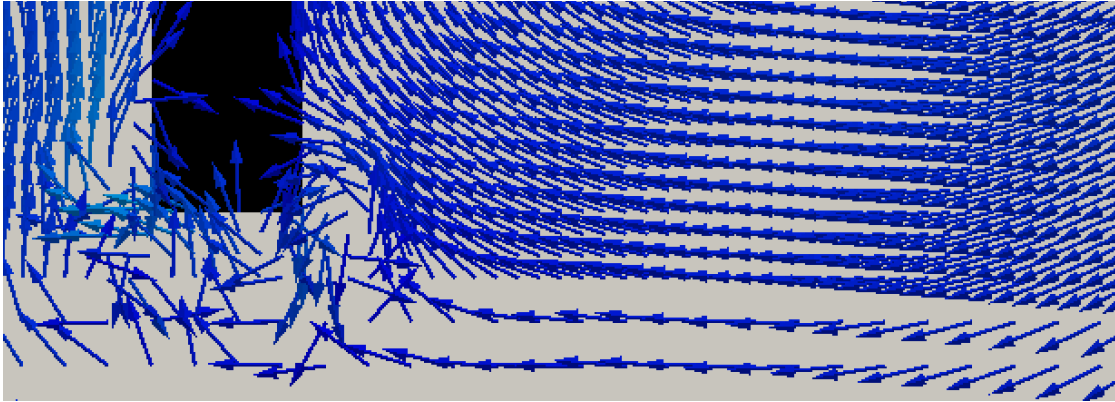


Figure 5.38: *Inviscid flow case with $d\omega = 0.05$: plot of velocity vectors around the column*

5.3.2 Force Results

Force results, force time series and force spectra, from the inviscid simulations for bi-chromatic waves of height $H = 6m$ are presented in figure 5.39 to 5.43. In figure 5.41 to 5.43, the force coefficient results from the inviscid flow simulations are plotted together with the viscous flow results. Figure 5.41 shows the coefficients of the mean drift force, Figure 5.42 shows the first-order force coefficients and Figure 5.43 the slow drift force coefficients.

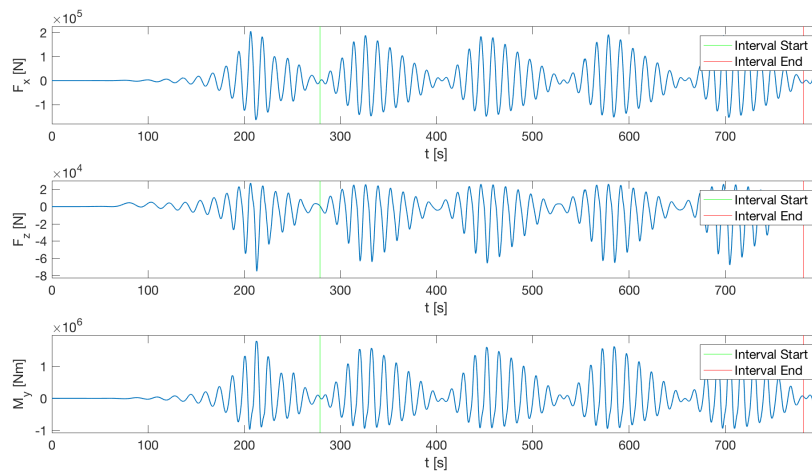


Figure 5.39: *Inviscid flow case with $d\omega = 0.05$: force time series for $H = 6m$*

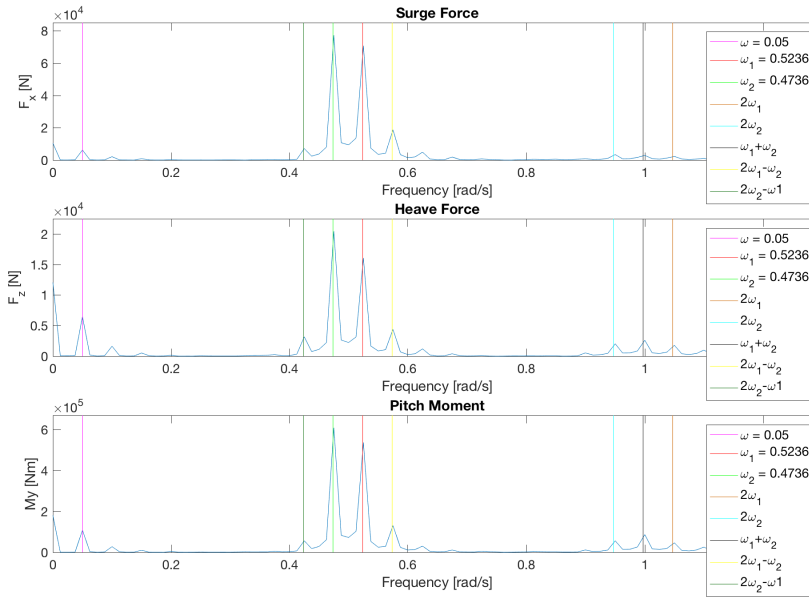


Figure 5.40: Inviscid flow case with $d\omega = 0.05$: force spectrum for $H = 6\text{ m}$

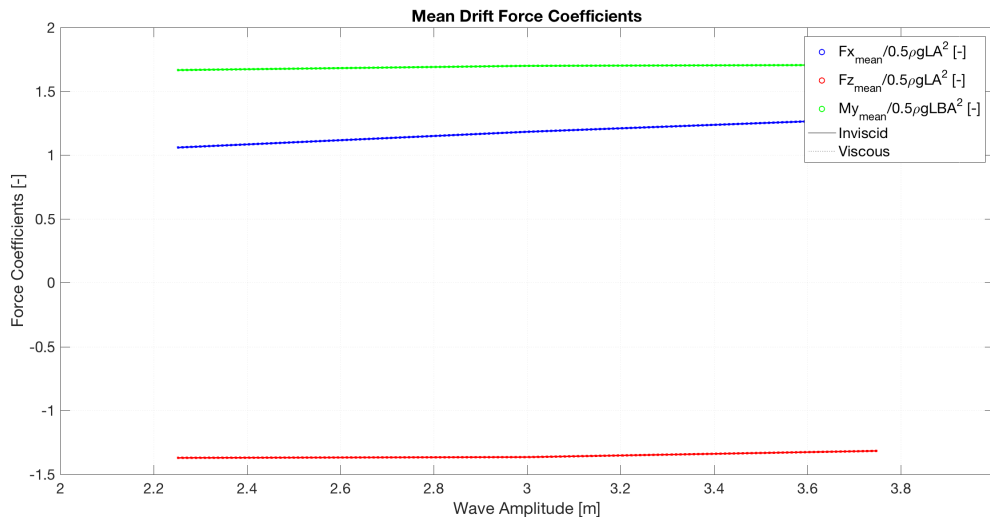


Figure 5.41: Inviscid and viscous flow results for $d\omega = 0.05$: mean drift force coefficients

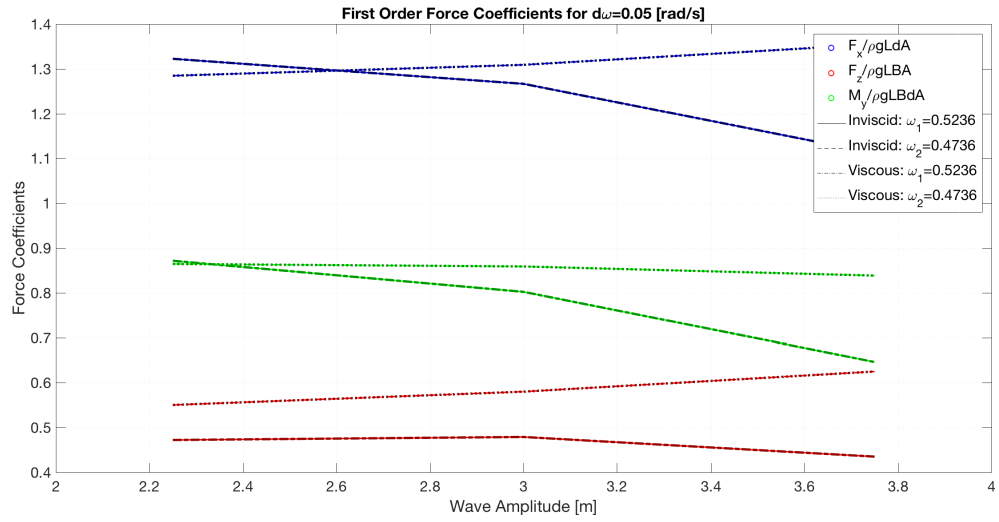


Figure 5.42: Inviscid and viscous flow results for $d\omega = 0.05$: first-order force coefficients

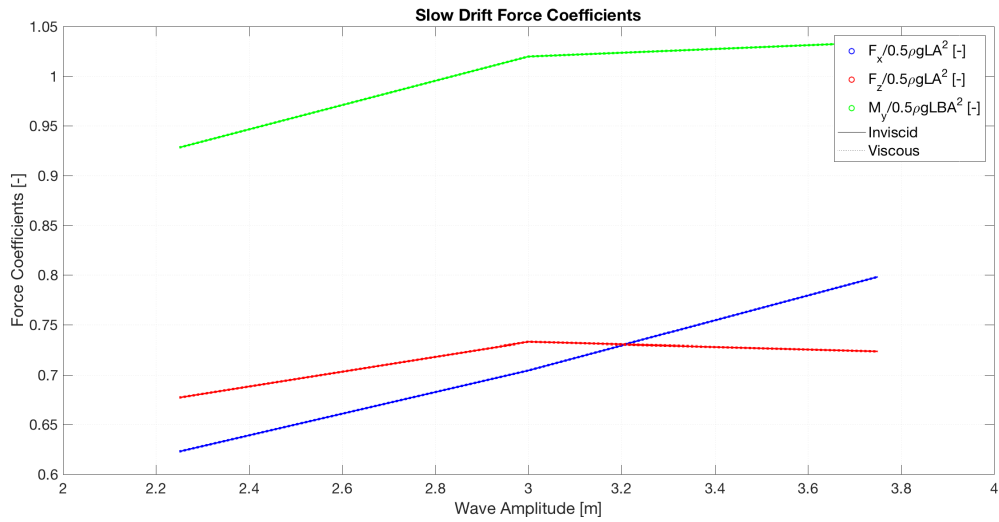


Figure 5.43: Inviscid and viscous flow results for $d\omega = 0.05$: slow drift force coefficients

Chapter 6

Discussion of Results from Numerical Study

This section covers a discussion of the results and findings presented in Chapter 5. As discussed in Chapter 1, this study is intended as the first step of a comprehensive study of wave drift forces on semi-submersible platforms. The focus has been on the numerical methodology and the analysis and understanding of the results. More attention has been directed towards the surge force as a consequence of what has been focused on in the literature.

6.1 Regular Waves

The wave elevation time series and the Fourier analysis of the time series shown in Figure 5.1 in Chapter 5 and B.1 and B.2 in Appendix B show three peaks at the wave frequencies which are present in the wave field, $\omega = 0$, ω_1 and $2\omega_1$. These force peaks represent the mean force, first-order force and second-order force, respectively. The single wave frequency component, corresponding to ω_1 , is much larger than the double-frequency component. This is expected. From the time series it can be seen that some time is required for the wave field to stabilise. The figures of the interval of the wave elevation time series presented in Section 4.5 show that the difference between the actual and theoretical wave increases slightly with increasing wave amplitude. As the wave height increases, the wave becomes more non-linear, and the wave will deviate from linear wave theory. This means that the run with an amplitude of 4.5 m most likely will give a more accurate result compared to the run with an amplitude of 7.5 m in terms of linear wave theory.

In the Fourier analysis of the force time series for the regular wave with 6 m wave height, presented in Figure 5.3 in Chapter 5, three major peaks are visible. These peaks represent the expected harmonic components, corresponding to the frequencies of the peaks in the wave elevation spectrum. The same can be noted from the rest of the results presented in Appendix B. As expected, the first-order force is the largest for all the runs, and is followed by the mean force and the second-order force. The force time series in Figure 5.2 show the interval in which the force spectrum has been calculated. It shows that steady state is reached quite quickly after the waves meet the column.

From the plots of the mean drift force coefficients in Figure 5.4 it is clear that the magnitude of the mean drift moment about y is the largest. The graphs are more or less constant with wave amplitude, which means that the mean drift forces are proportional to the amplitude squared. The mean drift force coefficients in x and z direction, surge and pitch, have about the same magnitude, however the vertical force is negative. It is important to note that the hydrostatic force has been subtracted from the heave force.

Figure 5.5, 5.6 and 5.7 show the same as stated from the Fourier analysis, namely that the first-order force components are much bigger than the second and third order force components. In x -direction, the coefficients are more or less constant with wave amplitude, however in z -direction and for the moment coefficient about y , the second-order force coefficients are increasing with increasing wave amplitude.

6.2 Bi-Chromatic Waves

The figures taken from paraView presented in Section 5.2.1, show the velocity and pressure distribution in the domain at fixed timesteps. Figure 5.8 shows the pressure distribution of the travelling wave when the hydrostatic pressure has been subtracted. High pressure, red, correspond to a wave crest and low pressure, blue, correspond to a wave trough. The modulated wave is clearly visible. Figure 5.9 shows the velocity distribution. The highest velocities are found close to the free surface and the highest wave amplitudes cause the air to flow faster. Figure 5.10 and 5.11 show the

velocity vectors around the column and at the inlet of the domain. The circular wave particle orbits are visible.

Figure 5.15 show the velocity distribution around the bottom of the column at two different time instants. High velocities are found close to the column and a pattern that look like vortices is present, although it is only slightly visible. Vortices are expected, because the flow separates at the sharp corners, but the element size might be too large in order to capture the vortex propagation clearly.

The effect of simulating bi-chromatic waves is clearly visible in the time series of the wave elevation, because of the modulated amplitudes. The wave spectra in Figure 5.16 to 5.19 show that non-linear effects from the wave-body interaction are present, because the wave spectra are broader. The sea states contains a wider range of excitation frequency content compared to the regular wave runs and all the wave frequencies are present. The same is visible in the result for the other cases included in Appendix B. As the wave height increases, the spectra becomes less clean and the energy is no longer limited and present only at the expected frequency peaks, additional force peaks appear. This might indicate that running cases with higher wave heights in openFoam are less accurate and appear more noisy, likely because of the difficulty of simulating steep waves accurately.

For the force time series and the associated Fourier analysis of the time series presented in Figure 5.20 to 5.27, the same harmonic components are present as in the wave spectra. The force time series show the same behavior as the wave elevation time series. The force spectra show that the first-order force components related to the single wave frequencies, ω_1 and ω_2 , are the largest components in all cases. However, for the heave force, in particular, the mean drift force is quite large relative to the first-order force components. The magnitude of the slow drift force peaks, for all the force components, are much smaller than the first-order and mean force peaks, but increase with increasing wave height.

An interesting observation from the wave amplitude and force spectra is the peaks at frequencies $2\omega_1 - \omega_2$ and $2\omega_2 - \omega_1$. This is an effect caused by interaction of first and second-order harmonics [Fonseca et al. \(2011\)](#). The Fourier analysis show that this effect is larger than the second-order

effect related to $2\omega_1$ and $2\omega_2$. The corresponding force coefficients are presented in Figure 5.36. The figure shows that the coefficients are increasing with wave amplitude.

The plots of the mean drift force coefficients in Figure 5.28 to 5.30 show that the mean drift force is increasing with increasing amplitude in surge and partly in pitch and decreasing in heave. From Table 5.2, it is clear that the change is most significant in surge and that the mean pitch moment is changing very little. The mean coefficient plot suggest that the surge coefficient is proportional to more than the amplitude squared. This may be explained by looking at Figure 5.12, 5.13 and 5.14. As shown in these figures, the asymmetry of the wave elevation on the upstream and downstream side of the column increases with growing wave height. This asymmetry can cause a considerable surge force and may explain the increasing coefficient. In addition, vortex shedding from the bottom of the column may become stronger with larger wave heights causing an increasing force coefficient.

Figure 5.29 shows that the mean force in heave is decreasing with increasing amplitude, especially when the difference frequency is 0.07 rad/s. A possible explanation can be that the local hydrostatic pressure, as a consequence of the wave run-up along the column wall, increases for higher wave heights and counteracts the dynamic pressure such that the total force decreases. This, however, needs to be further validated.

Considering the mean drift force coefficients, the cases behave in a similar manner regardless of difference frequency, except for pitch. However, the cases with a difference frequency of 0.07 rad/s have somewhat smaller values compared to the cases with difference frequency 0.05 rad/s, except for the highest amplitude in heave.

Figure 5.31, 5.32 and 5.33, presenting the slow drift force coefficients, show that the slowly varying forces are increasing with increasing wave amplitude for all the force directions. Table 5.3 shows that the relative increase is largest for surge and for a difference frequency of 0.07 rad/s. In addition, the figures imply that the slow drift force coefficients are proportional to more than the amplitude squared. The behaviour is similar regardless of difference frequency, but a difference frequency of 0.07 rad/s is connected to the largest force coefficients in surge and heave.

The first-order force coefficients with respect to ω_1 and ω_2 are shown in Figure 5.34 and 5.35. These plots together with Table 5.4 and 5.5 show that the first-order force coefficients connected to ω_2 increase while the coefficient related to ω_1 decrease with increasing wave amplitude. This is also shown in Table 5.4 and 5.5. However, the rate of change of the coefficients are varying.

6.3 Inviscid Flow Case

The results from the simulations with zero viscosity presented in Chapter 5 are very similar and almost equal to the results from the simulations with viscosity. This is clearly visible from the force coefficient plots in Figure 5.41 to 5.43. After defining the viscosity to be zero, the Euler equation is solved, as explained in Chapter 3. This means that the flow still is rotational and that vortices may exist in the fluid, and flow separation will occur at the sharp corners of the cylinder. The presented results indicate that non-viscous flow separation is more important than viscous flow separation. In addition, the viscous effects are most likely very small for the presented cases. This might be different in case of 3D simulation, when the flow of water around the cylinder can cause additional drag and frictional forces.

From Figure 5.38 it is clear that separation occurs at the two corners at the bottom of the column, and that vortices develop close to the column wall. However, the grid resolution is most likely too low to capture the possible vortices further downstream of the column. This means that the grid size may be too large in order to correctly capture the viscous effects in the viscous flow cases as well.

6.4 General Remarks

When discussing the force results it is important to keep the natural periods of the structure in mind. Even though this study has focused on a simple, fixed 2D geometry of quadratic shape, the overall goal is to eventually relate the results to a complete semi-submersible platform. The main

focus has been towards the mean and slowly varying drift forces in surge, which means that the sum-frequency components generally have been neglected in the discussion.

Although the first-order force components related to the frequencies of the two single waves are the largest, the slow drift force can become of great importance if the semi-submersible platform has a natural period close to the slowly varying wave period. The slowly varying wave periods are 125.6 s and 89.8 s which is in the range of the natural surge periods for semi-submersibles. In heave, the natural period is proportional to the water plane area and are over 20 s, corresponding to an angular frequency of about 0.3 rad/s. Looking at the wave elevation spectra for heave, there are no considerable energy located around this frequency, meaning that the heave excitation will be low. The surge excitation is therefore of greater interest.

However, there are limited connections to draw between these results and the total expected behaviour of a complete semi-submersible platform. A platform consists of several columns and pontoons that will cause coupled effects and interaction. In a real environment, the bottom of the column will not experience force directly from the wave, there will be forces on the pontoon. The behaviour and excitation of a structure depends on the system characteristics, and to be able to say anything definite and certain about a structures excitation or behaviour, the correct geometry must be investigated.

It is important to emphasize that this study has investigated the fundamental mechanisms for a simple geometry, which is important in order to understand the mechanisms in a real environment. It is difficult to understand the total picture when studying all the effects at the same time, and isolating and identifying the individual contributions, as done in this study, is valuable.

Due to the simple geometry, the presented force results can also be valuable for and related to other floating structures than semi-submersibles, for instance such as spread moored FPSO's (Floating Production, Storage and Offloading) subjected to incoming waves from the side and SPAR-buoys.

Chapter 7

Conclusions and Recommendations for Further Work

7.1 Conclusion

The presented results show that the expected dominating frequencies are present in the spectra of the forces and wave elevation. For the bi-chromatic wave cases, the mean drift force in surge is proportional to more than the wave amplitude squared. This is also the case for the slow drift forces, which clearly increase for higher wave amplitudes. Furthermore, the results show that the viscous contribution to the wave drift loads is small and that non-viscous flow separation is present at the sharp corners at the bottom of the column. However, the grid resolution might have been too large in order to capture the viscous effects correctly and the elements should be smaller, at least further below the column. The problem in this thesis has been limited to 2D, and 2D cases are quite far from a real situation. However, the findings and the methodology presented are valuable as a basis for a future study of the wave drift forces in three dimensions with additional features as for instance wave-current interaction.

7.2 Recommendations for Further Work

Further work on this problem is of great interest. This thesis has been more of an in-depth systematic study in order to clarify the general methodology of a numerical study of the wave drift

forces. This thesis represents the first step in the comprehensive numerical investigation, and it will be valuable to build the cases further. The grid resolution should be increased in order to be able to capture the viscous effects better, at least below the column. It would also be interesting to simulate steeper waves, which will require careful consideration and evaluation of the simulation and mesh parameters to ensure a stable solution.

Future investigation will benefit from building up the 3D case to study the 3D effects on the structure as well as the effect of viscosity. A 3D case allows for flow around the body which result in a larger wetted surface and probably larger drag forces. In addition, more model test results are available for 3D cases than for 2D cases. Furthermore, the empirical formula presented in Chapter 3 can be applied to investigate and compare against the simulation results.

This study has been focusing on a part of the over-all problem by concentrating on a single column representing a platform column. It will be valuable to eventually study and build up the case towards a complete semi-submersible, including the pontoons, in order to study how the different parts interact and influence the wave drift forces. Further, it will be valuable to include the radiation problem and not only the diffraction problem by creating a floating platform in order to simulate a more real environment. This, however, is a quite large task and it is assumed to be very time consuming to reach this step.

In general, CFD simulations should be performed together with model tests in order to verify the results against empirical data. In addition, the empirical formulas should be investigated and developed further, because they can be valuable for quick estimations of the forces. Comparing results from potential codes with CFD calculations can also be practical and efficient in order to investigate conditions where the potential and viscous theory differ.

Bibliography

3D Systems (2017). What is an stl file?

URL: <https://www.3dsystems.com/quickparts/learning-center/what-is-stl-file>

Ali, A. A., Peng, H. and Qui, W. (2017). Experimental and numerical investigation of the slowly varying wave exciting drift forces on a restrained body in bi-chromatic waves, *Proceedings of the ASME 2017 36th International Conference on Ocean, Offshore and Arctic Engineering OMAE2017*, Trondheim, Norway.

Berthelsen, P. A., Baarholm, R., Pákozdi, C. and Stansberg, C. T. (2009). Viscous drift forces and responses on a semisubmersible platform in high waves, *Proceedings of the ASME 2009 28th International Conference on Ocean, Offshore and Arctic Engineering OMAE2009*, Honolulu, Hawaii, USA.

Braaten, H. (2016). Report: Deepsea model tests.

CFD Direct (2016). Openfoam user guide: 2.3 breaking of a dam.

URL: <https://cfd.direct/openfoam/user-guide/damBreak/##x7-520002.3>

Dean, R. G. and Dalrymple, R. A. (1991). *Water Wave Mechanics for Engineers and Scientists (Advanced Series on Ocean Engineering-Vol2)*, World Scientific Publishing Company.

Dev, A. and Pinkster, J. (1995). Viscous mean drift forces on moored semi-submersibles, *Proceedings of the Fifth International Offshore and Polar Engineering Conference*, Vol. 3, The Hague, Netherlands.

Faltinsen, O. (1990). *Sea Loads on Ships and Offshore Structures*, Cambridge University Press, Cambridge, United Kingdom.

Fonseca, N. (2016). Report: Cat-d semi-submersible model tests.

Fonseca, N., Pessoa, J., Mavrakos, S. and Le Boulluec, M. (2011). Experimental and numerical investigation of the slowly varying wave exciting drift forces on a restrained body in bi-chromatic waves, *Ocean Engineering* 38.

Greco, M. (2012). *TMR 4215: Sea Loads Lecture Notes*, Department of Marine Technology, NTNU, Trondheim, Norway.

Hpc Group (2017). About vilje.

URL: <https://www.hpc.ntnu.no/display/hpc/About+Vilje>

Hu, J. and Zhou, L. (2015). Experimental and numerical study on wave drift forces on a semi-submersible platform in waves, *Ships and Offshore Structures*, Vol. 1-10.

Jacobsen, N. G. (2011). A wave generation toolbox for the open-source cfd library: Openfoam, *International Journal for Numerical Methods in Fluids*.

Kundu, P. and Cohen, I. (2007). *Fluid Mechanics*, Elsevier, United States.

Pettersen, B. (2007). *Marin Teknikk 3, Hydrodynamikk*, Department of Marine Technology, NTNU, Trondheim, Norway.

Stansberg, C., Baarholm, R. and Kristiansen, T. (2005). Extreme wave amplification and impact loads on offshore structures, *Offshore Technology Conference*, Huston, Texas, USA.

Stansberg, C. T., Fonseca, N., Nestegård, A., Bøckmann, A. and Baarholm, R. (2016). The exwave jip: Improved procedures to calculate slowly varying wave drift forces on floating units in extreme seas, *Proceedings of the ASME 2016 35th International Conference on Ocean, Offshore and Arctic Engineering OMAE2016*, Busan, South Korea.

Stansberg, C. T. and Nestegård, A. (2014). Report: Exwave pilot study task 2b - recommendations.

Stansberg, C., Yttervik, R. and Nielsen, F. (1998). Wave drift forces and responses in storm waves, *Proceedings of PRADS'98 Conference*.

Tanizawa, K., Minami, M. and Naito, S. (1999). Estimation of wave drift force by numerical wave tank, *Proceedings of the Ninth International Offshore and Polar Engineering Conference*, Brest, France.

Thys, M. and Ambrahamsen, B. C. (2016). Report: Songa dee model tests.

WAMIT (2017). Technical description.

URL: *<http://www.wamit.com/techdescription.htm>*

Appendix A

OpenFOAM Details

A.1 Overview of OpenFOAM Case Set-Up

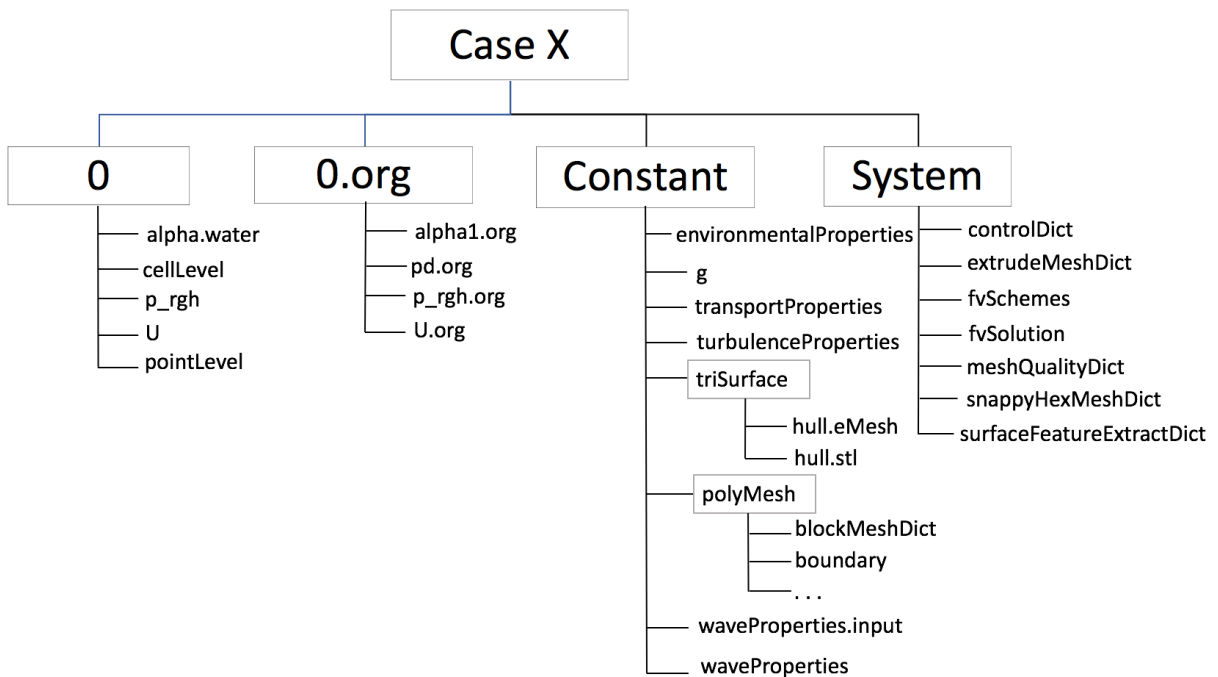


Figure A.1: Overview of initial programming set-up

Figure A.1 shows roughly how OpenFoam is organised. The boxes represent the different directories.

The folder *0.org* contains the initial conditions of the problem and the boundary conditions for the different parts of the domain boundaries.

The folder *constant* consists of several files that describe the constant properties of the problem, for instance the gravitational acceleration, the viscosity of the fluid, the structure geometry and mesh information. The folder also contains the files containing information about the waves and relaxation zones.

The *system* folder contains the information that controls how the problem is solved, for instance what kind of interpolation, integration and solver that are used. In addition, it contains the files that control the time step, the simulation time and how the meshing is performed.

After running the code and solving the problem, additional directories with results are saved. Figure A.2 shows some of these files.

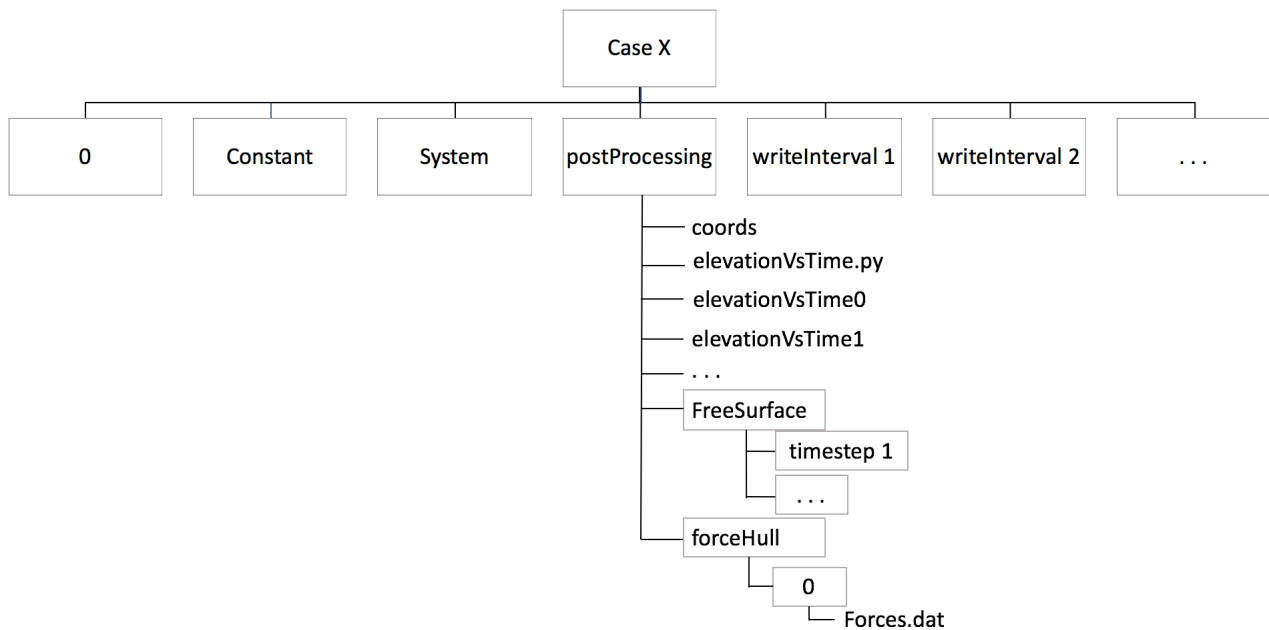


Figure A.2: Overview of programming set-up with result folders

The wave elevation information and the forces on the structure at each time step are found in the *postProcessing* folder. The *writeInterval i* folders contain the field solutions at the defined times. How many of these directories that appear are controlled by the *writeControl* option, described in 3., defines how often the results are saved.

A.2 Boundary Conditions and Explanation

Table A.1: *Boundary Conditions*

Surface	Velocity BC	Pressure BC	Volume fraction BC
inlet	waveVelocity	zeroGradient	waveAlpha
outlet	fixedValue	zeroGradient	zeroGradient
bottom	fixedValue	zeroGradient	zeroGradient
atmosphere	pressureInletOutletVelocity	totalPressure	inletOutlet
front	empty	empty	empty
back	empty	empty	empty
hull	fixedValue	zeroGradient	zeroGradient

Table A.2: *Boundary Condition Description (CFD Direct; 2016)*

Boundary condition	Description
waveVelocity	Special bc connected to waves2Foam toolbox
waveAlpha	Special bc connected to waves2Foam toolbox
fixedValue	Specified by a value
pressureInletOutletVelocity	Allow some inflow with unknown velocity
empty	For 2D cases
fixedFluxPressure	Adjusts pressure gradient to match velocity BC
zeroGradient	Normal gradient is zero
totalPressure	Fixed value condition from specified total pressure
inletOutlet	zeroGradient if fluid flows out of domain and fixedValue into domain

Appendix B

Additional Simulation Results

B.1 Regular Waves

B.1.1 Wave Elevation Results

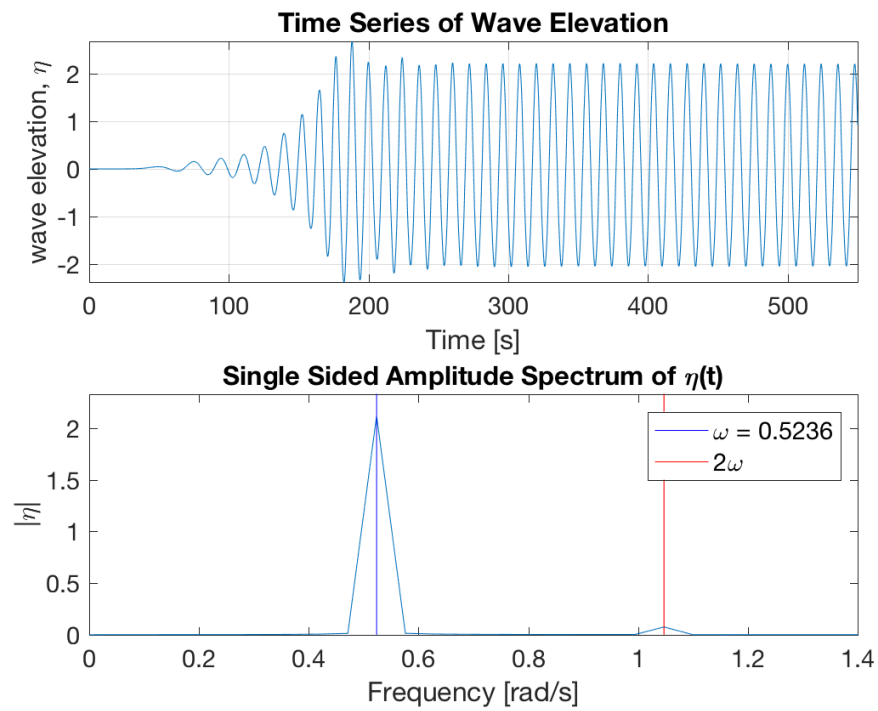


Figure B.1: Regular waves: wave elevation analysis for $H = 4.5m$

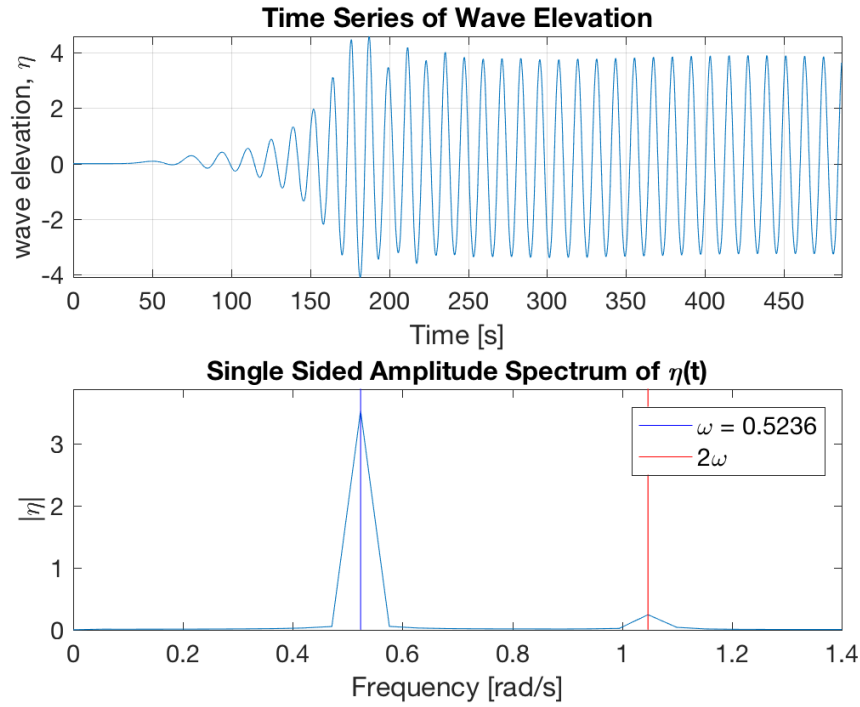


Figure B.2: Regular waves: wave elevation analysis for $H = 7.5m$

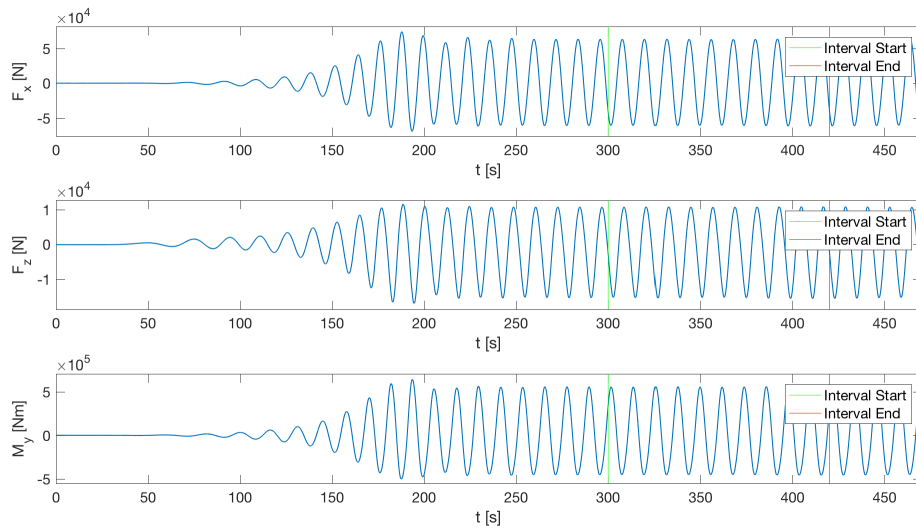


Figure B.3: Regular waves: force time series for $H = 4.5m$

B.1.2 Force Results

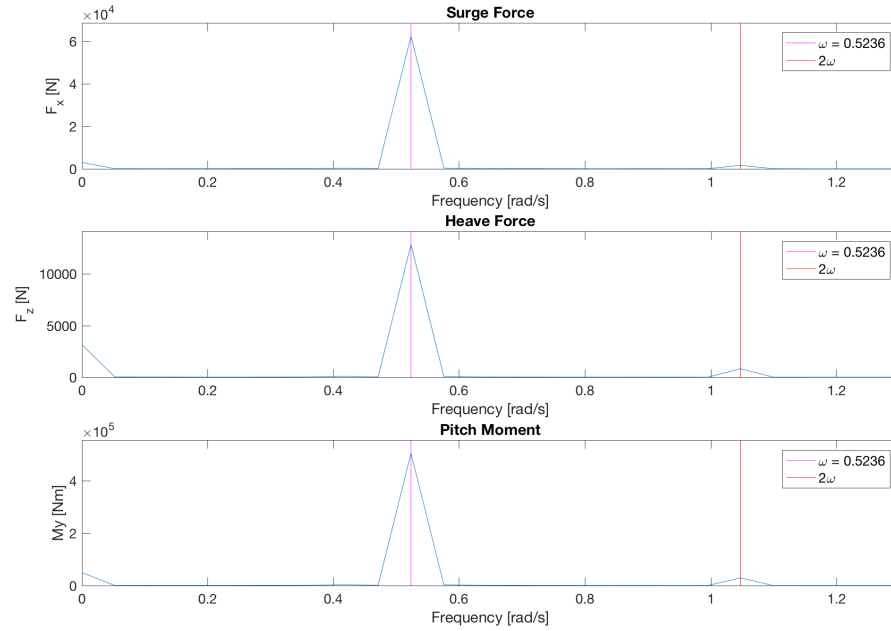


Figure B.4: Regular waves: force spectrum for $H = 4.5m$

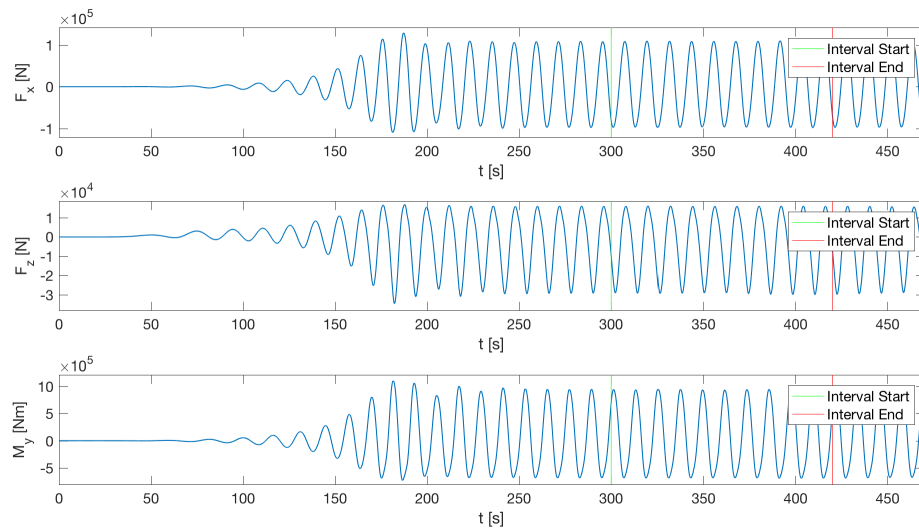


Figure B.5: Regular waves: force time series for $H = 7.5m$

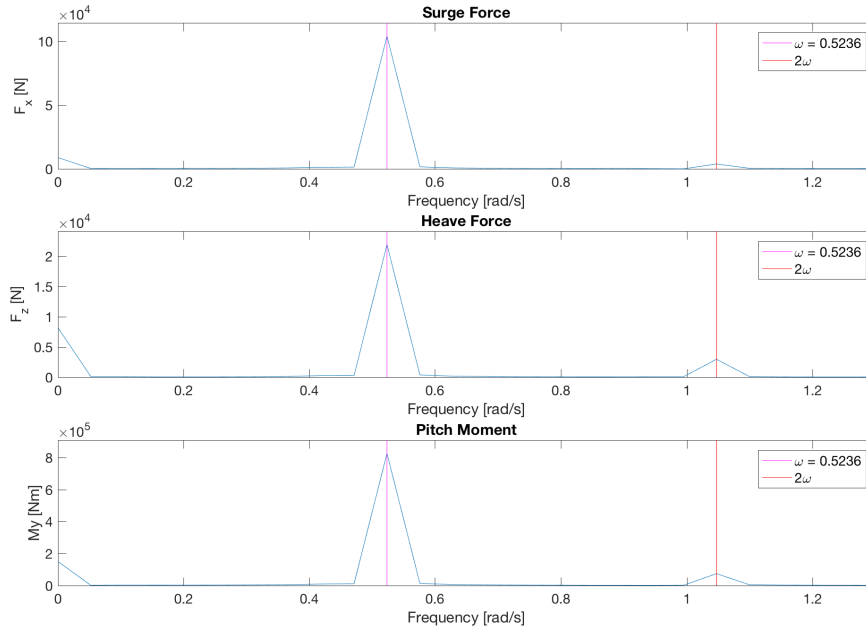


Figure B.6: Regular waves: force spectrum for $H = 7.5m$

B.2 Bi-Chromatic Waves

B.2.1 Wave Elevation Results

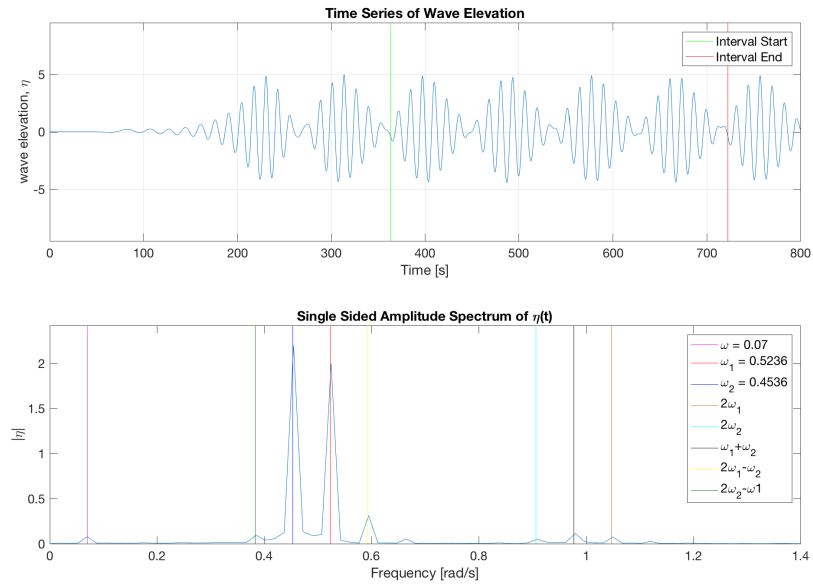


Figure B.7: *Bi-chromatic waves with $d\omega = 0.07$: wave elevation time series for $H = 4.5m$*

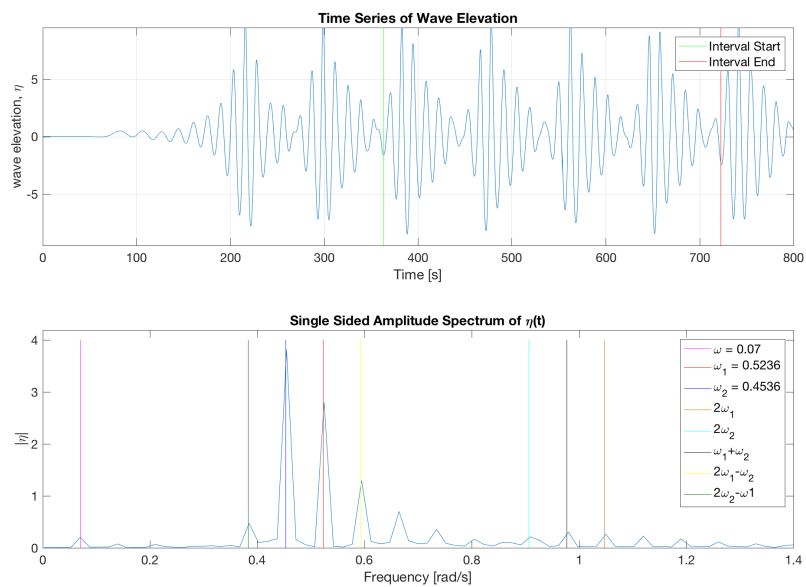


Figure B.8: *Bi-chromatic waves with $d\omega = 0.07$: wave elevation time series for $H = 7.5m$*

B.2.2 Force Results

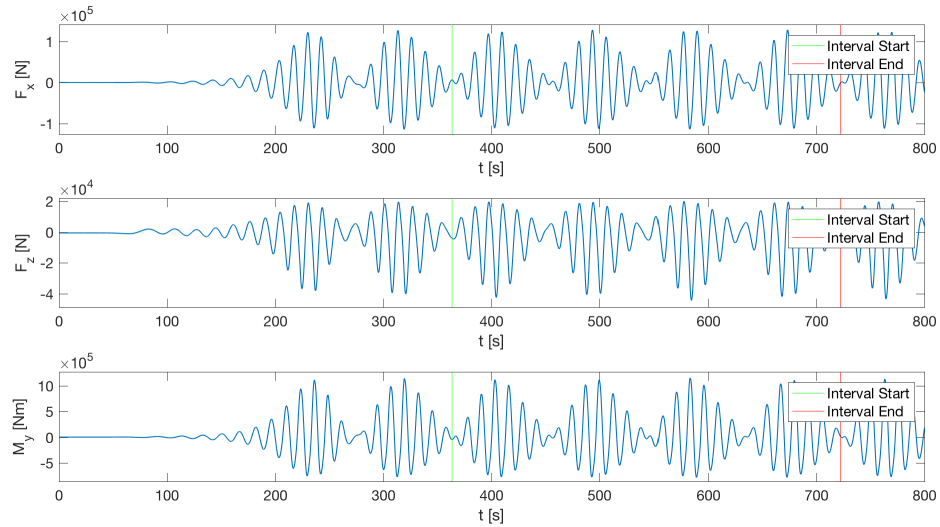


Figure B.9: Bi-chromatic waves with $d\omega = 0.07$: force time series for $H = 4.5m$

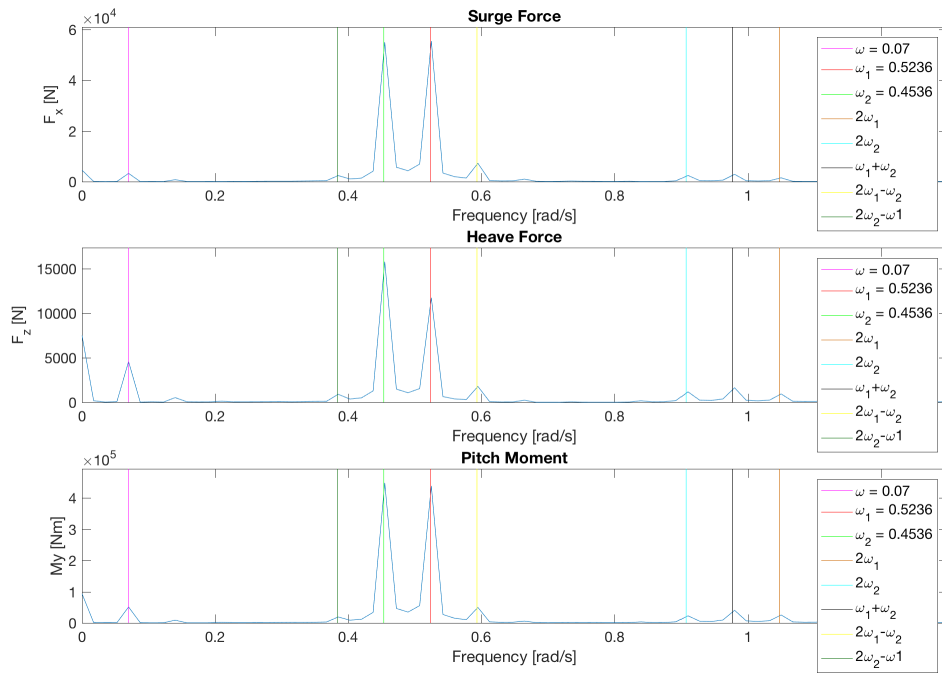


Figure B.10: Bi-chromatic waves with $d\omega = 0.07$: force spectrum for $H = 4.5m$

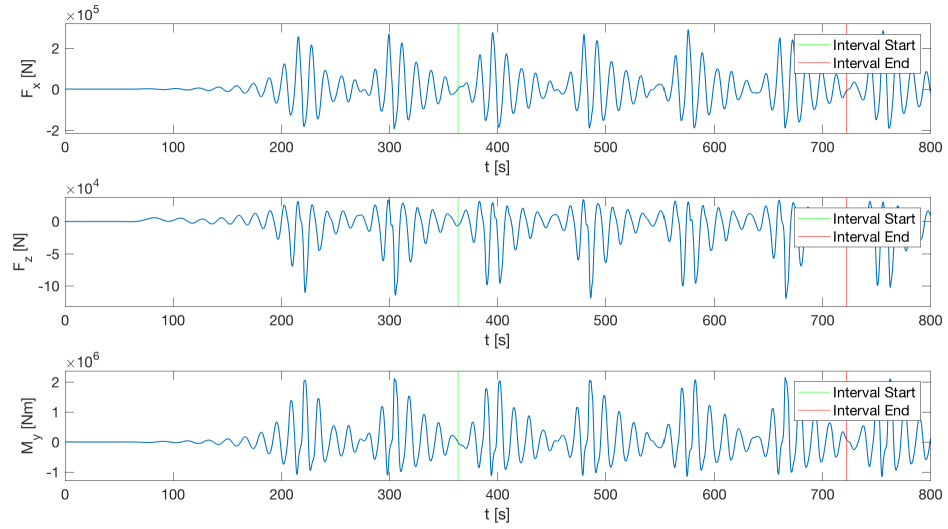


Figure B.11: Bi-chromatic waves with $d\omega = 0.07$: force time series for $H = 7.5m$

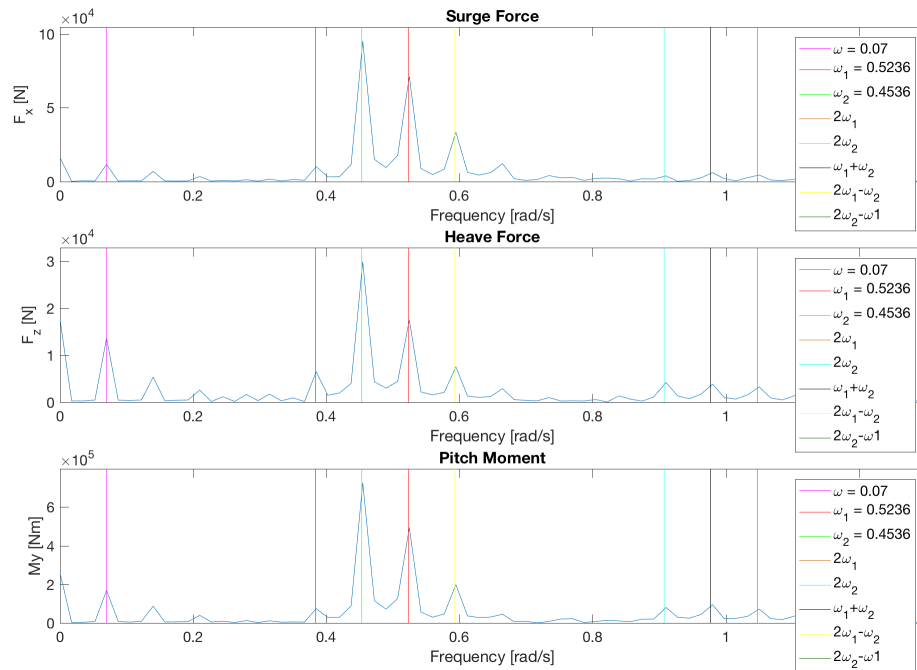


Figure B.12: Bi-chromatic waves with $d\omega = 0.07$: force spectrum for $H = 7.5m$

B.3 Inviscid Flow Case

B.3.1 Wave Elevation Results

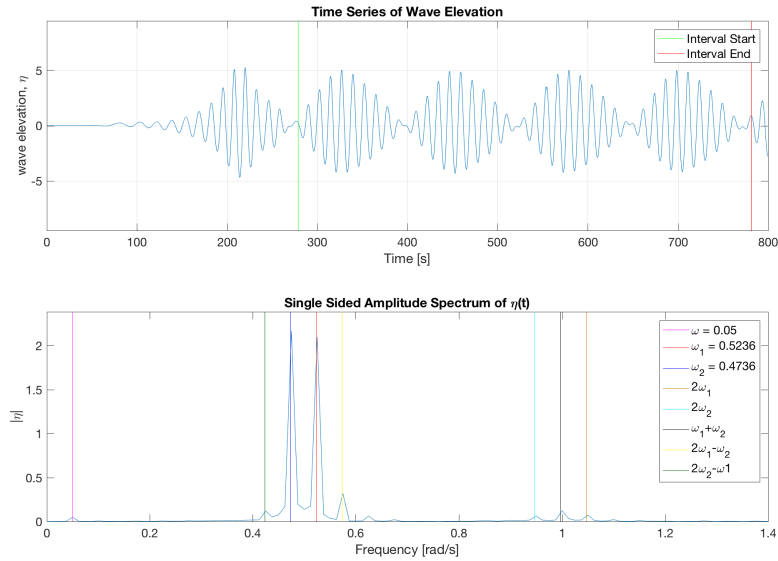


Figure B.13: Inviscid flow case with $d\omega = 0.05$: wave elevation time series and spectrum for $H = 4.5m$

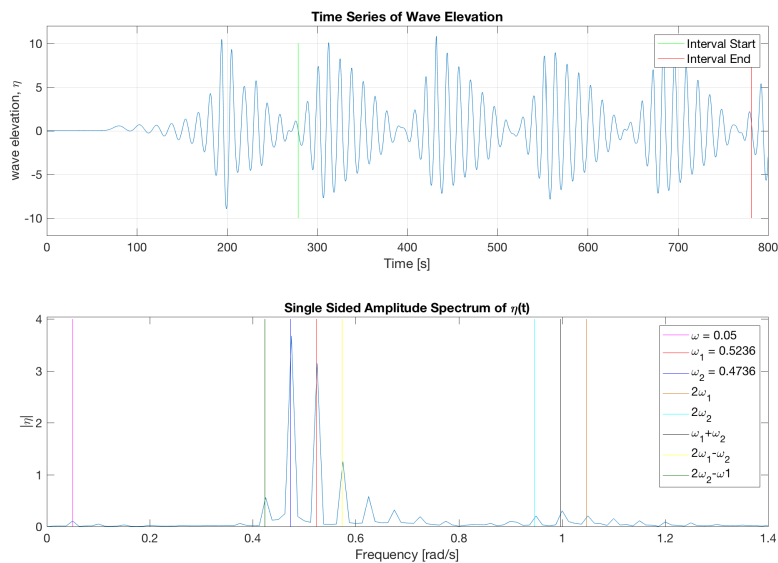


Figure B.14: Inviscid flow case with $d\omega = 0.05$: wave elevation time series and spectrum for $H = 7.5m$

B.3.2 Force Results

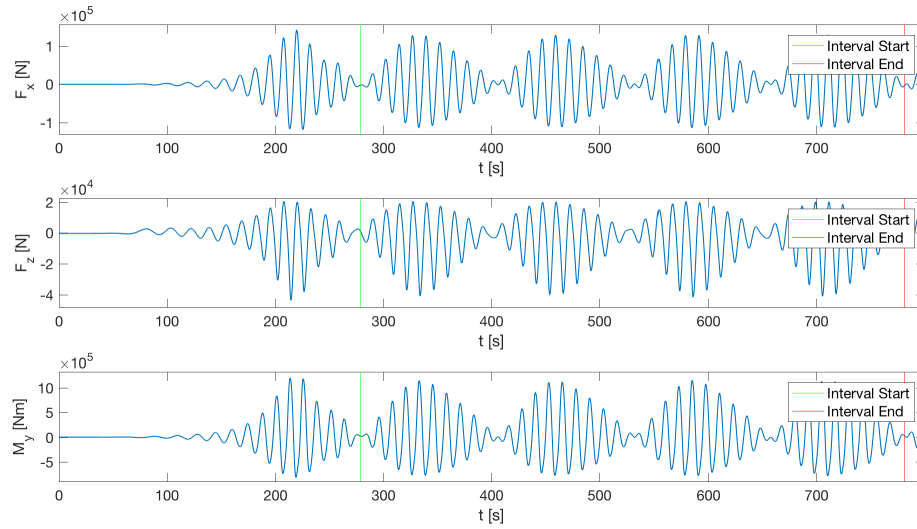


Figure B.15: Inviscid flow case with $d\omega = 0.05$: force time serie for $H = 4.5m$

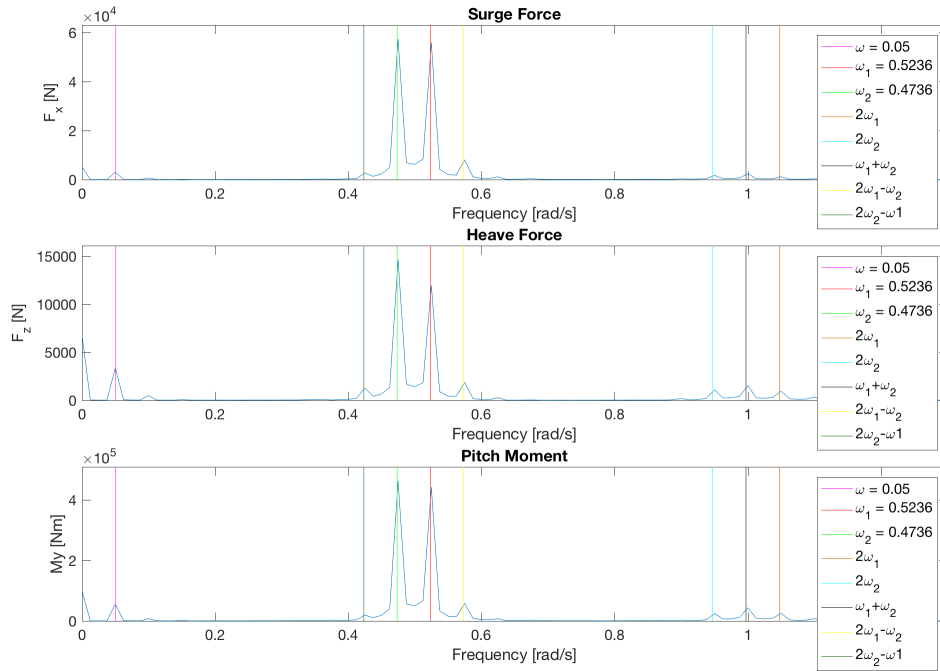


Figure B.16: Inviscid flow case with $d\omega = 0.05$: force spectrum for $H = 4.5m$

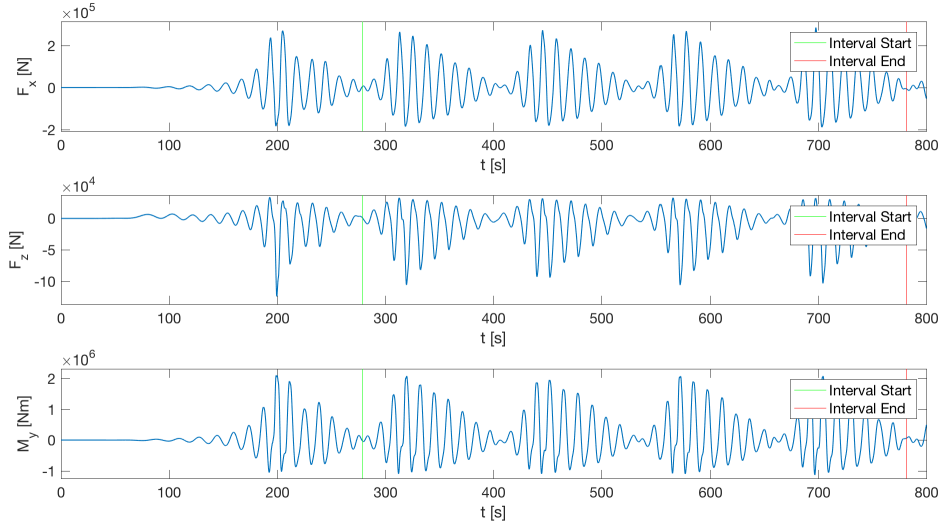


Figure B.17: Inviscid flow case with $d\omega = 0.05$: force time series for $H = 7.5m$

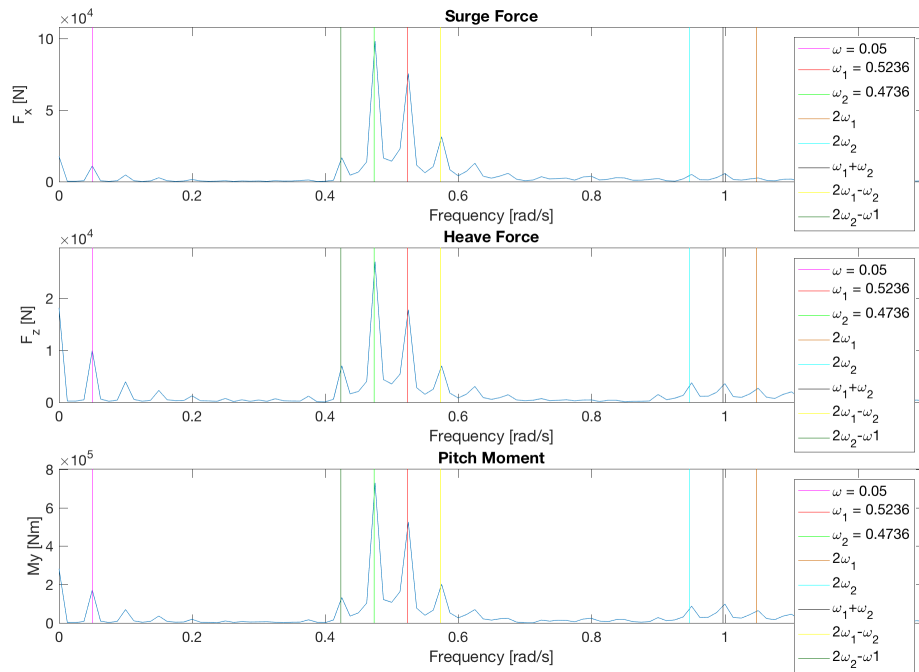


Figure B.18: Inviscid flow case with $d\omega = 0.05$: force spectrum for $H = 7.5m$

Appendix C

MATLAB Scripts

C.1 Case Generation Script

Bi-Chromatic Wave Case

```
1 % Prepares bi-chromatic wave cases to be simulated in openFOAM
2 % Based on script made by Babak Ommani
3
4 function generateRun()
5     workPath = ...
6     '/Users/julie/Documents/Marin5/Delt/runGeneration/MasterCases/Bichromatic';
7     sourcePath = '/Users/julie/Documents/Marin5/Delt/runGeneration';
8     templatePath = [sourcePath '/' 'projectfilesBodyBi'];
9
10 %% CASE PARAMETERS
11 T1 = 12;           % Period 1
12 H=[4.5 6 7.5];   % Wave height
13 draft = 20;
14 B = 12;           % Body breadth
15 dw = 0.05;       % Difference frequency
16
17 for i=1:3
18     omega1 = 2*pi/T1;
19     omega2 = omega1 - dw;
20     T2 = 2*pi/omega2; %Period 2
21     frequency1 = 1/T1;
22     frequency2 = 1/T2;
23     g = 9.81;
24     k1 = omega1^2/g;
```

```

25 k2 = omega2^2/g;
26 lambda1 = (2*pi)/k1;
27 lambda2 = (2*pi)/k2;
28 steep1_ka(i) = k1*(H(i)/2);
29 steep1_lam(i) = H(i)/lambda1;
30 steep2_ka(i) = k2*(H(i)/2);
31 steep2_lam(i) = H(i)/lambda2;
32 depth = 0.5*lambda2;
33 air = (depth/0.7)-depth;
34 tankL = 11*lambda2;
35 sizeCells = lambda2/20;
36 nCellXs = round(tankL/sizeCells);
37 nCellZs = round((depth+air)/(tankL/nCellXs));
38 dampstart = 0.82*tankL; %DAMPING AREA
39 damp_Yn = -1;
40 damp_Yp = 1;
41 inletDamp = 400;
42
43 endtime = 800;
44 vel_g = g/(2*omega1); % Group speed
45 vel_ph = g/(omega1); % Phase velocity
46
47 %stl file
48 yNeg=-5;
49 yPos=5;
50 LeftX=0.7*tankL;
51 rightX=0.7*tankL+B;
52 midX=LeftX+(B/2);
53 lowZ=-20;
54 midZ=0;
55 highZ(i)=2*H(i)+H(i)/2;
56 rotmomX = midX;
57 rotmomY = 0.15;
58 rotmomZ = 0;
59
60 %Snappyhexmesh
61 fsboxZlow = lowZ-4;
62 fsboxZhigh(i) = highZ(i)+2;
63 fsboxX = tankL+5;
64 fsrefine = 3;
65 brefone = 3;
66 breftwo = 3;
67 bodyXmin = LeftX-5;
68 bodyXmax = rightX+5;
69 bodyZmin = lowZ-2;
70 bodyZmax(i) = highZ(i)+1;

```

```
71
72 %Probe in front and back of body
73 front=midX-(2*B);
74 back=midX+(2*B);
75
76 %Coords for porbes
77 one = 0.2 * tankL;
78 two = 0.5 * tankL;
79 three = 0.7 * tankL;
80 four = LeftX - B;
81 five = rightX + B;
82 six = 0.79 * tankL;
83 seven = 0.9 * tankL;
84
85 end
86 %%
87     for ind = 1:3
88         %input parameters
89         inputs.nCellX = nCellXs;
90         inputs.L = tankL;
91         inputs.D = depth;
92         inputs.f = frequency1;
93         inputs.wH = H;
94         inputs.domend = air;
95         inputs.endt = endtime;
96         inputs.yNeg = yNeg;
97         inputs.yPos = yPos;
98         inputs.LeftX = LeftX;
99         inputs.rightX = rightX;
100        inputs.midX = midX;
101        inputs.lowZ = lowZ;
102        inputs.midZ = midZ;
103        inputs.highZ = highZ(ind);
104        inputs.fsboxZlow = fsboxZlow;
105        inputs.fsboxZhigh = fsboxZhigh(ind);
106        inputs.fsboxX = fsboxX;
107        inputs.fsrefine = fsrefine;
108        inputs.brefone = brefone;
109        inputs.breftwo = breftwo;
110        inputs.bodyXmin = bodyXmin;
111        inputs.bodyXmax = bodyXmax;
112        inputs.bodyZmin = bodyZmin;
113        inputs.bodyZmax = bodyZmax(ind);
114        inputs.nCellZ = nCellZs;
115        inputs.front = front;
116        inputs.back = back;
```

```
117     inputs.rotmomX = rotmomX;
118     inputs.rotmomY = rotmomY;
119     inputs.rotmomZ = rotmomZ;
120     inputs.dampstart = dampstart;
121     inputs.dampYn = damp_Yn;
122     inputs.dampYp = damp_Yp;
123     inputs.one = one;
124     inputs.two = two;
125     inputs.three = three;
126     inputs.four = four;
127     inputs.five = five;
128     inputs.six = six;
129     inputs.seven = seven;
130     inputs.T1 = T1;
131     inputs.T2 = T2;
132     inputs.inletDamp = inletDamp;
133     inputs.H = H(ind);
134
135     caseName = ['caseBi' num2str(ind), 'Inviscid'];
136
137     casePath = [workPath '/' caseName];
138     mkdir(casePath);
139     copyfile([templatePath '/*'], casePath);
140
141     applyInput(casePath, inputs);
142 end
143 end
144
145 function applyInput(casePath, inputs)
146
147     %-----
148     % block Mesh dic file
149     file = fullfile(casePath, 'constant', 'polyMesh/blockMeshDict');
150     params={};
151
152     param.name = '__nCellX__';
153     param.value = inputs.nCellX;
154     params{end+1} = param;
155
156     param.name = '__L__';
157     param.value = inputs.L;
158     params{end+1} = param;
159
160     param.name = '__domend__';
161     param.value = inputs.domend;
162     params{end+1} = param;
```



```
163
164     param.name = '__D__';
165     param.value = - inputs.D;
166     params{end+1} = param;
167
168     param.name = '__nCellZ__';
169     param.value = inputs.nCellZ;
170     params{end+1} = param;
171
172     replaceParams(file,params);
173     %-----
174     %stl file
175     file = fullfile(casePath,'constant','triSurface/hull.stl');
176     params={};
177
178     param.name = '__yPos__';
179     param.value = inputs.yPos;
180     params{end+1} = param;
181
182     param.name = '__yNeg__';
183     param.value = inputs.yNeg;
184     params{end+1} = param;
185
186     param.name = '__LeftX__';
187     param.value = inputs.LeftX;
188     params{end+1} = param;
189
190     param.name = '__midX__';
191     param.value = inputs.midX;
192     params{end+1} = param;
193
194     param.name = '__rightX__';
195     param.value = inputs.rightX;
196     params{end+1} = param;
197
198     param.name = '__lowZ__';
199     param.value = inputs.lowZ;
200     params{end+1} = param;
201
202     param.name = '__midZ__';
203     param.value = inputs.midZ;
204     params{end+1} = param;
205
206     param.name = '__highZ__';
207     param.value = inputs.highZ;
208     params{end+1} = param;
```

```
209
210     replaceParams(file,params);
211     %-----
212     %snappyHexMesh file
213     file = fullfile(casePath,'system','snappyHexMeshDict');
214     params={};
215
216     param.name = '__fsboxZlow__'; %for blocks
217     param.value = inputs.fsboxZlow;
218     params{end+1} = param;
219
220     param.name = '__fsboxZhigh__'; %for blocks
221     param.value = inputs.fsboxZhigh;
222     params{end+1} = param;
223
224     param.name = '__L__'; %for one block
225     param.value = inputs.L;
226     params{end+1} = param;
227
228     param.name = '__fsrefine__';
229     param.value = inputs.fsrefine;
230     params{end+1} = param;
231
232     param.name = '__brefine1__';
233     param.value = inputs.brefone;
234     params{end+1} = param;
235
236     param.name = '__brefine2__';
237     param.value = inputs.breftwo;
238     params{end+1} = param;
239
240     param.name = '__bodyXmin__';
241     param.value = inputs.bodyXmin;
242     params{end+1} = param;
243
244     param.name = '__bodyZmin__';
245     param.value = inputs.bodyZmin;
246     params{end+1} = param;
247
248     param.name = '__bodyXmax__';
249     param.value = inputs.bodyXmax;
250     params{end+1} = param;
251
252     param.name = '__bodyZmax__';
253     param.value = inputs.bodyZmax;
254     params{end+1} = param;
```

```
255
256     replaceParams(file, params);
257     %-----
258     % waveProperties.input
259     file = fullfile(casePath, 'constant', 'waveProperties.input');
260     params={};
261
262     param.name = '__D__';
263     param.value = inputs.D;
264     params{end+1} = param;
265
266     param.name = '__damping__';
267     param.value = inputs.dampstart;
268     params{end+1} = param;
269
270     param.name = '__dampYn__';
271     param.value = inputs.dampYn;
272     params{end+1} = param;
273
274
275     param.name = '__dampYp__';
276     param.value = inputs.dampYp;
277     params{end+1} = param;
278
279     param.name = '__L__';
280     param.value = inputs.L;
281     params{end+1} = param;
282
283     param.name = '__T1__';
284     param.value = inputs.T1;
285     params{end+1} = param;
286
287     param.name = '__T2__';
288     param.value = inputs.T2;
289     params{end+1} = param;
290
291     param.name = '__inletDamp__';
292     param.value = inputs.inletDamp;
293     params{end+1} = param;
294
295     param.name = '__H__';
296     param.value = inputs.H;
297     params{end+1} = param;
298
299     replaceParams(file, params);
300     %-----
```

```
301     % controldict
302     file = fullfile(casePath, 'system', 'controlDict');
303     params={};
304
305     param.name = '__end__';
306     param.value = inputs.endt;
307     params{end+1} = param;
308
309     param.name = '__midX__';
310     param.value = inputs.midX;
311     params{end+1} = param;
312
313     param.name = '__midZ__';
314     param.value = inputs.midZ;
315     params{end+1} = param;
316     replaceParams(file,params);
317
318     param.name = '__rotmomX__';
319     param.value = inputs.rotmomX;
320     params{end+1} = param;
321
322     param.name = '__rotmomY__';
323     param.value = inputs.rotmomY;
324     params{end+1} = param;
325
326     param.name = '__rotmomZ__';
327     param.value = inputs.rotmomZ;
328     params{end+1} = param;
329
330     replaceParams(file,params);
331     %-----
332     % coords
333     file = fullfile(casePath, 'postProcessing', 'coords');
334     params={};
335
336     param.name = '__one__';
337     param.value = inputs.one;
338     params{end+1} = param;
339
340     param.name = '__two__';
341     param.value = inputs.two;
342     params{end+1} = param;
343
344     param.name = '__three__';
345     param.value = inputs.three;
346     params{end+1} = param;
```

```

347
348     param.name = '__four__';
349     param.value = inputs.four;
350     params{end+1} = param;
351
352     param.name = '__five__';
353     param.value = inputs.five;
354     params{end+1} = param;
355
356     param.name = '__six__';
357     param.value = inputs.six;
358     params{end+1} = param;
359
360     param.name = '__seven__';
361     param.value = inputs.seven;
362     params{end+1} = param;
363
364     replaceParams(file,params);
365 end
366
367
368 function replaceParams(filePath, params)
369
370     txt = fileread(filePath);
371
372     for ind = 1:length(params)
373         param = params{ind};
374         txt = strrep(txt, param.name, num2str(param.value));
375     end
376
377     fid = fopen(filePath,'wt');
378     fprintf(fid, '%s', txt);
379     fclose(fid);
380
381 end

```

C.2 Post-Processing Scripts

C.2.1 FFT of Wave Elevation

```

1 % Script to perform FFT on the wave elevation time series and plot the
2 % Time series together with the spectra
3

```

```

4  close all;
5  clear;
6  clc;
7  %SET PARAMETERS
8  wavemax=12;
9  wavemin=-12;
10 numProbes=7;
11 legend1={};
12 legend2={};
13 legend3={};
14
15 %IMPORT WAVEDATA FROM FILES
16 for i=1:numProbes
17     name=['probe',num2str(i)];
18     pathname=['elevationVsTime',num2str(i-1)];
19     data.(name) = importdata(pathname);
20     depth(i)=mean(data.(name)(:,2));
21 end
22
23 %SET WAVE PARAMETERS
24 w = 0.05;
25 %w = 0.07; % MUST CHANGE WITH CASE
26 omega = [0.05 0.5236 0.4736];
27 %omega = [0.07 0.5236 0.4536]; % MUST CHANGE WITH CASE
28 Tw=2*pi/w; % MUST CHANGE WITH CASE
29 g =9.81;
30 numT = 4; % Number of periods to use in validation
31 Tstart = 2.22; %4.05; % Number periods at interval start
32 delT=0.001; % Timestep in interpolation
33 dt=0.01; % Time step used in OpenFOAM simulation
34 t_start_sec=Tstart*Tw; % Time in sekunder
35 t_start=t_start_sec*1/dt; % Time in "elements"
36 t_delta_sec=numT*Tw; % Delta time in seconds
37 t_delta=t_delta_sec*1/dt; % Delta time in elements
38 t_end_sec=round(t_start_sec+t_delta_sec,1); % End time seconds
39 t_end=t_start+t_delta; % End time in elements
40
41 %RUN AND PLOT
42 for i=4
43     name=['probe',num2str(i)];
44     m=1/dt;
45
46     t=data.(name)(t_start:t_end,1);
47     y=data.(name)(t_start:t_end,2) - mean(data.(name)(t_start:t_end,2));
48     newt = t_start_sec:delT:t_end_sec;
49     newy = interp1(t,y,newt);

```

```

50 newy(isnan(newy)) = 0;
51 newL=length(newt)*1;
52 newFs=1/delT;
53 freq=2*pi*((0:newL-1)*newFs/newL);
54 x=fft(newy);
55 mag=abs(x);
56
57 if i==4
58     fig = figure;
59     hold on;
60
61     set(gcf, 'PaperUnits', 'centimeters');
62     paperSize = [18 1.4*18*sqrt(2)/3]*2;
63     figureSize = [0 0 paperSize(1) paperSize(2)-0.01];
64     axesfontSize = 14;
65
66     subplot( 2, 1, 2 )
67     plot(freq(1:newL/2), (2/newL*mag(1:newL/2)));
68     title('Single Sided Amplitude Spectrum of \eta(t)')
69
70     h = zeros(6, 1);
71     h(1)=line([omega(1) omega(1)], [0 4], 'Color', 'm'); % line through freq
72     h(2)=line([omega(2) omega(2) ], [0 4], 'Color', 'r');
73     h(3)=line([omega(3) omega(3)], [0 4], 'Color', 'b');
74     h(4)=line([2*omega(2) 2*omega(2)], [0 4], 'Color', ...
75         [204/255 102/255 0/255]);
76     h(5)=line([2*omega(3) 2*omega(3)], [0 4], 'Color', 'c');
77     h(6)=line([omega(2)+omega(3) omega(2)+omega(3)], [0 4], 'Color', 'k');
78     h(7)=line([2*omega(2)-omega(3) 2*omega(2)-omega(3)], [0 4], ...
79         'Color', 'y');
80     h(8)=line([2*omega(3)-omega(2) 2*omega(3)-omega(2)], [0 4], 'Color', ...
81         [0/255 102/255 0/255]);
82     legend1 = ['\omega = ', num2str(omega(1))];
83     legend2 = ['\omega_1 = ', num2str(omega(2))];
84     legend3 = ['\omega_2 = ', num2str(omega(3))];
85     legend4 = ['2\omega_1'];
86     legend5 = ['2\omega_2'];
87     legend6 = ['\omega_1+\omega_2'];
88     legend7 = ['2\omega_1-\omega_2'];
89     legend8 = ['2\omega_2-\omega_1'];
90     legObj=legend(h, legend1, legend2, legend3, legend4, legend5, legend6, ...
91         legend7, legend8);
92     legObj.FontSize=14;
93     xlabel('Frequency [rad/s]')
94     ylabel('\eta')
95     xlim([0 1.4])

```

```
96     ylim([0 1.1*max(2/newL*mag(1:newL/2))])
97     box on;
98     set( gca, 'FontSize', axesfontSize );
99
100    subplot( 2, 1, 1)
101    plot(data.probe4(:,1),data.probe4(:,2))
102    h = zeros(2, 1);
103    h(1)=line([t_start_sec t_start_sec], [-10 10], 'Color','g');
104    h(2)=line([t_end_sec t_end_sec], [-10 10], 'Color','r');
105    legend1 = ['Interval Start'];
106    legend2 = ['Interval End'];
107    legObj=legend(h,legend1,legend2);
108    legObj.FontSize=14;
109    title('Time Series of Wave Elevation')
110    xlabel('Time [s]')
111    ylabel('wave elevation, \eta')
112    ylim([wavemin wavemax])
113    xlim([0 data.probe1(end,1)])
114    grid;
115    box on;
116    set( gca, 'FontSize', axesfontSize );
117
118    plotname =...
119    '/Users/julie/Documents/Marin5/Master/Master-set-up/fig/H7/dw005FFT';
120    set(gcf,'PaperSize',paperSize*1.05)
121    set(gcf,'PaperPosition',figureSize*1.05)
122    set(gca, 'LooseInset', get(gca, 'TightInset'));
123    print(gcf,'-dpng', plotname);
124 end
125 end
```

C.2.2 FFT of Force Data

```
1 % Performs FFT on the force results and plots the force time series and the
2 % force spectra
3
4 close all;
5 clear;
6 clc;
7 fourierData={};
8 hAll = [4.5 6 7.5 8]; %j
9 zetaAll=[2.25 3 3.75 4];
10 progressBar=0;
11 output={};
12
```



```

13 for kk=1:2;
14     if kk==1
15         w = [0.05 0.5236 0.4736]; %i
16     elseif kk==2
17         w = [0.07 0.5236 0.4536];
18     else
19         disp('error1')
20     end
21     for j=1:3;
22         H=hAll(j);
23         for i=1;
24             %close all;
25
26             B = 12;
27             d = 20;
28             L = 0.1;
29             zeta_A = zetaAll(j); % NOMINAL AMPLITUDE
30             if w(1)==0.05
31                 nTStart=2.22;
32             elseif w(1)==0.07
33                 nTStart=4.05;
34             else
35                 disp('error');
36             end
37
38             numT = 4.00; %number of periods in fourier analysis
39
40             rho = 1000.0;
41             g = 9.81;
42             Tw = 2.0*pi/w(1);
43             k = (w(1)^2.0)/g;
44             % Load data, wave loads
45
46             filename=['BiH', num2str(floor(H)), 'dw00', num2str(w(1)*100), ...
47                 't001'];
48             output= [output; filename num2str(i) num2str(j) num2str(kk)];
49
50             run(filename);
51
52             t0 = time(4:end);
53             dt0 = t0(2)-t0(1);
54             fx0 = fpx(4:end)+fvx(4:end);
55             fz0 = fpz(4:end)+fvz(4:end) - rho*g*d*B*L;
56             my0 = mpy(4:end)+mvy(4:end);
57
58             % Harmonic components

```

```
59     % Analysis window
60     t_start= nTStart*Tw;
61     t_end = t_start + numT*Tw; %+0.1*dt;
62     t_end = round(t_end);
63     delT = 0.001; %timestep in interpolation
64
65     % FORCE X (SURGE)
66     newt = t_start:delT:t_start+(numT*Tw);
67     newfx = interp1(t0,fx0,newt);
68     newLx = length(newt)*1;
69     newFsx = 1/delT;
70     freq = 2*pi*((0:newLx-1)*newFsx/newLx);
71     fftx = fft(newfx,length(freq));
72     magx = abs(fftx);
73     [ampx, I] = max(2/newLx*magx);
74     Fq = freq(I);
75
76     % FORCE Z (HEAVE)
77     name=['fz'];
78     newt = t_start:delT:t_start+(numT*Tw);
79     newfz = interp1(t0,fz0,newt);
80     newLz=length(newt);
81     newFsz=1/delT;
82     freq=2*pi*((0:newLz-1)*newFsz/newLz);
83     fftz=fft(newfz,length(freq));
84     magz=abs(fftz);
85     [ampz, I]=max(2/newLz*magz);
86     Fq=freq(I);
87
88     % MOMENT Y (PITCH)
89     name=['my'];
90     newt = t_start:delT:t_start+(numT*Tw);
91     newmy = interp1(t0,my0,newt);
92     newLy=length(newt)*1;
93     newFsy=1/delT;
94     freq=2*pi*((0:newLy-1)*newFsy/newLy);
95     fftmy=fft(newmy,length(freq));
96     magmy=abs(fftmy);
97     %magmy(1)=0;
98     [ampmy, I]=max(2/newLy*magmy);
99     Fq=freq(I);
100
101     % FIGURES
102     fig=figure;
103     hold on;
104     set(gcf, 'PaperUnits', 'centimeters');
```

```

105     paperSize = [18 1.4*18*sqrt(2)/3]*2;
106     figureSize = [0 0 paperSize(1) paperSize(2)-0.01];
107     axesfontSize = 14;
108
109     subplot( 3, 1, 1 )
110     plot(freq(1:floor(newLx/2)),(2/newLx*magx(1:floor(newLx/2))));
111     title('Surge Force')
112     h = zeros(6, 1);
113     h(1)=line([w(1) w(1)], [0 1.1*ampx],'Color','m'); %plot line
114     h(2)=line([w(2) w(2)], [0 1.1*ampx],'Color','r');
115     h(3) = line([w(3) w(3)], [0 1.1*ampx],'Color','g');
116     h(4)=line([2*w(2) 2*w(2)], [0 1.1*ampx],'Color',...
117         [204/255 102/255 0/255]); % []
118     h(5)=line([2*w(3) 2*w(3)], [0 1.1*ampx],'Color','c');
119     h(6)=line([w(2)+w(3) w(2)+w(3)], [0 1.1*ampx],'Color','k');
120     h(7)=line([2*w(2)-w(3) 2*w(2)-w(3)], [0 1.1*ampx],'Color','y');
121     h(8)=line([2*w(3)-w(2) 2*w(3)-w(2)], [0 1.1*ampx],'Color',...
122         [0/255 102/255 0/255]);
123     legend1 = ['\omega = ', num2str(w(1))];
124     legend2 = ['\omega_1 = ', num2str(w(2))];
125     legend3 = ['\omega_2 = ', num2str(w(3))];
126     legend4 = '2\omega_1';
127     legend5 = '2\omega_2';
128     legend6 = '\omega_1+\omega_2';
129     legend7 = ['2\omega_1-\omega_2'];
130     legend8 = ['2\omega_2-\omega_1'];
131     legObj=legend(h,legend1,legend2,legend3,legend4,legend5,...
132         legend6,legend7,legend8);
133     legObj.FontSize=axesfontSize;
134     xlabel('Frequency [rad/s'],'FontSize', axesfontSize)
135     ylabel( 'F_x [N]', 'FontSize', axesfontSize );
136     xlim([0 1.3])
137     ylim([0 1.1*ampx])
138     box on;
139
140     set( gca, 'FontSize', axesfontSize );
141
142     subplot( 3, 1, 2)
143     plot(freq(1:floor(newLz/2)),(2/newLz*magz(1:floor(newLz/2))));
144     title('Heave Force')
145     h = zeros(8, 1);
146     h(1)=line([w(1) w(1)], [0 1.1*ampz],'Color','m'); %plot line
147     h(2)=line([w(2) w(2)], [0 1.1*ampz],'Color','r');
148     h(3)=line([w(3) w(3)], [0 1.1*ampz],'Color','g');
149     h(4)=line([2*w(2) 2*w(2)], [0 1.1*ampz],'Color',...
150         [204/255 102/255 0/255]);

```

```

151     h(5)=line([2*w(3) 2*w(3)], [0 1.1*ampz], 'Color','c');
152     h(6)=line([w(2)+w(3) w(2)+w(3)], [0 1.1*ampz], 'Color','k');
153     h(7)=line([2*w(2)-w(3) 2*w(2)-w(3)], [0 1.1*ampz], 'Color','y');
154     h(8)=line([2*w(3)-w(2) 2*w(3)-w(2)], [0 1.1*ampz], 'Color',...
155         [0/255 102/255 0/255]);
156     legend1 = ['\omega = ', num2str(w(1))];
157     legend2 = ['\omega_1 = ', num2str(w(2))];
158     legend3 = ['\omega_2 = ', num2str(w(3))];
159     legend4 = ['2\omega_1'];
160     legend5 = ['2\omega_2'];
161     legend6 = ['\omega_1+\omega_2'];
162     legend7 = ['2\omega_1-\omega_2'];
163     legend8 = ['2\omega_2-\omega_1'];
164
165     legObj=legend(h,legend1,legend2,legend3,legend4,legend5,...
166         legend6,legend7, legend8);
167     legObj.FontSize=axesfontSize;
168     xlabel('Frequency [rad/s'],'FontSize', axesfontSize)
169     ylabel('F_z [N]', 'FontSize', axesfontSize );
170     xlim([0 1.3])
171     ylim([0 1.1*ampz])
172     box on;
173
174     set( gca, 'FontSize', axesfontSize );
175
176     subplot( 3, 1, 3)
177     plot(freq(1:floor(newLy/2)),(2/newLy*magmy(1:floor(newLy/2))));
178     title('Pitch Moment')
179
180     h = zeros(6, 1);
181     h(1)=line([w(1) w(1)], [0 1.1*ampmy], 'Color','m'); %plot line
182     h(2)=line([w(2) w(2)], [0 1.1*ampmy], 'Color','r');
183     h(3)=line([w(3) w(3)], [0 1.1*ampmy], 'Color','g');
184     h(4)=line([2*w(2) 2*w(2)], [0 1.1*ampmy], 'Color',...
185         [204/255 102/255 0/255]);
186     h(5)=line([2*w(3) 2*w(3)], [0 1.1*ampmy], 'Color','c');
187     h(6)=line([w(2)+w(3) w(2)+w(3)], [0 1.1*ampmy], 'Color','k');
188     h(7)=line([2*w(2)-w(3) 2*w(2)-w(3)], [0 1.1*ampmy], 'Color',...
189         'y');
190     h(8)=line([2*w(3)-w(2) 2*w(3)-w(2)], [0 1.1*ampmy], 'Color',...
191         [0/255 102/255 0/255]);
192     legend1 = ['\omega = ', num2str(w(1))];
193     legend2 = ['\omega_1 = ', num2str(w(2))];
194     legend3 = ['\omega_2 = ', num2str(w(3))];
195     legend4 = ['2\omega_1'];
196     legend5 = ['2\omega_2'];

```

```

197         legend6 = ['\omega_1+\omega_2'];
198         legend7 = ['2\omega_1-\omega_2'];
199         legend8 = ['2\omega_2-\omega_1'];
200         legObj=legend(h,legend1,legend2,legend3,legend4,legend5,...
201             legend6,legend7,legend8);
202         legObj.FontSize=axesfontSize;
203         xlabel('Frequency [rad/s'],'FontSize', axesfontSize)
204         ylabel('My [Nm]', 'FontSize', axesfontSize );
205         xlim([0 1.3])
206         ylim([0 1.1*ampmy])
207         box on;
208         set( gca, 'FontSize', axesfontSize );
209
210         plotname=...
211         ['/Users/julie/Documents/Marin5/Master/Master-set-up/fig/fftForceBiH',...
212             num2str(floor(H),'dw00',num2str(w(1)*100),'t001'];
213         set(gcf,'PaperSize',paperSize*1.05)
214         set(gcf,'PaperPosition',figureSize*1.05)
215         set(gca, 'LooseInset', get(gca, 'TightInset'));
216         print(gcf,'-dpng', plotname);
217         progressBar=progressBar+1;
218         progress=round(progressBar/6*100);
219         clc; %clearing "chat"
220         loadingText=['Simulation is ',num2str(progress),'% done'];
221         disp(loadingText);
222         hold off;
223         close all;
224     end
225 end
226 end
227 clc;
228 disp('Complete')

```

C.2.3 Fourier Analysis of Force Data

```

1 % Script to perform Fourier analysis on the force results
2 % Based on the script made by Finn-Christian Hanssen
3 % Uses the function intergral values.m and fourier_comp.m
4 % Outputs a matrix with all the dimensionless force coefficients
5
6 clear all; clc; close all;
7
8 %Basic data
9 fourierData={};
10 fourierDataThird={};

```

```

11 hAll = [4.5 6 7.5];      %Wave heigt, index j
12 zetaAll=[2.25 3 3.75]; %Wave Amp
13 progressBar=0;
14
15 for kk=1:2;
16     if kk==1
17         w = [0.05 0.5236 0.4736]; % frequencies, index i
18     elseif kk==2
19         w = [0.07 0.5236 0.4536];
20     else
21         disp('error1')
22     end
23     for j=1:3;
24         H=hAll(j);
25         for i=1:3;
26
27             B = 12;          % Breadth of column
28             d = 20;          % Draft of column
29             L = 0.1;         % Domain size in y - thickness of body
30             zeta_A = zetaAll(j);% NOMINAL AMPLITUDE
31             if w(1)==0.05
32                 nTStart=2.22; %Start of interval for diff. freq 0.05
33             elseif w(1)==0.07
34                 nTStart=4.05; %Start of interval for diff. freq 0.07
35             else
36                 disp('error');
37             end
38
39             n_Tw = 4.00;      %Number of periods in fourier analysis
40
41             rho = 1000.0;
42             g = 9.81;
43             Tw = 2.0*pi/w(1);
44             k = (w(i)^2.0)/g;
45
46             % Load data, wave loads
47             filename=...
48             ['BiH',num2str(floor(H)), 'dw00', num2str(w(1)*100), 't001.m'];
49
50             run(filename); %Runs script collecting force data from file
51
52             t0 = time(4:end);
53             dt0 = t0(2)-t0(1);
54             fx0 = fpx(4:end)+fvx(4:end);
55             fz0 = fpz(4:end)+fvz(4:end);
56             my0 = mpy(4:end)+mvy(4:end);

```

```

57
58     % Resample data . interpolate
59     t = t0( 1 ):( dt0/10 ):t0( end );
60     dt = t( 2 ) - t( 1 );
61     t = t';
62     fx = interp1( t0, fx0, t );
63     fz = interp1( t0, fz0, t ) - rho*g*d*B*L;
64     my = interp1( t0, my0, t );
65
66     % Harmonic components
67     % Analysis window
68     t1 = nTStart*Tw;
69     t2 = t1 + n_Tw*Tw + 0.1*dt;
70
71     % Zeroth order
72     n = 0;
73     [ a0.fx, b0.fx ] = fourier_comp( n, t, fx, w(i), t1, t2 );
74     [ a0.fz, b0.fz ] = fourier_comp( n, t, fz, w(i), t1, t2 );
75     [ a0.my, b0.my ] = fourier_comp( n, t, my, w(i), t1, t2 );
76     a0.fx = a0.fx/2.0;
77     a0.fz = a0.fz/2.0;
78     a0.my = a0.my/2.0;
79
80     % First order
81     n = 1;
82     [ a1.fx, b1.fx ] = fourier_comp( n, t, fx, w(i), t1, t2 );
83     [ a1.fz, b1.fz ] = fourier_comp( n, t, fz, w(i), t1, t2 );
84     [ a1.my, b1.my ] = fourier_comp( n, t, my, w(i), t1, t2 );
85
86     % Second order
87     n = 2;
88     [ a2.fx, b2.fx ] = fourier_comp( n, t, fx, w(i), t1, t2 );
89     [ a2.fz, b2.fz ] = fourier_comp( n, t, fz, w(i), t1, t2 );
90     [ a2.my, b2.my ] = fourier_comp( n, t, my, w(i), t1, t2 );
91
92     % Third order
93     n = 3;
94     [ a3.fx, b3.fx ] = fourier_comp( n, t, fx, w(i), t1, t2 );
95     [ a3.fz, b3.fz ] = fourier_comp( n, t, fz, w(i), t1, t2 );
96     [ a3.my, b3.my ] = fourier_comp( n, t, my, w(i), t1, t2 );
97     nn = 1;
98     w1 = 2*w(2)-w(3);%2w1-w2
99     w2 = 2*w(3)-w(2);%2w2-w1
100    [ a3w1.fx, b3w1.fx ] = fourier_comp( nn, t, fx, w1, t1, t2 );
101    [ a3w1.fz, b3w1.fz ] = fourier_comp( nn, t, fz, w1, t1, t2 );
102    [ a3w1.my, b3w1.my ] = fourier_comp( nn, t, my, w1, t1, t2 );

```

```

103
104     [ a3w2.fx, b3w2.fx ] = fourier_comp( nn, t, fx, w2, t1, t2 );
105     [ a3w2.fz, b3w2.fz ] = fourier_comp( nn, t, fz, w2, t1, t2 );
106     [ a3w2.my, b3w2.my ] = fourier_comp( nn, t, my, w2, t1, t2 );
107
108
109     % Nondimensional forces
110     fd_x = a0.fx/( 0.5*rho*g*L*zeta_A^2.0 );
111     fd_z = a0.fz/( 0.5*rho*g*L*zeta_A^2.0 );
112     fd_my = a0.my/( 0.5*rho*g*L*B*zeta_A^2.0 );
113
114     fx1 = sqrt( a1.fx^2 + b1.fx^2 )/( rho*g*L*d*zeta_A );
115     fz1 = sqrt( a1.fz^2 + b1.fz^2 )/( rho*g*L*B*zeta_A );
116     my1 = sqrt( a1.my^2 + b1.my^2 )/( rho*g*L*B*d*zeta_A );
117     fxSlow = sqrt( a1.fx^2 + b1.fx^2 )/( rho*g*L*zeta_A^2 );
118     fzSlow = sqrt( a1.fz^2 + b1.fz^2 )/( rho*g*L*zeta_A^2 );
119     mySlow = sqrt( a1.my^2 + b1.my^2 )/( rho*g*L*B*zeta_A^2 );
120
121     fx2 = sqrt( a2.fx^2 + b2.fx^2 )/( rho*L*d*g*zeta_A );
122     fz2 = sqrt( a2.fz^2 + b2.fz^2 )/( rho*L*B*g*zeta_A );
123     my2 = sqrt( a2.my^2 + b2.my^2 )/( rho*g*L*B*d*zeta_A );
124
125     fx3 = sqrt( a3.fx^2 + b3.fx^2 )/( rho*L*d*g*zeta_A );
126     fz3 = sqrt( a3.fz^2 + b3.fz^2 )/( rho*L*B*g*zeta_A );
127     my3 = sqrt( a3.my^2 + b3.my^2 )/( rho*g*L*B*d*zeta_A );
128     fx3w1 = sqrt( a3w1.fx^2 + b3w1.fx^2 )/( rho*L*d*g*zeta_A );
129     fz3w1 = sqrt( a3w1.fz^2 + b3w1.fz^2 )/( rho*L*B*g*zeta_A );
130     my3w1 = sqrt( a3w1.my^2 + b3w1.my^2 )/( rho*g*L*B*d*zeta_A );
131     fx3w2 = sqrt( a3w2.fx^2 + b3w2.fx^2 )/( rho*L*d*g*zeta_A );
132     fz3w2 = sqrt( a3w2.fz^2 + b3w2.fz^2 )/( rho*L*B*g*zeta_A );
133     my3w2 = sqrt( a3w2.my^2 + b3w2.my^2 )/( rho*g*L*B*d*zeta_A );
134
135     fourierData=[fourierData; fd_x fx1 fz1 my1 fx2 fz2 my2 fx3...
136         fz3 my3 fd_z fd_my fxSlow fzSlow mySlow i j kk];
137     fourierDataThird=[fourierDataThird;...
138         fx3w1 fz3w1 my3w1 fx3w2 fz3w2 my3w2 i j kk];
139     progressBar=progressBar+1;
140     progress=round(progressBar/18*100);
141     clc;
142     loadingText=['Simulation is ',num2str(progress),'% done'];
143     disp(loadingText);
144     end
145 end
146 end
147 fourierData = cell2mat(fourierData);
148 fourierDataThird = cell2mat(fourierDataThird);

```



```

149 clc;
150 disp('Done');

```

C.2.4 Input Function in `fourier_analysist001.m`

```

1 % Made by Finn-Christian Hanssen
2 % Used by the script fourier_analysist001.m
3 % Uses the function integral_values.m
4
5 function [ an, bn ] = fourier_comp( n, t, y, w, t1, t2 )
6
7 % Determine vectors for integration
8 ind = find( ( t >= t1 ) & ( t <= t2 ) );
9 ti = t( ind );
10 yi = y( ind );
11 T = ti( end ) - ti( 1 );
12
13 for i = 1:length( ti )
14     tt = ti( i );
15     yy = yi( i );
16     [ ian( i ), ibn( i ) ] = integral_values( n, w, tt, yy );
17 end
18
19 % Perform trapezoidal integration
20 an = ( 2/T)*trapz( ti, ian );
21 bn = ( 2/T)*trapz( ti, ibn );
22
23 end

```

C.2.5 Input Function in `fourier_comp.m`

```

1
2 % Made by Finn-Christian Hanssen
3 % Input function to fourier_comp.m
4
5 function [ ia, ib ] = integral_values( n, w, t, y )
6 ia = y*cos( n*w*t );
7 ib = y*sin( n*w*t );
8 end

```

C.2.6 Script Used to Plot Mean Drift Force Coefficients

```

1  % Script to plot the mean drift force coefficients
2  % Uses Matrix output from fourier_analysis.m
3
4  run fourier_analysist001.m
5
6  close all;
7  figure
8
9  grid on
10 hold on
11 colorVector=['b' 'r'];
12 lineVector={'-', '-.', ':'};
13 legendString={};
14
15 for kk=1:2;
16     if kk==1
17         w = [0.05 0.5236 0.4736]; %i
18     elseif kk==2
19         w = [0.07 0.5236 0.4536];
20     else
21         disp('error1')
22     end
23 for i=1
24 plotY=fourierData(9*(kk-1)+((i-1)+1:3:(i-1)+9),1);
25 plotXentry=fourierData(9*(kk-1)+((i-1)+1:3:(i-1)+9),17); %track wave height
26 heightVector=[2.25 3 3.75];
27 plotX=[heightVector(plotXentry(1)) heightVector(plotXentry(2))...
28     heightVector(plotXentry(3))];
29
30 set(gcf, 'PaperUnits', 'centimeters')
31 paperSize = [18 1.1*18*sqrt(2)/3]*2;
32 figureSize = [0 0 paperSize(1) paperSize(2)-0.01];
33 axesfontSize = 16;
34
35 plotOption = [cellstr(lineVector(i)), colorVector(kk)];
36 plotOption = strjoin(plotOption);
37 plot(plotX,plotY,plotOption,'LineWidth',1.5)
38 legendString=[legendString ['d\omega = ' num2str(w(1))]];
39 legend(legendString,'Location', 'NorthEast');
40
41 xlim([2 4]);
42 %ylim([0.75 1]);
43
44 set(gca,'GridLineStyle',':')
45 set(gcf,'PaperSize',paperSize*1.05)
46 set(gcf,'PaperPosition',figureSize*1.05)

```

```
47 set(gca, 'LooseInset', get(gca, 'TightInset'));
48 set(gca, 'FontSize', axesFontSize)
49 prcentChangeMeanForceX(:,kk) = ((plotY(3)-plotY(1))/plotY(1))*100;
50 end
51 end
52
53 plotname =...
54     '/Users/julie/Documents/Marin5/Master/Master-set-up/fig/MeanCoeffX';
55 legend(legendString);
56 xlabel('Wave Amplitude [m]');
57 ylabel('Fx{mean}/0.5\rho g L A2 [-]');
58 title('Mean Drift Force Coefficients in x-Direction');
59 box on;
60 print(gcf, '-dpng', plotname)
61 hold off
```